2018

Tailoring Polybenzimidazole Membranes For Enhanced Performance In Electrochemical Devices

Andrew T. Pingitore
University of South Carolina - Columbia

TAILORING POLYBENZIMIDAZOLE MEMBRANES FOR ENHANCED PERFORMANCE IN ELECTROCHEMICAL DEVICES

by

Andrew T. Pingitore

Bachelor of Arts
Washington & Jefferson College, 2014

Submitted in Partial Fulfillment of the Requirements

For the Degree of Doctor of Philosophy in

Chemistry

College of Arts and Sciences

University of South Carolina

2018

Accepted by:

Brian C. Benicewicz, Major Professor

Chuanbing Tang, Committee Member

John W. Weidner, Committee Member

Aaron Vannucci, Committee Member

Cheryl L. Addy, Vice Provost and Dean of the Graduate School

DEDICATION

In loving memory of my grandmothers, Irene Fischer and Margaret Snyder, and grandfather, Gerred Snyder.

ACKNOWLEDGEMENTS

First and foremost I would like to thank my research advisor, Dr. Brian C. Benicewicz, for all of his support and guidance on my research projects. It would take more than one Ph.D. to acquire a fragment of his knowledge and creativity in polymer science and his enthusiastic approach and love of science helped to keep me motivated through all those late nights in the lab. I am sincerely grateful for all the opportunities and experiences I was given in his group.

I would like thank Dr. John W. Weidner for the opportunity to collaborate with his group and his support through my Ph.D. candidacy. I would also like to thank Dr. Chuanbing Tang for his guidance and interest in my research. I would also like to thank Dr. Aaron Vannucci for his support and valuable suggestions on my research. - Thank you all for being on my doctoral committee, as well.

I would like to thank the entire Benicewicz Group, both past and present, for all of the support, suggestions and friendship. I would especially like to thank Kayley Fishel-Hayat for mentoring me in beginning years and being a truly great lab mate and even better friend. The fun and laughs we shared were invaluable and truly missed. I'd also like to thank Julia Pribyl for our office vent sessions and for all of the support and ideas. I would also like to thank Zachary Marsh for being a great friend and all of the support, fun, and beers we had along the way. I would also like to thank Kayla Lantz for her friendship, support, listening to me vent.

Next, I would like to thank my parents, siblings, and loving grandparents for their unwavering support, availability to talk no matter what time of the day, and traveling to visit me. I would also like to give my deepest gratitude to my girlfriend, Tori Fecteau, who has been extremely supportive and helpful throughout my program, putting up with all of the late nights and weekends I'd spend in the lab, and subsequently taking care of my dog Bill; who I would also like thank for always be so happy when I got home.

Finally, I would like to acknowledge all of the funding support and research opportunities I was given through my collaborations with BASF GmbH, United Technologies Research Center, Johnson R&D Co., and PBI Performance Products.

ABSTRACT

After approximately 15 years of development, polybenzimidazole (PBI) chemistries and the concomitant manufacturing processes have evolved into commercially produced membrane electrode assemblies (MEAs). PBI MEAs can operate reliably without complex water humidification hardware and are able to run at elevated temperatures of 120-180 ^{O}C due to the physical and chemical robustness of PBI membranes. These higher temperatures improve the electrode kinetics and conductivity of the MEAs, simplify the water and thermal management of the systems, and significantly increase their tolerance to fuel impurities. Membranes cast by a newly developed polyphosphoric acid (PPA) Process possessed excellent mechanical properties, higher phosphoric acid (PA)/PBI ratios, and enhanced proton conductivities as compared to previous methods of membrane preparation. *p*-PBI and *m*-PBI are the most common polymers in PBI-based fuel cell systems, although AB-PBI and other derivatives have been investigated. The work presented in this dissertation demonstrates the chemical flexibility of PBI polymers which enables the tailoring of specific membrane properties enhancing performance in new and different electrochemical devices with diverse operating conditions.

TABLE OF CONTENTS

LIST OF TABLES

LIST OF FIGURES

LIST OF SYMBOLS

E_{Nernst}	Nernst Potential
$E°$	Standard Potential
R	Universal Gas Constant
T	Temperature
F	Faraday's Constant
i_o	Exchange Current Density
J_s^0	Creep Compliance
d	Distance between the two inner electrodes.
l	Thickness of the membrane.
w	Membrane width
R_m	Membrane ohmic resistance
dJ/dt	Creep Rate
R_A	Specific Area Resistance
HFR	High Frequency Resistance
iR_A	Ohmic Resistance in the Membrane
U_{eq}	Equilibrium Potential
MSE	Mixed Solvent Electrolyte Thermodynamics Framework Package
k	Kinetic Term Dependent on Temperature in The Arrhenius Relationship
η_a	Anodic Overpotential

$c_r(t)$ Receptor $VOSO_4$ Concentration at Time t in Permeability Cell

$c_r(0)$ Donor Initial $VOSO_4$ Concentration in Permeability Cell

V Volume of the Donor and Receptor Permeability Cell

d Thickness of Membrane used in Permeability Testing

A Active Area of the Membrane used in Permeability Testing

P_s Permeability of Salt Through the Membrane

LIST OF ABBREVIATIONS

PEM ..... Polymer Electrolyte Membrane

PEMFC ..... Polymer Electrolyte Fuel Cell

MEA ..... Membrane Electrode Assembly

PA ..... Phosphoric Acid

SA ..... Sulfuric Acid

TFA ..... Trifluoroacetic Acid

PBI ..... Polybenzimidazole

PPA ..... Polyphosphoric Acid

RU ..... Repeat Unit

PSA ..... Pressure Swing Absorption

PFSA ..... Perfluorosulfonic Acid

EHS ..... Electrochemical Hydrogen Separation

HyS ..... Hybrid Sulfur Cycle

HT-PEM ..... High Temperature Polymer Electrolyte Fuel Cell

LT-PEM ..... Low Temperature Polymer Electrolyte Fuel Cell

DMAc ..... N,N'-Dimethylacetamide

TPA ..... Terephthalic Acid

IPA ..... Isophthalic Acid

TAB ..... 3,3',4,4'-tetraamine-(1,1'-biphenyl)

R.H. ..... Relative Humidity

GDE ..... Gas Diffusion Electrode

DCX ..... α,α'-Dichloro-*p*-xylene

DCB .....4,4'-Bis(chloromethyl)biphenyl

s-PBI .....Sulfonated Polybenzimidazole

SDE ..... SO_2 Depolarized Electrolyzer

S-TAB Sulfonylbis-1,2-benzenediamine

s-TPA .....Monosodium 2-Sulfoterephthalate

SAXS .....Small Angle X-Ray Scattering

WAXS..... Wide Angle X-Ray Scattering

CHAPTER 1

GENERAL INTRODUCTION

REPRINTED IN PART WITH PERMISSION FROM SPRINGER INTERNATIONAL PUBLISING

Pingitore, A. T., Molleo, M., Schmidt T. J., Benicewicz B. C. *Polybenzimidazole Fuel Cell Technology: Theory, Performance, and Applications;* Springer International Publishing, 2018.

1.1 Abstract.

After approximately 15 years of development, polybenzimidazole (PBI) chemistries and the concomitant manufacturing processes have evolved into commercially produced membrane electrode assemblies (MEAs). PBI MEAs can operate reliably without complex water humidification hardware and are able to run at elevated temperatures of 120-180 ^{O}C due to the physical and chemical robustness of PBI membranes. These higher temperatures improve the electrode kinetics and conductivity of the MEAs, simplify the water and thermal management of the systems, and significantly increase their tolerance to fuel impurities. Membranes cast by a newly developed polyphosphoric acid (PPA) Process possessed excellent mechanical properties, higher phosphoric acid (PA)/PBI ratios, and enhanced proton conductivities as compared to previous methods of membrane preparation. *p*-PBI and *m*-PBI are the most common polymers in PBI-based fuel cell systems, although AB-PBI and other derivatives have been investigated. This chapter reports on the chemistries and sustainable usages of PBI-based high temperature proton exchange membrane fuel cells (PEMFCs).

1.2 Introduction to Polybenzimidazole Fuel Cell Sustainability.

Alternative energy is often defined as any energy derived from sources other than fossil fuels or nuclear fission. These alternative energy sources, which include solar, wind, hydro, and geothermal energy, are considered renewable because they are naturally replenished and their supply is seemingly limitless. In contrast, the Earth's supply of fossil fuels is constantly being diminished. Fossil fuels, which include crude oil, coal, and natural gas, continue to be the dominating sources of energy in the world (**Figure 1.1**). Fossil fuels provide more than 86% of the total energy consumed globally.(1, 2) In 2009, the electrical

power sector was the largest source of carbon dioxide emissions (40% of all energy-related CO_2 emissions) and was followed closely by the transportation sector which was 34% of the total.(3) It is predicted that the global demand for fossil fuels will continue to increase over the next 10-20 years due to economic growth. One may conclude that the importance of renewable energy will steadily increase as the Earth's supply of fossil fuels continues to be depleted.

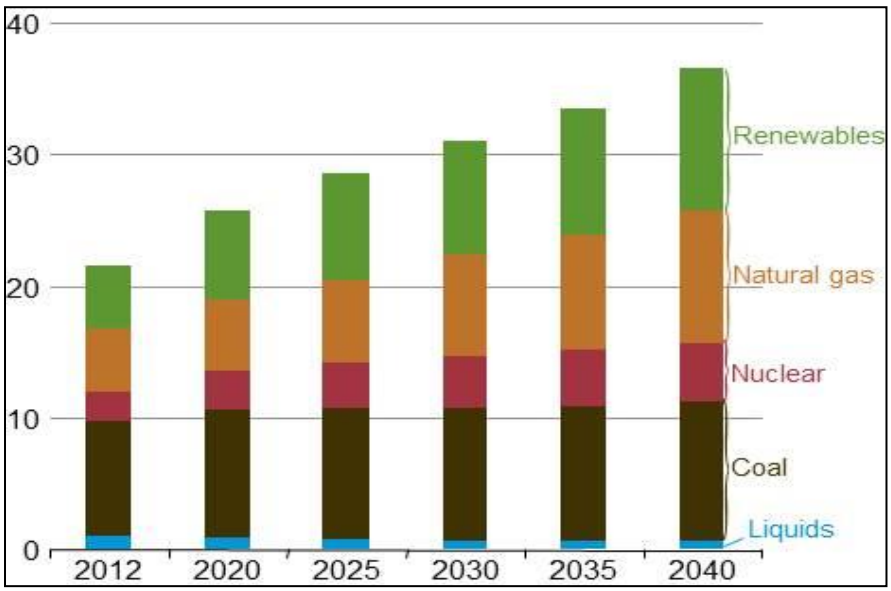

Figure 1.1: World net electricity production by source, 2012-40 (trillion kilowatt hours). (1)

Polymer electrolyte membrane (PEM) fuel cells, also known as proton exchange membrane fuel cells (PEMFCs), are energy conversion devices that could provide the world with clean and efficient energy. Due to their excellent energy production, inexpensive starting materials, and lack of pollutant byproducts, these cells have exponentially gained in popularity over the past decade. Electricity is produced at the heart of the fuel cell by the membrane electrode assembly (MEA), a component that is comprised

of a proton exchange membrane sandwiched between two electrodes. Fueled by a hydrogen-based source, a metal catalyst at the anode splits the hydrogen into protons and electrons. As the protons are transported through the proton electrolyte membrane to the cathode, the electrons provide electrical work by traveling around the membrane through an external circuit from the anode to the cathode. The protons and electrons react with an oxidant (typically air or pure oxygen) at the cathode to form water, thereby completing the electrochemical cycle. Hydrogen gas is commonly used as a fuel source for the cells, but other fuels such as methane, methanol, and ethanol have been explored.

PEM fuel cells provide multiple advantages over conventional fossil fuel energy production. Because water is the only byproduct of the electrochemical process, these fuel cells are clean and environmentally friendly. If one considers the tremendous amount of carbon dioxide created by energy production on the global scale (**Figure 1.2**), PEM fuel cells offer a method to significantly reduce hazardous gas emissions. Minimal moving parts reduces the amount of maintenance of each cell, and the lack of combustion significantly decreases the amount of harmful pollutants such as sulfur oxides and nitrogen oxides. In addition, PEM fuel cells are much more efficient at producing energy and, much like a combustion engine, the cell can run continuously as long as fuel and oxidant are provided. Although fuel cells are an environmentally friendly energy conversion device, one must consider the way hydrogen is gathered. Both hydrogen production and conversion from chemical to electrical energy need to be sustainable to make the overall process sustainable. Hydrogen production, however, will only briefly be discussed in this chapter.

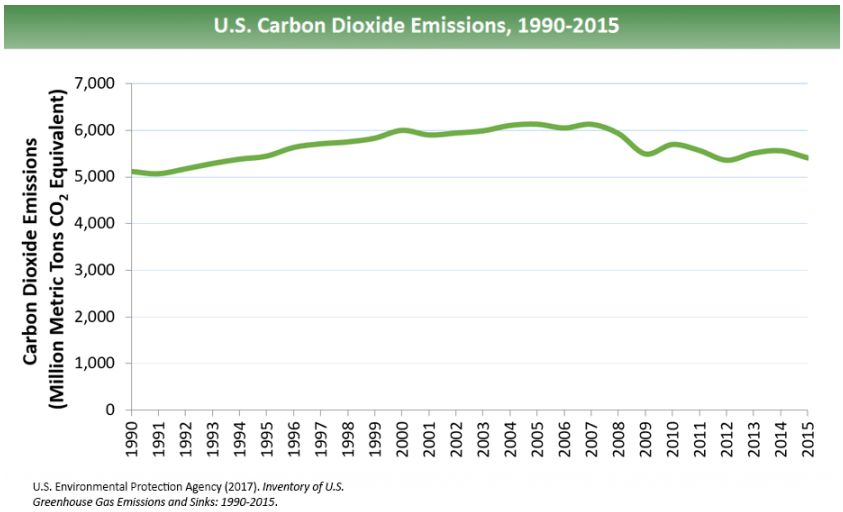

Figure 1.2 Global production of carbon dioxide annually from 1990-2015.(4)

The efficiency of a PEM fuel cell is largely dependent on the materials used and their arrangement in the cell. Fuel cells use an array of different catalysts, electrodes, membranes, and dopants, each of which function under specific operating conditions. Cells that use low-boiling dopants, such as water, operate at approximately 60-80^{o}C to avoid vaporization of the proton-transfer agent. Large heat exchangers are required to ensure the heat generated by the cell does not vaporize the electrolyte. Consequently, system complexity is increased as extra components and controls are required to ensure that the membrane remains hydrated during operation. Moreover, cell operation at such low temperatures allows trace amounts of reformate byproducts, especially carbon monoxide, to bind to the catalyst. These highly-competitive, non-reversible reactions “poison” the catalyst, thereby decreasing and possibly terminating the functionality of the fuel cell. Therefore, low temperature fuel cells require an extremely pure fuel source.

In contrast to low-temperature cells, high-temperature PEMs use high-boiling dopants, such as phosphoric acid and sulfuric acid, and function at temperatures of 120-200^{o}C. Operating at elevated temperatures alleviates the need for excessive heat exchangers and at these temperatures fuel pollutants bind reversibly to the catalyst, which helps to prevent catalyst poisoning. Consequently, high-temperature PEMs can use reformed gases with much higher levels of impurities and lower reformation costs. Furthermore, high temperatures typically improve both the electrode kinetics and operating abilities of the cell. This chapter reports on the chemistries and sustainable usages of PBI-based high temperature PEMFCs.

1.3 History of PBI Membranes.

Polybenzimidazoles (PBIs) are a class of polymers recognized for their excellent thermal and chemical stability. PBI is used in multiple applications including matrix resins, high strength adhesives, thermal and electrical insulating foams, and thermally resistant fibers. PBI fibers were originally synthesized in the early 1960's by a cooperative effort of the United States Air Force Materials Laboratory with Dupont and the Celanese Research Company. One of the first PBIs to be widely investigated was poly(2,2'-*m*-phenylene-5,5'-bibenzimidazole), which is commonly referred to as *m*-PBI (**Figure 1.3**). Because *m*-PBI is non-flammable, resistant to chemicals, physically stable at high temperatures, and can be spun into fibers, this polymer has been used in astronaut space suits, firefighter's turnout coats and suits, and high temperature protective gloves.

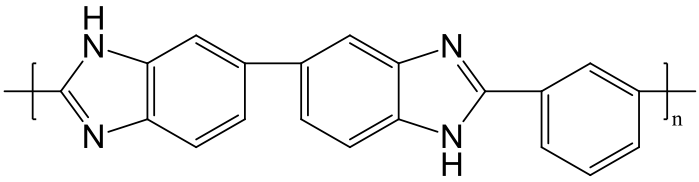

Figure 1.3 Chemical structure of poly(2,2'-*m*-phenylene-5,5'-bibenzimidazole) (*m*-PBI).

Polybenzimidazole membranes are excellent candidates for high-temperature fuel cells because of their thermal and chemical stability and proton conducting ability when properly doped. The stability of PBIs is attributed to its aromatic structure (alternating single and double bonds) and the rigid nature of its bonds.(5) While the membrane structure allows protons to flow from one side to the other, it acts as a barrier to the crossover of gases and electrons. The chemical stability of PBIs allows the membranes to withstand the chemically reactive environments of the anode and cathode. Furthermore, the basic nature of the polymer allows it to be highly doped with phosphoric or sulfuric acid. The dopants interact with the polymer matrix and provide a network through which protons can be transported. These acids are used as electrolytes because of their high conductivity, thermal stability, and enhanced proton-transport capabilities. It is important to note that the proton conductivity of PBI membranes without a dopant is negligible. For liquid phosphoric acid, the proton jump rate is orders of magnitude larger than the diffusion of the phosphoric acid molecule as a whole.(6) Additionally, it has been reported that both protons and phosphate moieties have a substantially decreased diffusion coefficient when blended with basic polymers as opposed to liquid phosphoric acid.(7) Therefore, a heterogeneous, two-phase system in which the PBI membrane is phase-separated and imbibed with phosphoric acid has a higher conductivity than its homogeneous counterpart.(8) More recently, Kreuer et al. demonstrated that the interaction of phosphoric acid and PBI reduces the hydrogen bond

network frustration, which in turn reduces phosphoric acid's very high acidity and hygroscopicity; reducing electroosmotic drag as well. They suggest this to be a reason why, in fuel cells, PBI-phosphoric acid membranes perform better than other phosphoric acid containing electrolytes with higher protonic conductivity.(9) As evidence of the growing attention in this area, a book on high temperature PEM fuel cells has recently been released.(10)

1.4. Synthesis of Polybenzimidazoles

One of the first PBI membranes investigated for fuel cell use was poly(2,2'-*m*-phenylene-5,5'-bibenzimidazole) (*m*-PBI). At the time, there was a vast amount of research previously reported on *m*-PBI and it was renowned for its excellent thermal and mechanical properties.(6) The polymer is synthesized by the reaction of 3,3',4,4'-tetraaminobiphenyl (TAB) with diphenylisophthalate (DPIP) during a melt/solid polymerization (**Scheme 1.1**). The resulting polymer is extracted and has an inherent viscosity (IVs) between 0.5-0.8 dL g^{-1}, which corresponds to a polymer with low to moderate molecular weight. The *m*-PBI is further purified by dissolving it in a solution of N,N-dimethylacetamide and lithium chloride (DMAc/LiCl) under 60-100 psi and 250 ^{o}C and then filtering; this step removes any crosslinked *m*-PBI. The polymer is then cast as a film and dried at 140 ^{o}C under vacuum to evaporate the solvent. The *m*-PBI membrane is washed in boiling water to remove any residual DMAc/LiCl solution trapped in the polymer matrix. After the polymer has been dried, an acid bath is used to dope the membrane; the doping level of the membrane can be partially controlled by varying the concentration of acid in the bath. Originally, this conventionally imbibed process created membranes with molar ratios of phosphoric acid/polymer repeat unit (PA/PRU) approximately 6-10.(11) A "direct acid

casting" (DAC) technique was later developed to allow the PBI membrane to retain more PA.(12) Both the conventional imbibing process and DAC were developed following the research performed by Jean-Claude Lasegues, who was one of the first scientists that investigated basic polymeric acid systems (a summary of his work is reviewed in reference (13)). The DAC technique consists of extracting low molecular weight PBI components from PBI powder, and then dissolving the high molecular weight PBI components in trifluoroacetic acid (TFA). Phosphoric acid is added to the TFA/PBI mixture, which is then cast onto glass plates with a casting blade. One may tune the doping level of the polymer by adjusting the amount of phosphoric acid that is added to the TFA/PBI mixture. However, as one increases the PA doping level of a DAC PBI membrane, its mechanical strength decreases to the point where it can no longer be used in a fuel cell. Modern imbibing processes can increase the PA/PBI ratio to 12-16, and these fuel cell membranes are reported to have proton conductivities as high as 0.08 S cm^{-1} at 150 $^{\circ}$C at various humidities.

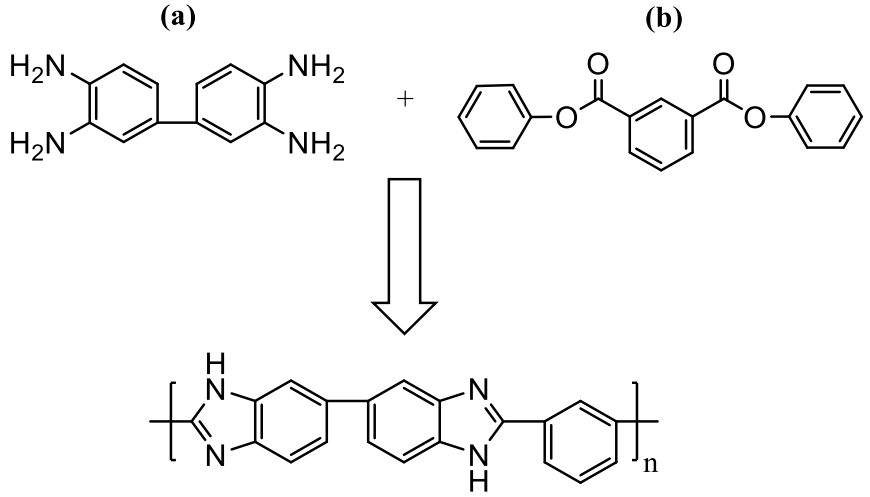

Scheme 1.1 Polymerization of 3,3',4,4'-tetraaminobiphenyl (a) and diphenylisophthalate (b) to form *m*-PBI

A novel synthetic process for producing high molecular weight PBIs, the "PPA Process" was developed at Rensselaer Polytechnic Institute with cooperation from BASF Fuel Cell GmbH. This process has previously been discussed by Xiao *et al*.(14) The general synthesis of PBI by this method requires the combination of a tetraamine with a dicarboxylic acid in polyphosphoric acid (PPA) in a dry environment. The step-growth polycondensation reaction typically occurs ca. 200 °C for 16-24 hours in a nitrogen atmosphere, producing high molecular weight polymer. This solution is cast directly from PPA as a thin film on a substrate, and upon absorption of water, the PPA hydrolyzes *in situ* to form phosphoric acid. Note that PPA is a good solvent for many PBIs while PA is a poor solvent. Under controlled hydrolysis conditions, a mechanically stable PBI gel membrane that is highly doped with phosphoric acid is produced. The multiple physical and chemical transformations that explain the solution-to-gel phase transition are summarized in **Figure 1.4**.

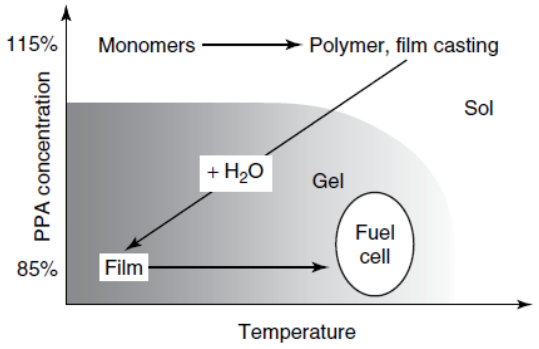

Figure 1.4: State diagram of the PPA Sol-Gel Process.(14)

The PA doped *m*-PBI fuel cell membrane maintains thermal and physical stability while operating at high temperature. To illuminate the fundamental differences in polymer

film architecture, polymers with similar physical characteristics were prepared by the conventional and PPA Process (**Table 1.1**). Even though the ratio of phosphoric acid-to-polymer repeat unit (PA/PRU) achieved by both processes were nearly identical, the PPA Process produces membranes with much higher proton diffusion coefficients and conductivities. One can conclude that the PPA Process creates a membrane with a proton transport architecture superior to that of the conventionally imbibed PBI membrane. The higher proton diffusion coefficients of the membranes produced by the PPA process versus conventionally imbibed membranes were confirmed by NMR.(15) In addition, inherent viscosity data indicates that the PPA Process produces polymers of much higher molecular weight.(14) It was subsequently shown that improved membrane morphology and increased molecular weight allow the polymer to retain much more phosphoric acid than traditionally cast PBI membranes. An increased PA doping level typically improves the conductivity of the membrane and may even increase the performance of the cell.

Table 1.1 Comparison of conventionally imbibed m-PBI vs. m-PBI synthesized from the PPA Process.(16)

IV[a] (dl g^{-1})	Film process	Polymer (wt%)	PA (wt%)	Water (wt%)	PA/PBI (molar ratio)	Proton diffusion coefficient[b] ($cm^2\ s^{-1}$)	Conductivity[c] ($S\ cm^{-1}$)
0.89	Conventionally imbibed	15.6	60.7	23.7	12.2	10^{-7}	0.048
1.49	PPA process	14.4	63.3	22.3	13.8	3×10^{-6}	0.13

[a] Inherent viscosity (IV) was measured at a polymer concentration of 0.2 g dl^{-1} in concentrated sulfuric acid (96%) at 30 °C, using a Canon Ubbelohde viscometer
[b] Estimation of upper bound for conventionally imbibed *m*-PBI at 180 °C; PPA-prepared *m*-PBI measured at 180 °C
[c] Measured at 160 °C after an initial heating to 160 °C to remove water

1.5. Electrochemical Devices

An electrochemical device is a device capable of either generating electrical energy from chemical reactions or using electrical energy to cause chemical reactions; the former

are voltaic or galvanic cells, while the later are electrolytic cells. Electrochemical reactions are as diverse as snowflakes enabling a robust number of applications; this includes the well-known lithium ion battery, to fuel cells, and even now in biological sensors. Of these electrochemical devices, fuel cells, electrochemical hydrogen separations, flow batteries, SO_2 depolarized electrolyzers, and hydrogen batteries will be discussed in further detail as well as the membrane work tailored to each application.

1.5.1. Fuel Cells.

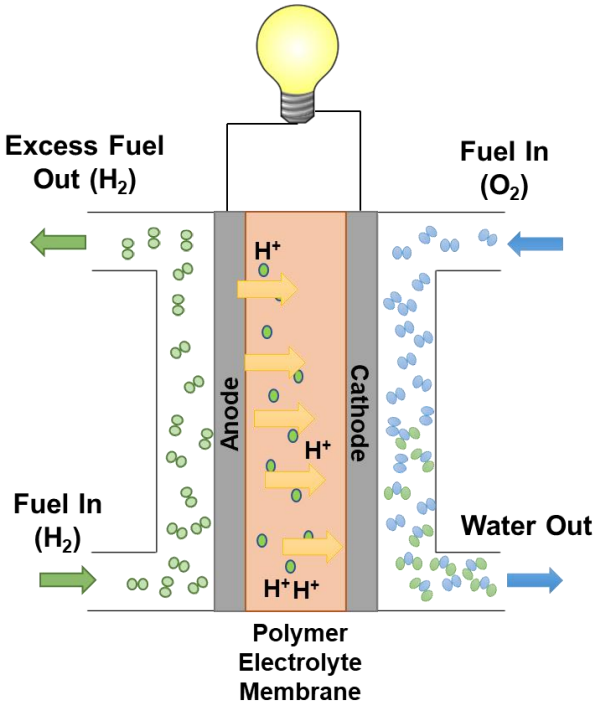

Figure 1.5 Polymer electrolyte membrane fuel cell.

Fuel cells are electrochemical devices that create an electrical energy through a pair of chemical reactions typically involving the oxidation of H_2 and the reduction of oxygen to form water. Hydrogen is flowed through the anode of the device where it is easily split into protons and electrons. The protons are carried through a membrane separator (in the

case of this dissertation, a polymer electrolyte membrane (PEM)) and the electrons flow through an external circuit producing direct current electricity. The protons can then interact with oxygen on the cathode side to generate water and heat, **Figure 1.5**.

1.5.2. Electrochemical Hydrogen Separation

Efficient purification of hydrogen is becoming a common interest in both the industrial and energy sectors. Technology which can efficiently purify, pump, and pressurize hydrogen at low to moderate flow rates is needed, but is not readily available. Of course, there are existing methods for hydrogen purification which include various combinations of mechanical compression with cryogenic cleanup, palladium membranes, pressure swing absorption, and passive membrane separators to name a few. However, these technologies are challenged by certain limitations: 1) cryogenic cleanup produces high purity hydrogen, but requires costly refrigeration equipment and is suitable for very large-scale specialty applications; 2) palladium membrane purification can be fairly simple in design and construction, but requires pressurization to drive the hydrogen separation process and suffers from poor utilization when purifying hydrogen from gases containing low fractions of hydrogen; 3) pressure swing absorption (PSA) is widely used in high volume industrial processes and relies on large, mechanical components that are subject to frequent maintenance and inherent inefficiency. Such devices are not easily scaled to smaller sizes or localized generation/purification needs. Furthermore, it is important to state that all of the above processes require expensive, high maintenance, compressors.

Electrochemical hydrogen separation, or H_2 pumping, is not a new concept and has in fact been utilized as a diagnostic technique within the electrochemical industry for years. General Electric developed this concept in the early 1970's.(17)

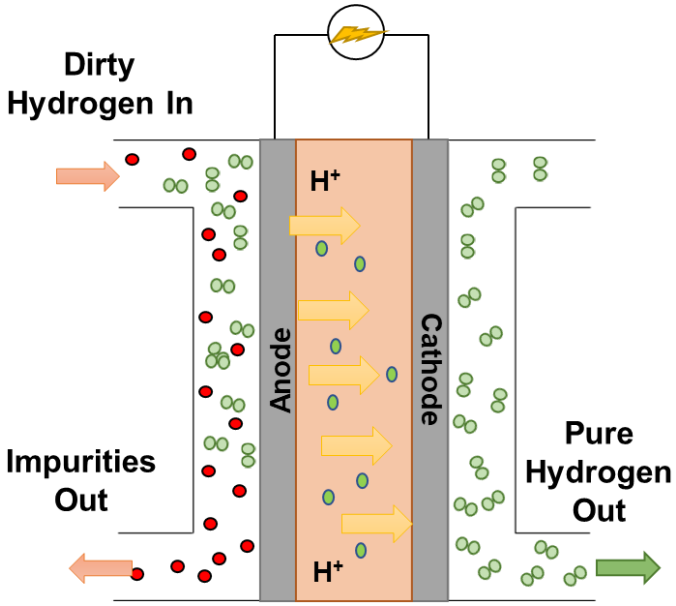

Figure 1.6 Polymer electrolyte membrane used for hydrogen electrolysis

The use of polymer electrolyte membranes for electrochemical hydrogen compression has been demonstrated in water electrolysis (H_2 generation) devices at United Technologies Corporation, reaching 3000 psi_a (18), as well as studied in academic institutions.(19) The electrochemical hydrogen pump, first developed in the 1960's and 1970's, was derived from the original proton exchange membrane fuel cell efforts. The concept is simple, requires little power, and has been shown to pump hydrogen to high pressures. In the original work, the membrane transport medium was a perfluorosulfonic acid (PFSA) material, similar to the material used in many fuel cells today.

The process is quite elegant in that, like a fuel cell, molecular hydrogen enters the anode compartment, is oxidized to protons and electrons at the catalyst, and then the protons are driven through the membrane while the electrons are driven through the electrically conductive elements of the cell, **Figure 1.6**.

The major difference in this cell as compared to a fuel cell is that the pump is operated in an electrolytic mode, not galvanic, meaning that power is required to "drive" the proton movement. Once the protons emerge from the membrane at the cathode, they recombine with electrons to form molecular hydrogen. Thus, hydrogen can be pumped and purified in a single step with a non-mechanical device. The pump concept builds upon the understanding of proton transport membranes. The overall chemical reaction is described by Equation 1:

Equation 1:

$$Anode: H_2 \rightarrow 2H^+ + 2e^+$$

$$Cathode: 2H^+ + 2e^- \rightarrow H_2$$

$$Total\ Reaction: H_2(anode) \rightarrow H_2(cathode)$$

The cell voltage between the anode and cathode can then be described by Equation 2. The Nernst potential, E_{Nernst}, is given by the Nernst Equation 3, where $E^{\circ}$is the standard potential of a hydrogen reaction, R is the gas constant, T is the temperature in Kelvin, F is Faraday's constant, and p_{cathode} and p_{andode} are the partial pressures of hydrogen at the anode and cathode respectively.

Equation 2:

$$E = E_{Nernst} - E_{polarization} - E_{ohmic}$$

Equation 3:

$$E_{Nernst} = E° - \frac{RT}{2F} \ln \frac{p_{cathode}}{p_{anode}}$$

$E_{polarization}$ is the polarization overpotential which is the sum of the polarization overpotentials at the anode and cathode. This can be described using the Butler-Volmer equation. The polarization overpotential can be approximated at low overpotentials, Equation 4, where R is the gas constant, T is the temperature in Kelvin, F is Faraday's constant, i is the current density, and i_0 is the exchange current density.

Equation 4:

$$E_{polarization} = \frac{RTi}{2Fi_0}$$

Clearly, the proton conducting membrane properties are critical. Desirable properties include: high proton conductivity, mechanical stability, low solubility and permeability of impurity gases, and sufficient operating temperature to support tolerance to impurities (CO and H_2S) found in reformed gases. The application of the PBI membrane to electrochemical hydrogen pumping provides high proton conductivity (0.2 – 0.4 S/cm), mechanical stability, enhanced gas separation, and up to 180 °C operation. The high operating temperature eliminates water management difficulties typically experienced with the low operating temperatures of PFSA membranes while also providing tolerance to poisonous gas species such as CO. This is a crucial quality in electrochemical hydrogen pumping as many of the common impurities being removed from the feed stream are

known to poison the catalyst. As such, the PBI membrane and electrode assembly represents a significant new opportunity and paradigm shift in electrochemical hydrogen pumps as well as in advancing the science of hydrogen separation, purification, and pressurization. This concept has been evaluated and demonstrated in recent work using PBI membranes.(20) The hydrogen pump was shown to operate with fairly low power requirements, and generally needed less than 100 mV when operating at 0.2-0.4 A/cm^2. This was accomplished without the critical water management commonly encountered in low temperature, water-based membranes. The cathodic flow of hydrogen from the device was nearly identical to the theoretical Faradic flows. This suggests that the hydrogen pump could have applications as a hydrogen metering device since the hydrogen flow could be easily and accurately controlled by the current of the power source. The initial work reported devices that could operate for several thousand hours with little change in the operating parameters. This would be expected from the related work on PBI membranes for fuel cells which show outstanding long-term durability. In fuel cell applications, the ability to operate at high temperatures provides benefits for gas cleanup and durability on reformed fuels. In hydrogen pump applications, this tolerance to fuel impurities enables the hydrogen pump to purify hydrogen from hydrogen gas feeds containing such impurities. **Figure 1.7** shows the operation of a PBI-based hydrogen pump operating on pure hydrogen, as well as two different synthetic reformates. The flow rates are nearly unaffected by the composition of the gas feed at the various operating conditions (the data points are superimposed for the different gases). The data demonstrates that the pump was capable of operating at high CO levels (1% in this work) and extracting hydrogen from dilute feed streams (<40% hydrogen). Additionally, the hydrogen pump was capable of

producing hydrogen with purities greater than 99%, with the final purity dependent on operating conditions. This device could play a prominent role for both the current industrial hydrogen users, as well as in a future economy that is more heavily reliant on hydrogen as an energy carrier. Commercial development of this device is underway.

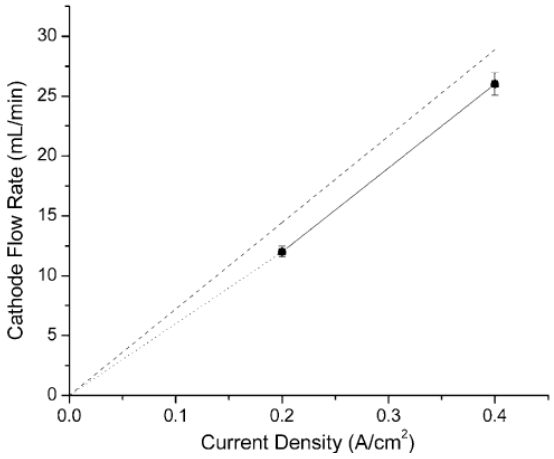

Figure 1.7 The cathodic flow rates of a hydrogen pump operated at 160 ^{O}C and 0% relative humidity and fueled by pure hydrogen (unfilled squares), a reformate gas comprised of 35.8% H_2, 11.9% CO_2, 1906 ppm CO, and 52.11% N_2 (filled circles), and a reformate gas comprised of 69.17% H_2, 29.8% CO_2, and 1.03% CO (filled triangles). The values are nearly identical, and thus, the symbols appear superimposed. The dotted line represents the theoretical flow rate at 100% efficiency.(20)

1.5.3. Flow Batteries

Flow batteries are a type of rechargeable battery that utilize chemical reactions of compounds dissolved in an electrolyte. Two sets of reactants are stored in opposite reservoirs usually separated by a membrane that allows the transfer of some species that facilitates the reaction, in most cases this is a proton. As the battery charges, the compounds in one reservoir oxidizes and the other reduces, storing electrons. Upon discharge the opposite reactions occur spontaneously if the circuitry allows. To be more precise, during discharge the anode side of the battery is at a high chemical potential state. The compounds

in the negative electrolyte can undergo a spontaneous oxidation where the electron is moved through an external circuit and do useful work. The electron finally makes it way to the cathode where it is accepted in a reduction reaction of the compounds in the positive electrolyte. The chemistry of the active redox species in the electrolytes determine the total potential energy battery.

The amount of energy that can be stored in a flow battery is directly related to the amount of redox active species that are available in the electrolyte and thus the volume of electrolyte that is held in the storage tanks. Since adding additional electrolyte storage tanks (or making them larger) is relatively easy, flow batteries are advantageous for large scale energy storage.

Flow battery technology is much like conventional batteries with one major fundamental difference; how the energy is stored. Flow batteries store energy in the electrolyte that flows through the system, whereas, the energy is typically stored in the electrode material for a conventional battery.

1.5.4. The Hybrid Sulfur Cycle (SO_2 Depolarized Electrolyzers)

More recently, the hybrid sulfur thermochemical cycle has drawn a great amount of attention due to its potential to provide clean hydrogen on a large scale using considerably less energy than water electrolysis. The hybrid sulfur (HyS) process contains two steps: [1] a high temperature decomposition of sulfuric acid to produce sulfur dioxide, oxygen, and water and [2] a low temperature electrochemical oxidation of sulfur dioxide in the presence of water to form sulfuric acid and gaseous hydrogen. The entire process recycles sulfur compounds which leaves a net reaction of splitting water into hydrogen and

oxygen. Herein we describe advancements in the low temperature sulfur oxidation step that could be coupled with next generation solar power plants or high temperature nuclear reactors.(21, 22)

Since the HyS process involves the transfer of protons it is not surprising that proton exchange membranes (PEMs) are the most investigated materials. Historically, Nafion has been usually the most widely studied due to its availability. Nafion's performance in the HyS electrolyzer has been thoroughly examined with the prediction of mass transport through the membrane as a function of operating potential and other design variables. Nafion does, however, have many drawbacks including the inability to operate at elevated temperatures (above 100 °C) and since water is needed for its conductivity, there is decreased performance at high acid concentrations or low water concentrations.(22)

Polybenzimidazole (PBI) membranes are high temperature PEMs that are imbibed with acid as its electrolyte. We have shown that PBI membranes are a good alternative to Nafion in fuel cells and offer a solution to the HyS process as an avenue to higher temperature operation, which minimizes voltage losses, as well as the ability to perform under high acid concentration conditions that allow for reduced energy demands necessary for water separation.(23-28) Weidner *et al.* show the successful operation of the HyS electrolyzer using sulfuric acid doped PBI membranes and have determined that the area-specific resistance of sulfonated PBI (s-PBI) compares favorably with Nafion, yet is not adversely affected by concentrated sulfuric acid conditions within the electrolyzer. Importantly, the PBI based cell could be operated at low pressures and without significant water dilution of the sulfuric acid produced. Additionally, a model for high temperature and high-pressure operation of the s-PBI membrane in the electrolyzer has been

constructed allowing for further analysis of the system to determine operating conditions for economically viable operation.(22, 29)

As new devices emerge and old ones are being rejuvenated, requiring a distinct set of operating conditions and fundamental necessities, a handle for adaptable material synthesis is needed. Polybenzimidazole is a versatile, stable polymer holding exceptional inherent properties and the capability of finely tuning those properties, both directly (polymer synthesis) and indirectly (membrane processing techniques), for different applications. The bulk of this dissertation is focused on studying the structure/property (transport, chemical and mechanical stability, etc.) relationships of PBI gel membranes in an effort to design and synthesize new materials for optimal performance in various electrochemical devices.

1.6 References.

1. EIA, International Energy Outlook 2016, in, U.S. Energy Information Administration (2016).
2. EIA, Annual Energy Review 2008, in, U.S. Energy Information Administration (2009).
3. EIA, Emissions of Greenhouse Gases in the United States 2009, in, U.S. Energy Information Administration (2011).
4. EPA, Overview of Greenhouse Gases: Carbon Dioxide Emissions, in, U.S. Environmental Protection Agency, U.S. Environmental Protection Agency (2017).
5. J. Wainright, J. Wang, D. Weng, R. Savinell and M. Litt, *J. Electrochem. Soc.*, **142**, L121 (1995).
6. T. Dippel, K. D. Kreuer, J. C. Lassègues and D. Rodriguez, *Solid State Ionics*, **61**, 41 (1993).
7. A. Bozkurt, M. Ise, K. D. Kreuer, W. H. Meyer and G. Wegner, *Solid State Ionics*, **125**, 225 (1999).
8. J. Weber, K.-D. Kreuer, J. Maier and A. Thomas, *Advanced Materials*, **20**, 2595 (2008).
9. J. P. Melchior, G. Majer and K. D. Kreuer, *Physical Chemistry Chemical Physics*, **19**, 601 (2017).
10. Q. li, D. Aili, H. A. Hjuler and J. O. Jensen, *High Temperature Polymer Electrolyte Membrane Fuel Cells*, Springer International Publishing Switzerland (2016).
11. J. Mader, L. Xiao, T. Schmidt and B. C. Benicewicz, *Adv. Polym. Sci.*, **216**, 63 (2008).
12. J. S. Wainright, R. F. Savinell and M. H. Litt, *Fuel Cell Handbook* (2003).
13. P. Colomban, *Proton conductors: solids, membranes, and gels - materials and devices*, Cambridge University Press, Cambridge (1992).
14. L. Xiao, H. Zhang, E. Scanlon, L. S. Ramanthan, E. W. Choe, D. Rogers, T. Apple and B. C. Benicewicz, *Chem. Mater.*, **17**, 5328 (2005).
15. J. R. P. Jayakody, S. H. Chung, L. Durantino, H. Zhang, L. Xiao, B. C. Benicewicz and S. G. Greenbaum, *Journal of The Electrochemical Society*, **154**, B242 (2007).
16. D. C. Seel, B. C. Benicewicz, L. Xiao and T. J. Schmidt, *Handbook of Fuel Cells*, **5**, 300 (2009).
17. H. J. R. Maget, Process for Gas Purification, U.S. Patent 3489670, in (Jan. 13,1970).
18. J. F. McElroy, in *Energy Conversion Engineering Conference*, p. 1631, Proceedings of the 24th Intersociety, Washington, DC, USA (Aug. 1989).
19. B. Rohland, K. Eberle, R. Strobel, J. Scholta and J. Garche, *Electrochem. Acta.*, **43**, 3841 (1998).
20. K. A. Perry, G. A. Eisman and B. C. Benicewicz, *J. Power Sources*, **177**, 478 (2008).
21. C. Corgnale, S. Shimpalee, M. B. Gorensek, P. Satjaritanun, J. W. Weidner and W. A. Summers, *International Journal of Hydrogen Energy* (2017).

22. J. W. Weidner, *Journal of Applied Electrochemistry*, **46**, 829 (2016).
23. M. B. Gorensek, J. A. Staser, T. G. Stanford and J. W. Weidner, *International Journal of Hydrogen Energy*, **34**, 6089 (2009).
24. J. Staser, R. P. Ramasamy, P. Sivasubramanian and J. W. Weidner, *Electrochemical and Solid State Letters*, **10**, E17 (2007).
25. J. A. Staser, M. B. Gorensek and J. W. Weidner, *Journal of the Electrochemical Society*, **157**, B952 (2010).
26. J. A. Staser, K. Norman, C. H. Fujimoto, M. A. Hickner and J. W. Weidner, *Journal of the Electrochemical Society*, **156**, B842 (2009).
27. J. A. Staser and J. W. Weidner, *Journal of the Electrochemical Society*, **156**, B16 (2009).
28. J. A. Staser and J. W. Weidner, *Journal of the Electrochemical Society*, **156**, B836 (2009).
29. T. R. Garrick, A. Gulledge, J. A. Staser, B. Benicewicz and J. W. Weidner, *ECS Transactions*, **66**, 31 (2015).

CHAPTER 2

DURABLE HIGH POLYMER CONTENT M/P-PBI POLYBENZIMIDAZOLE

MEMBRANES FOR EXTENDED LIFE-TIME ELECTROCHEMICAL DEVICES

2.1 Abstract.

A series of high polymer content phosphoric acid doped meta/para (*m*/*p*) polybenzimidazole (PBI) copolymer membranes were prepared via the Polyphosphoric acid (PPA) Process. These copolymer membranes showed much higher solubility in solution compared to the homopolymer *para*-PBI which translated to higher polymer solids content in the PPA processed doped membranes. The synergistic approach of increasing the solubility of the polymer via copolymer design and utilizing the unique gel membrane structure afforded from the PPA process allowed for the preparation of membranes with high proton conductivities and high creep resistance that can be used in electrochemical devices requiring long operational life-times with low voltage decay.

2.2 Introduction.

Phosphoric acid (PA) doped polybenzimidazole (PBI) membranes have long been studied as high temperature polymer electrolyte membranes (HT-PEMs) and considerable progress has been made in the past 10 years. Throughout this time many members of the PBI family were extensively investigated for use in high temperature polymer electrolyte membrane fuel cells (HT-PEMFCs), which include *meta*-PBI,(1) *para*-PBI,(2) AB-PBIs,(3, 4) partially fluorinated PBIs,(5, 6) hydroxylated PBIs,(7) sulfonated PBIs,(8) pyridine PBIs,(9-11) and their copolymers. Compared to low temperature polymer electrolyte membranes (LT-PEMs) based on perfluorosulfonic acid (PFSA) ionomers, such as Dupont's Nafion®, PA doped PBI membranes have high proton conductivity at high operational temperatures (up to 200 °C), low reactant permeability, high fuel impurity tolerance, excellent oxidative and thermal stability, and nearly zero electroosmotic drag coefficient(12-17) that are useful in multiple device applications. In this operational

temperature range (120 - 200 °C) heat and water management is greatly simplified. Additionally, the reaction kinetics of the catalysts on the electrode increase with increasing temperature, which opens the possibility of using cheaper catalyst materials to replace the expensive platinum (Pt) electrode catalyst typically used in fuel cells.(18) Moreover, due to the high temperature stability and strong acid resistance of the PBI family of polymers, they have been found to be good candidates for a variety of electrochemical devices other than fuel cells; e.g., electrochemical hydrogen pumps and electrolyzers for the hybrid sulfur cycle.(19-21)

Traditionally, PA doped PBI membranes are prepared from *meta*-PBI polymer produced from a two-step melt-solid polymerization. The produced polymer powders are dissolved in a polar aprotic solvent, such as N,N'-dimethylacetamide (DMAc) at high temperatures. The solution is filtered to remove undissolved parts. The solution is then cast and the solvent evaporated to obtain a dry membrane. Finally, the dry membranes are soaked in phosphoric acid to prepare the doped film. This time consuming, costly, environmentally unfriendly, multi-step process is referred to as the "conventional imbibing process."(22) To mitigate the issues with this technique Xiao et al. developed the novel "PPA Process" to prepare phosphoric acid doped PBI membranes.(2) This is a one-pot polymerization of tetraamines and diacids (and optionally AB monomers) in polyphosphoric acid (PPA) where the formed PBI/PPA solution can be directly cast and exposed to atmospheric moisture or controlled humidity conditions to hydrolyze the PPA, a good solvent for PBI, to phosphoric acid (PA), a poor solvent for PBI. The hydrolysis process is usually conducted at room temperature. The coupling of these factors induces a state transition from solution to gel. The PPA Process is a simpler, less costly, and time-

effective alternative process over the conventional imbibing method that also produces membranes with high proton conductivities due to the high phosphoric acid doping levels. Poly(2,2'-(1,4-phenylene)5,5'-bibenzimidazole) (*para*-PBI) membranes prepared by the PPA process have high proton conductivities (>0.25 S/cm at 160 °C), which is attributed to their high phosphoric acid doping level (>20 PA/PBI repeat unit). Excellent fuel cell performances have also been demonstrated with these PA doped *para*-PBI membranes – greater than 0.65 V at 0.2 A/cm^2 for hydrogen and air at 160 °C and lifetimes of at least 2 years under steady-state conditions.(2, 23)

When considering PA doped PBI membranes prepared via the conventional imbibing process, a trade-off between two key properties of the membrane is realized, i.e., proton conductivity and mechanical properties. For example, to obtain a high proton conducting membrane PA doping levels must be high, however, this leads to lower mechanical properties of the membrane. The "practical" phosphoric acid doping level of a conventionally imbibed membrane is ~6-10 moles of PA/PBI r.u. and the resulting membrane (at ~6PA/PBI r.u.) exhibited 11 MPa Young's modulus, however the proton conductivity was only 0.04-0.06 S/cm. With doping levels greater than 6 PA/PBI r.u., the membranes become very soft and mechanical properties of the resulting membranes quickly dropped to levels too low to fabricate a membrane electrode assembly.(22)

More recently, Chen et al. conducted a thorough study characterizing the creep compliance of a multitude of PA doped PBI membrane chemistries. The creep compliance of high temperature PEMs is a relatively new aspect of characterizing films for long-term durability, as creep deformation was identified as the likely primary failure mode of PBI membranes prepared through the PPA Process. Their work showed a strong correlation

between the membranes final polymer content and its resistance to creep. For example, *para*-PBI membranes prepared via the PPA route have high PA doping levels (>20 PA/PBI r.u.) and a polymer content of just 4-5 wt %. The membrane mechanical properties were evaluated and showed a Young's modulus of ~2 MPa, and creep compliance (J_s^0) values of ~9.0x10^6 Pa^{-1} from dynamic mechanical analysis. Furthermore, a direct correlation was found for *para*-PBI membranes where an increase in final polymer solids decreased creep deformation. A similar trend was also found for the *meta*-PBI family of polymer membranes, however, the more flexible chain linkage reduced the overall efficacy of polymer solids to lower creep compliance.(24)

Herein, we investigate a novel series of *meta*/*para*-PBI random copolymer membranes synthesized via the PPA Process. Introducing the more soluble *meta*-PBI repeat unit into the less soluble *para*-PBI, in PPA, resulted in more concentrated copolymer/PPA solutions having processable viscosities and producing membranes with much higher polymer content. Membrane properties, i.e., proton conductivity, mechanical properties and creep resistance of these PA doped *meta*/*para*-PBI copolymer gel membranes were explored and compared to *meta*-PBI membranes prepared via the conventional imbibing process and *para*-PBI membranes prepared by the PPA Process. The new membranes were also tested in different electrochemical devices such as high temperature PEM fuel cells and electrochemical hydrogen pumps.

2.3 Experimental.

2.3.1 Materials.

3,3',4,4'-Tetraaminobiphenyl (TAB, polymer grade, ~97.5%) was donated by BASF Fuel Cell, Inc. and used as received. Isophthalic acid (IPA, >99% purity) and

terephthalic acid (TPA, >99% purity) were purchased from Amoco and used as received. Polyphosphoric acid (115%) was supplied from FMC Corporation and used as received. Reformate test gas (30% H_2, 3% CO, 67% N_2 – mol %) was mixed by AirGas and used as received.

2.3.2 Polymer synthesis and membrane fabrication.

A typical polymerization consisted of 64.28 g tetraaminobiphenyl (TAB, 300 mmol), 43.62 g isophthalic acid (IPA, 262.5 mmol), and 6.23g terephthalic acid (TPA, 37.5 mmol) added to 1050 g polyphosphoric acid, mixed with an overhead stirrer and purged with dry nitrogen. The contents were heated in a high temperature silicone oil bath, and the temperature was controlled by a programmable temperature controller with ramp and soak features. In a typical polymerization, the final reaction temperature was approximately 195 °C and held for 12 hours. Once the reaction was completed, determined by visual inspection of viscosity, the polymer solution was cast onto clear glass plates using a doctor blade with a controlled gate thickness of 15 mils. The cast solution was hydrolyzed into membranes in a humidity chamber regulated to 55% R.H. at 25 °C.

2.3.3 Membrane composition.

The composition of phosphoric acid-doped PBI membranes was determined by measuring the relative amounts of polymer solids, water, and acid in the membranes. The phosphoric acid (PA) content of a membrane was determined by titrating a membrane sample with standardized sodium hydroxide solution (0.10 M) using a Metrohm 716 DMS Titrino autotitrator. Once titrated, the sample was thoroughly washed with DI water and dried at reduced pressures at 120 °C overnight. The dried sample was then weighed to determine the polymer solids content of the membrane.

Using **equations 1 and 2**, the polymer weight percentage and phosphoric acid weight percentage can be determined, respectively;

$$Polymer\ w/w\ \% = \frac{W_{dry}}{W_{sample}} \cdot 100 \qquad (1)$$

$$Acid\ w/w\ \% = \frac{M_{acid} \cdot V_{NaOH} \cdot c_{NaOH}}{W_{sample}} \qquad (2)$$

where W_{sample} is the weight of the sample before titration, W_{dry} is the weight of final dried sample after titration, M_{acid} is the molecular weight of phosphoric acid, and V_{NaOH} and c_{NaOH} are the volume and concentration of the sodium hydroxide solution required to neutralize the phosphoric acid to the first equivalence point.

The number of moles of phosphoric acid per mole of PBI repeat unit (or the PA doping levels, X) were calculated from the equation:

$$X = \frac{V_{NaOH} \cdot c_{NaOH}}{W_{dry} \Big/ M_{polymer}} \qquad (3)$$

where V_{NaOH} and c_{NaOH} are the volume and concentration of the sodium hydroxide solution required to neutralize the phosphoric acid to the first equivalence point, W_{dry} is the final weight of the dried sample after titration, and $M_{polymer}$ is the molecular weight of the polymer repeat unit.

2.3.4 Tensile properties.

The tensile properties of the membranes were tested at room temperature using an Instron Model 5543A system with a 10 N Load cell and crosshead speed of 5 mm/min. Dog-bone shaped specimens were cut according to ASTM standard D683 (Type V specimens) and preloaded to 0.1 N prior to testing.

2.3.5 Compression creep and creep recovery experiment.

The compression creep and creep recovery method was used to study the time-dependent creep behavior of the prepared membranes in a TA RSA III dynamic mechanical analyzer using its built-in functionality for creep testing. A typical experiment consisted of a 20-hour creep phase followed by a 3-hour recovery phase. During the creep phase, a constant compressive force equivalent to a stress level of 0.1 MPa was applied, and this force was removed at the start of the recovery phase. All experiments were carried out at 180 ± 0.5 °C in a temperature-controlled oven with dry air circulation. The creep test was repeated 2-4 times for each gel membrane.

2.3.6 Proton conductivity.

Proton conductivities of the membrane were measured by a four-probe electrochemical impedance spectroscopy method using a Zahner IM6e electrochemical workstation over the frequency range from 1 Hz to 100 kHz with an amplitude of 5 mV. A two-component model with an ohmic resistance in parallel with a capacitor was employed to fit the experimental data. The conductivities of the membrane at different temperatures were calculated from the membrane resistance obtained from the model simulation with the following equation:

$$\sigma = \frac{d}{l \cdot w \cdot R_m} \qquad (4)$$

Where d is the distance between the two inner probes, l is the thickness of the membrane, w is the width of the membrane, and R_m is the ohmic resistance determined by the model fitting. Membrane samples underwent two heating ramps to 180 °C. Conductivity data reported was recorded on the second heat ramp, after water was removed from the membrane during the first heating cycle.

2.3.7 Membrane electrode assembly (MEA) preparation and fuel cell testing

The gas diffusion electrodes (GDE, acquired from BASF Fuel Cell, Inc) with a platinum loading of 1.0 mg/cm^2 were used for this study. Where applicable, the GDE was treated with a fluorinated PBI solution. The MEA was fabricated by hot pressing a piece of membrane between two Kapton framed electrodes. MEAs were then assembled into single cell fuel cell test equipment. The gas flow plates used were constructed from graphite with triple serpentine gas channels. Stainless steel end plates with attached heaters were used to clamp the graphite flow plates. A commercial fuel cell testing station (Fuel Cell Technology, Inc.) was used for cell testing. The instrument was controlled by home-programmed LabView software (National Instruments, Austin, TX). Fuel cell testing was conducted on 50 cm^2 cells and electrochemical hydrogen pumping tests were conducted on 10 cm^2 cells.

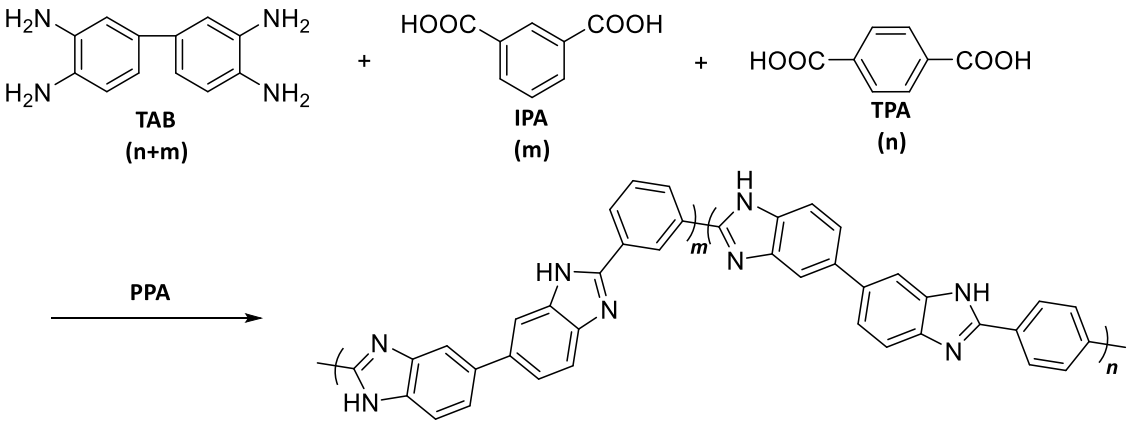

Scheme 2.1. Synthesis of *meta*/*para*-PBI in PPA. Detailed polymerization conditions are provided in Table 1.

2.4 Results and Discussion.

2.4.1 Polymer synthesis and membrane fabrication.

The *meta*/*para*-PBI copolymers and membranes were prepared via the PPA process, as shown in **Scheme 1**. *Para*-PBI membranes prepared by the PPA Process typically have only 4-5 wt% polymer content. Our group has previously shown that low polymer content leads to limiting creep and creep compliance properties of polymer gel membranes.(24) Two different techniques were attempted to increase final membrane solids; (1) directly increasing monomer charge in the polymerization and by adding pre-formed *para*-PBI polymer powder to the polymerization during its later stages. However, these techniques limited processability of the PBI/PPA solution due to the low solubility of *para*-PBI in PPA and to the high viscosities of the final polymer solution. The upper limit of processability for hand casting *para*-PBI/PPA solutions was 2.8 wt% *para*-PBI content (3.5 wt% of monomer charge). By introducing a more soluble *meta*-PBI repeat unit

into the polymer backbone, higher monomer charges up to 10 wt% (or 8 wt% of polymer in the PBI/PPA casting solution) could be polymerized without any evidence of early polymer precipitation. These PBI/PPA solutions retained suitable viscosities to process into films, thus producing high polymer content phosphoric acid doped PBI membranes. The monomer ratio was also used to adjust the viscosity of the PBI/PPA casting solution with identical monomer or polymer wt% charges. For the same polymer content in the casting solution, the viscosity of the PBI/PPA casting solution decreased with increasing *meta*-PBI content in the copolymer. However, this was ultimately limited by the upper solubility limit of the composition. As shown in Table 1, at 50% para content, the maximum monomer concentration achieved was 7 wt%, and this composition had to be cast prematurely (i.e., at low IV) to avoid precipitation or solidification of the polymerization solution.

Table 2.1. Polymer solution characteristics and membrane composition

Monomer charge wt% (Molar Ratio meta:para)	Polymer wt% in casting solution	I.V. (dL/g)	Polymer wt% in the membranes	PA wt% in the membranes	PA/PBI r.u.
7(5:1)	5.6	2.45	14.9	54.3	12
7(5:2)	5.6	2.78	14.0	54.4	12
7(1:1)	5.6	1.60	10.8	66.8	19.5
10(7:1)	8.0	3.67	17.5	52.6	9.5
10(4:1)	8.0	3.77	17.3	51.7	9.4
p-PBI	1.6	3-5	5.0	56.6	30
m-PBI	6.8	1.8	10	65	20.4

The inherent viscosities of all *meta*/*para*-PBI polymers that did not exhibit early solidification during the polymerization were above 2.0 dL/g, similar to *para*-PBI polymers prepared via the PPA Process, and higher than *meta*-PBI polymers used for the conventionally imbibed PBI membranes (typically 0.6-0.8 dL/g). Generally, these inherent viscosities indicate that the synthesized copolymers achieved high molecular weights.

2.4.2 Membrane characterization.

The proton conductivities of PA doped *meta*/*para*-PBI and *para*-PBI membranes made by the PPA Process are shown in **Figure 2.1**. The *para*-PBI membranes prepared by the PPA process had high phosphoric acid doping levels (~30 PA/PBI r.u.), engendering the high measured proton conductivities of approximately 0.30 S/cm at 180 °C. However, even with relatively low PA doping levels, 12 and 10 PA/PBI r.u., the *meta*/*para*-PBI copolymers still had relatively high conductivities ranging from 0.26 to 0.17 S/cm at 180 °C, respectively. The measured high proton conductivities for these membranes is consistent with previously reported comparisons between conventionally imbibed and PPA processed membranes.(22)

Typically, the mechanical properties for *para*-PBI membranes with acid loadings of 25-30 PA/PBI r.u. (< 5 wt% *para*-PBI) are 2 MPa tensile strength and 0.5 MPa Young's modulus. The phosphoric acid doping levels of the *meta*/*para*-PBI membranes were approximately 10 PA/PBI r.u., considerably lower than the *para*-PBI membranes, resulting in stronger membranes (7 MPa tensile strength and 11 MPa Young's modulus) and were similar to the membranes prepared by the conventionally imbibed process.(13, 22, 25)

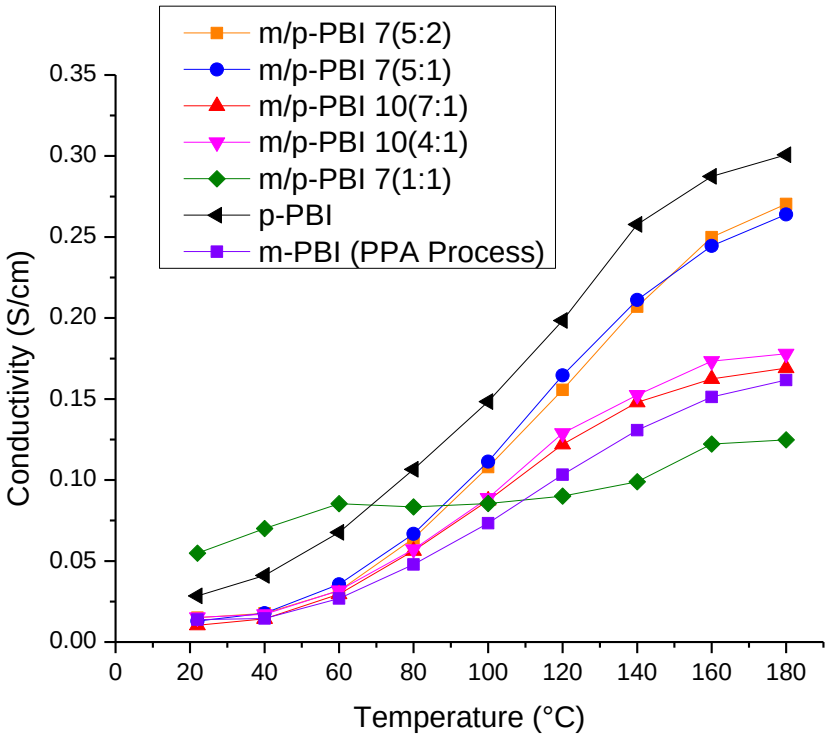

Figure 2.1 Proton conductivities of the *meta*/*para*-PBI copolymer membranes made from different monomer ratios and charges. Both *para*-PBI and *meta*-PBI are included for reference.

Figure 2.2 shows the high temperature creep properties of the high solids content *meta*/*para*-PBI, *meta*-PBI and *para*-PBI membranes. When considering the critical membrane creep properties, both the steady-state recoverable compliance, J_s^0 (creep compliance extrapolated to t = 0) and creep rate, dJ/dt, indicate that the high solids membranes are more mechanically durable materials under compressive loads. The improved mechanical properties are likely due to the combined effects of the higher polymer content in the membrane, high molecular weights of the copolymer and the copolymer composition.

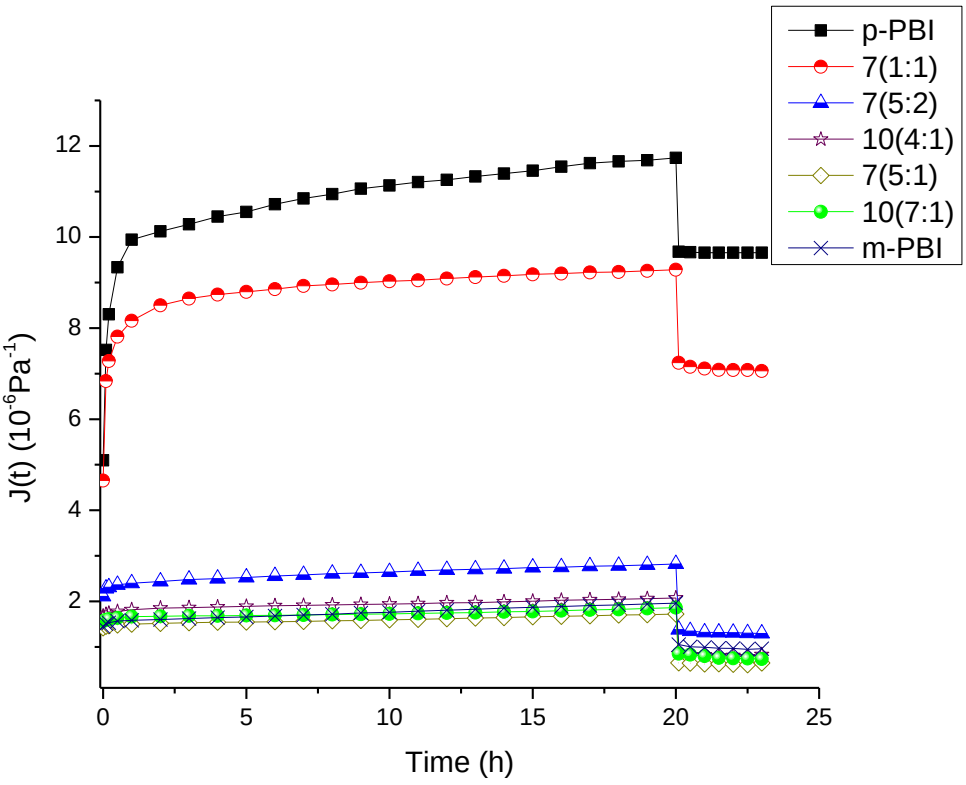

Figure 2.2 Creep deformation of *meta/para* PBI copolymers compared to *para*- and *meta*-PBI homopolymers. Membranes were conditioned for 24 hours at 180 °C. Strain was recorded under a static compression load for 20 hours at 180 °C.

2.4.3 Fuel cell performance.

Meta/*para*-PBI synthesized at 10 wt% monomer charge with a 7:1 ratio of *meta*:*para* isomers was selected for further studies due to its high mechanical properties and proton conductivity. The membrane was constructed into a membrane electrode assembly (MEA) by first dipping into an 85 % phosphoric acid bath for less than 30 seconds and then hot pressing between two Pt/C electrodes with 1 mg/cm^2 Pt loading on the anode and 1 mg/cm^2 Pt alloy loading on the cathode (BASF Fuel Cell, Inc.). The short-term acid dipping of the membrane into acid was conducted to wet the membrane surface and reduce

interfacial resistances between the membrane and electrodes. The MEA was assembled into a single cell fuel cell and tested at 180 °C with hydrogen and air or oxygen at 1.2 and 2.0 stoichiometric flows, respectively. The gases were supplied at atmospheric pressure and dry (without external humidification). **Figure 2.3** shows the polarization curves for the high solids membrane with both H_2/air and H_2/oxygen, which are slightly lower than *para*-PBI and consistent with the slightly lower conductivity. At 0.2 A/cm^2 using H_2/air (1.2/2.0 stoichiometries), the potential was 0.676 V and using H_2/O_2 (1.2/2.0 stoichiometries) the potential was 0.758 V. At approximately 0.6 A/cm^2 the high solids membrane MEA exhibited mass transfer losses. However, very little optimization of MEA pressing conditions has been conducted for these new membranes compared to the extensive development for *para*-PBI based MEAs.

Long-term steady-state durability tests were performed on a membrane with the same selected copolymer ratio and monomer charge (10 wt% monomer charge at 7:1 *meta*:*para*). The test was performed at 160 °C, 0.2 A/cm^2, using H_2/Air at 1.2:2.0 stoichiometric ratios. **Figure 2.4** shows the voltage response at constant load. The copolymer membrane showed excellent long-term stability at constant current density, running over 17,500 hours before a catastrophic (flooding) event in the building resulted in an irrecoverable fuel cell test. The voltage decay for this MEA measured from approximately 5500 hours to end-of-life was 0.69 $\mu V \cdot h^{-1}$, a value much lower than previously reported for *para*-PBI (~ 6 $\mu V \cdot h^{-1}$).(26, 27) Recently, Sondergaard et al. reported long term durability of a thermally crosslinked *meta*-PBI membrane prepared by

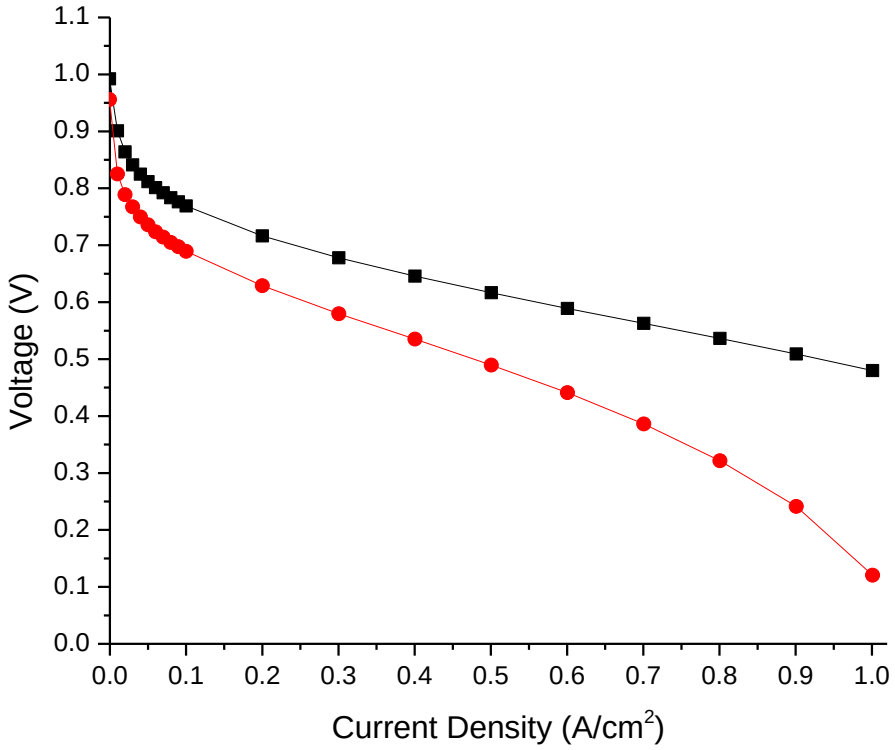

Figure 2.3 *Meta*/*para*-PBI 10(7:1) copolymer fuel cell performance data: (red circles) 180 °C H_2/Air = 1.2/2.0 stoichiometric flows, (black squares) 180 °C H_2/O_2 = 1.2/2.0 stoichiometric flows; no external humidification.

the conventional imbibing process. They recorded a voltage degradation rate of 0.5 $\mu V \cdot h^{-1}$ for the first 9200 hours of operation, and 5.0 $\mu V \cdot h^{-1}$ for the next 3800 hours of operation. Both studies indicate that PBI membranes have great potential for meeting the requirements of many devices for long-term durability.

Figure 2.5 shows the phosphoric acid evaporative loss for the first 4,500 hours of the test. The PA evaporative loss rate at the anode and cathode were 2.2 $ng \cdot cm^{-2} \cdot h^{-1}$ and 7.7 $ng \cdot cm^{-2} \cdot h^{-1}$, respectively. The amount of PA lost from the cathode was expectedly higher than that from the anode due to water vapor generation at the cathode during operation. At

these PA loss rates, the total amount of acid lost from the membrane for a 40,000 hour lifetime would represent < 1.5% of the total acid in the original membrane.

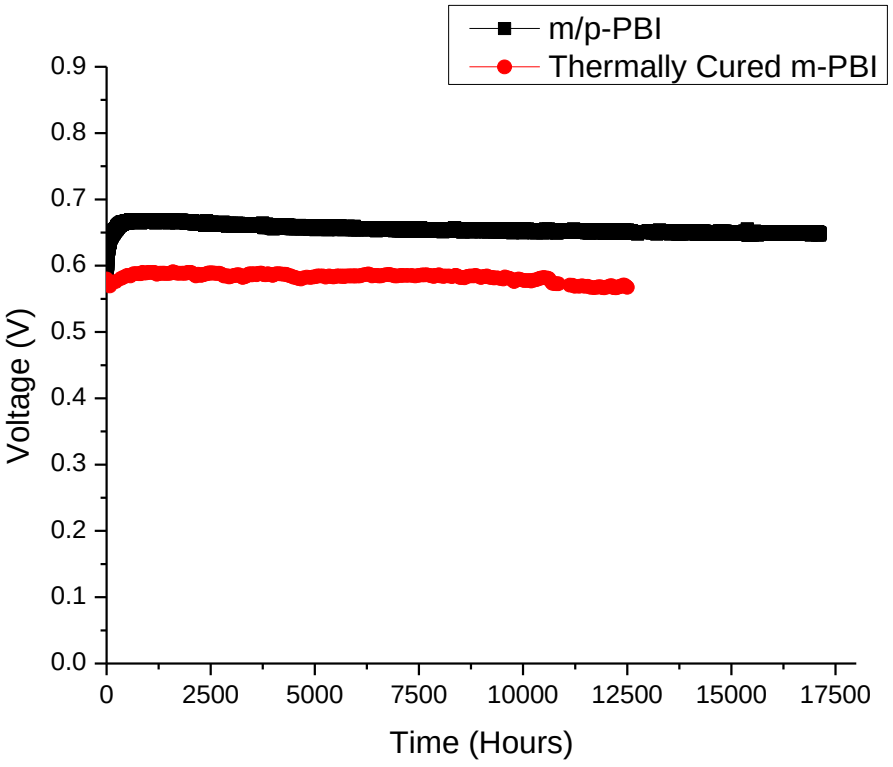

Figure 2.4 Long-term steady-state (0.2 A/cm^2) durability test of *meta/para*-PBI (7:1) copolymer (top curve) using H_2/Air = 1.2/2.0 stoichiometric flows at 160 °C compared to Sondergaard et al. for a thermally cured m-PBI (bottom curve, H_2/Air = 2.0/4.0 stoichiometric flows at 160 °C).*(25)*

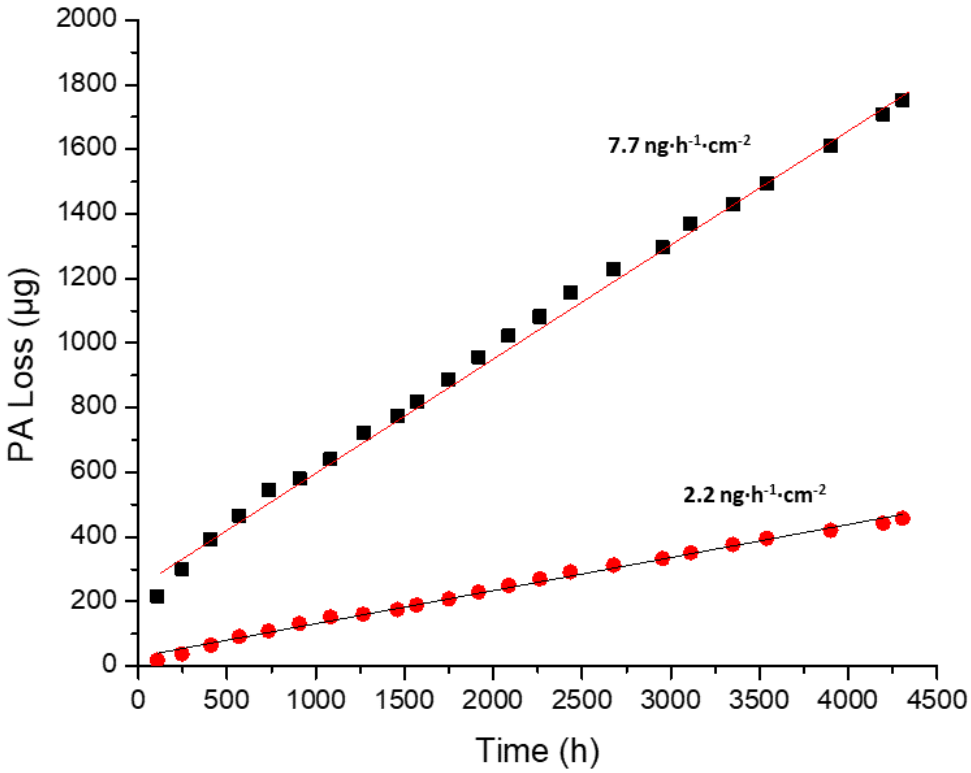

Figure 2.5 PA loss rates from the anode (red circles) and cathode (black squares) of the *meta*/*para*-PBI copolymer measured during steady-state fuel cell operation at 0.2 A/cm^2, 160˚C.

2.4.4 Electrochemical hydrogen pump operation

MEA fabrication for electrochemical hydrogen pump tests was similar to that for fuel cells except they were constructed with symmetrical electrodes, 1 mg/cm^2 Pt on both the anode and cathode (BASF Fuel Cell, Inc.). The MEAs were assembled into the same cell hardware used for fuel cell performance testing. Polarization curves were recorded (**Figure 2.6**) at 160, 180 and 200°C with 1.2 stoichiometric flow of H_2 supplied to the anode and without a sweep gas applied to the cathode. The voltage required to pump pure H_2 across the membrane showed a distinct linear dependence on current density, which

was directly related to the resistance across the cell. *para*-PBI displayed lower voltages than the *meta*/*para*-PBI copolymer consistent with its higher proton conductivity. Interestingly, the expected trend of the voltage decreasing with increasing temperature is observed for the *meta*/*para* copolymer membrane but reversed for the *para*-PBI membrane. At this time, we conjecture that this is due to increasing interfacial resistances from the para-PBI membranes which become "softer" at the higher temperatures (see discussion on compression creep properties).

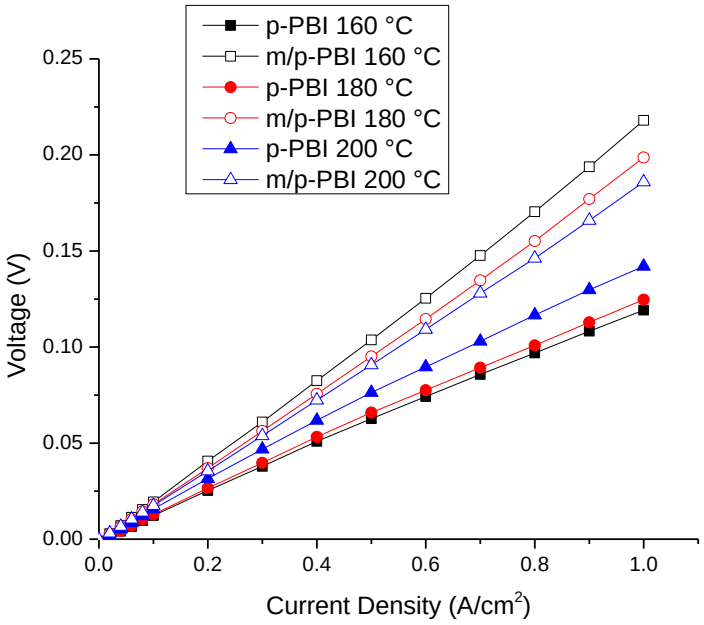

Figure 2.6 Electrochemical pump polarization curves for *meta*/*para* (7:1) PBI copolymer and *para*-PBI membranes using humidified hydrogen (anode gas humidified with 45 °C water bottle).

The MEAs were also subjected to hydrogen purification tests using a reformate test gas (30% H_2, 3% CO, and 67% N_2 – mol %) supplied at 1.2 stoichiometric hydrogen flow on the anode and without a sweep gas on the cathode, at 200 °C, 180 °C and 160 °C (**Figure**

2.7). These tests clearly demonstrate two critical factors that affect electrochemical hydrogen purification, membrane conductivity and Pt catalyst tolerance to CO. At all temperatures, the higher conductivity of *para*-PBI membranes compared to the *meta*/*para*-PBI membrane results in much lower voltages and thus lower power requirements for hydrogen purification. These effects were also obvious from the data in **Figure 2.6** using pure hydrogen. However, the temperature effects on Pt tolerance to CO, especially using a dilute hydrogen source, are prominent. The reversibility of CO binding to Pt dominates the performance of the device and both membranes show much improved operation (lower voltages and power requirements) at 180˚C compared to 160˚C and 200 °C compared to both 180 and 160 °C. Previous work on CO poisoning of Pt in phosphoric acid environments indicates that substantial differences in polarization losses and surface coverage of CO on Pt are observed in this temperature range and at this CO level, consistent with our hydrogen purification data.(28) When the combined effects of high proton conductivity and high operational temperatures are considered (para-PBI at 180˚C), hydrogen purification can be efficiently performed using a dilute hydrogen feed stream with large amounts of CO, producing a fairly pure hydrogen product. For example, at a target current density of 0.5 A/cm^2, hydrogen purification from this mixed gas required approximately 100 mV. The purity of the separated hydrogen was measured via an Agilent 490 micro gas chromatography inline with the cathode exhaust. With handmade MEAs, hydrogen purity was typically found to be >99 % with ~5 ppm carbon monoxide crossover, and ppm levels of nitrogen gas from the mixture as well.

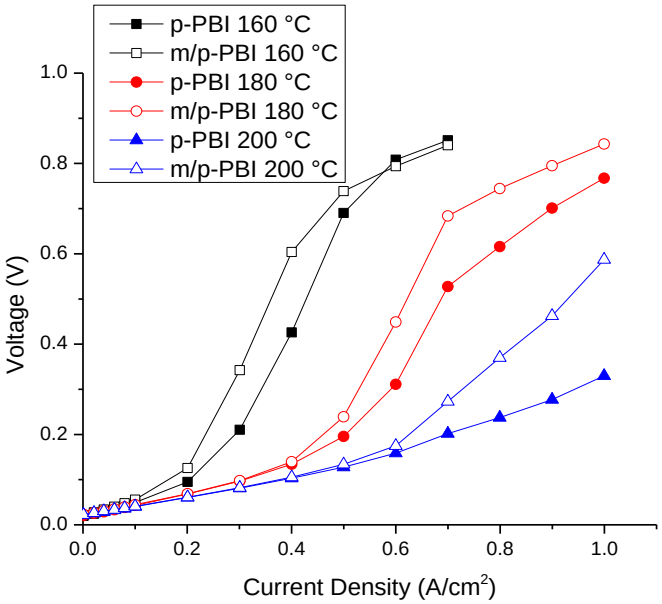

Figure 2.7 Electrochemical pump polarization curves for *meta*/*para*-PBI (7:1) copolymer and *para*-PBI membranes using a humidified reformate (30% H_2, 3% CO, and 67% N_2) test gas (anode gas humidified through 45 °C water bottle), 1.25 stoichiometry to H_2. Anode and cathode held at 7.5 psi back pressure.

2.5 Conclusion.

PBI copolymers based on commercially available monomers were synthesized and characterized as membranes for fuel cells and related electrochemical devices. As the solubility of the copolymers in PPA increased, higher monomer charges could be used which resulted in higher polymer solids content in the cast membranes. However, the balance of *meta*- and *para*- oriented monomers also had an effect on membrane conductivity and short term creep properties that are used to predict long term durabilty. A copolymer composition was chosen for further studies that balanced the properties of ionic conductivity, polymer solids content in the membrane and low creep compliance. Fuel cell performance was shown to be comparable to *para*-PBI. However, the long-term

steady-state test resulted in an exceptionally low degradation rate measured over a 2-year run time, and was ascribed to the low mechanical creep of the high solids content membrane. The copolymers also performed effectively in an electrochemical hydrogen separation device, demonstrating the low power requirements for separating and purifying hydrogen without the need for large pressure differentials required for diffusion based membranes and tolerance to catalyst poisons such as CO when operated at temperatures of 160˚C or higher.

2.6 References.

1. J. Mader, L. Xiao, T. Schmidt and B. C. Benicewicz, *Adv. Polym. Sci.*, **216**, 63 (2008).
2. L. Xiao, H. Zhang, E. Scanlon, L. S. Ramanthan, E. W. Choe, D. Rogers, T. Apple and B. C. Benicewicz, *Chem. Mater.*, **17**, 5328 (2005).
3. A. L. Gulledge, B. Gu and B. C. Benicewicz, *Journal of Polymer Science Part A: Polymer Chemistry*, **50**, 306 (2012).
4. J. A. Asensio and P. Gomez-Romero, *Fuel Cells*, **5**, 336 (2005).
5. X. Li, G. Qian, X. Chen and B. C. Benicewicz, *Fuel Cells*, **13**, 832 (2013).
6. G. Qian and B. C. Benicewicz, *J. Polym. Sci., Part A*, **47**, 4064 (2009).
7. S. Yu and B. C. Benicewicz, *Macromolecules*, **42**, 8640 (2009).
8. J. A. Mader and B. C. Benicewicz, *Macromolecules*, **43**, 6706 (2010).
9. M. A. Molleo, X. Chen, H. J. Ploehn and B. C. Benicewicz, *Fuel Cells*, **15**, 150 (2015).
10. M. A. Molleo, X. Chen, H. J. Ploehn, K. J. Fishel and B. C. Benicewicz, *Fuel Cells*, **14**, 16 (2014).
11. L. Xiao, H. Zhang, T. Jana, E. Scanlon, R. Chen, E. W. Choe, L. S. Ramanthan, S. Yu and B. C. Benicewicz, *Fuel Cells*, **5**, 287 (2005).
12. J. P. Melchior, G. Majer and K. D. Kreuer, *Physical Chemistry Chemical Physics*, **19**, 601 (2017).
13. Q. Li, H. A. Hjuler and N. J. Bjerrum, *J. Appl. Electrochem.*, **31**, 773 (2001).
14. J. H. Liao, Q. F. Li, H. C. Rudbeck, J. O. Jensen, A. Chromik, N. J. Bjerrum, J. Kerres and W. Xing, *Fuel Cells*, **11**, 745 (2011).
15. T. Dippel, K. D. Kreuer, J. C. Lassègues and D. Rodriguez, *Solid State Ionics*, **61**, 41 (1993).
16. M. A. Hickner, H. Ghassemi, Y. S. Kim, B. R. Einsla and J. E. McGrath, *Chem. Rev.*, **104**, 4587 (2004).
17. R. Savinell, E. Yeager, D. Tryk, U. Landau, J. Wainright, D. Weng, K. Lux, M. Litt and C. Rogers, *Journal of The Electrochemical Society*, **141**, L46 (1994).
18. R. Gokhale, T. Asset, G. Qian, A. Serov, K. Artyushkova, B. C. Benicewicz and P. Atanassov, *Electrochemistry Communications*, **93**, 91 (2018).
19. T. R. Garrick, C. H. Wilkins, A. T. Pingitore, J. Mehlhoff, A. Gulledge, B. C. Benicewicz and J. W. Weidner, *Journal of The Electrochemical Society*, **164**, F1591 (2017).
20. K. A. Perry, G. A. Eisman and B. C. Benicewicz, *J. Power Sources*, **177**, 478 (2008).
21. R. Peach, H. Krieg, A. Kruger, D. Bessarabov and J. A. Kerres, *ECS Transactions*, **85**, 21 (2018).
22. K. A. Perry, K. L. More, E. Andrew Payzant, R. A. Meisner, B. G. Sumpter and B. C. Benicewicz, *Journal of Polymer Science Part B: Polymer Physics*, **52**, 26 (2014).
23. T. Sondergaard, L. N. Cleemann, H. Becker, D. Aili, T. Steenberg, H. A. Hjuler, L. Seerup, Q. F. Li and J. O. Jensen, *Journal of Power Sources*, **342**, 570 (2017).
24. X. M. Chen, G. Q. Qian, M. A. Molleo, B. C. Benicewicz and H. J. Ploehn, *Journal of Polymer Science Part B-Polymer Physics*, **53**, 1527 (2015).

25. T. Søndergaard, L. N. Cleemann, H. Becker, D. Aili, T. Steenberg, H. A. Hjuler, L. Seerup, Q. Li and J. O. Jensen, *Journal of Power Sources*, **342**, 570 (2017).
26. T. J. Schmidt, *ECS Transactions*, **1**, 19 (2006).
27. T. J. Schmidt and J. Baurmeister, *ECS Transactions*, **3**, 861 (2006).
28. H. P. Dhar, L. G. Christner and A. K. Kush, *Journal of The Electrochemical Society*, **134**, 3021 (1987).

CHAPTER 3

TAILORING PBI MEMBRANES FOR ELECTROCHEMICAL HYDROGEN SEPARATION

3.1 Abstract.

Industrial demand for hydrogen has rapidly increased alongside growing business sectors related, but not limited to hydrogen cracking, desulphurization and catalytic reforming in petroleum-based applications, and hydrogenation of oils in the food industry. As societal needs depend on these growing processes, a reliable source of hydrogen is essential. Electrochemical hydrogen separation (EHS) is a low-energy consumption method capable of capturing pure hydrogen from multi-component source feeds. This can be advantageous in many industrial applications where hydrogen is a waste byproduct and can be captured and redistributed as a pure commodity, or when hydrogen is a process component, EHS can be used to mitigate reactant losses by providing an efficient means of hydrogen recycling. Furthermore, EHS is a possible hydrogen transportation/storage method applicable with existing infrastructure.

EHS can be a powerful tool in tomorrow's hydrogen economy or a cost-effective tool for current industries. This research work set out to lay the foundation for designing polymer electrolyte membranes (PEMs) dedicated for EHS applications with varying needs and specifications. PEMs are the heart of the stack and contribute greatly to the desired performance. Arising from this work is the inherent trade-off between power efficiency and durability of PEMs under unique conditions. From this, membrane durability *in-situ* has been related to *ex-situ* testing methods for enhanced material screening. Also demonstrated is the profound effect of membrane humidification, or lack-there-of, including efforts to alleviate the need. Additionally, membrane electrode assemblies (MEAs) were subjected to harsh reactant conditions where catalyst poisoning is a

fundamental issue, and utilization of high-temperature PEMs (HT-PEMs) implicitly enhances performance.

These results demonstrate the broad EHS application scope of polybenzimidazole (PBI) based PEMs, but also exhibit a deep-rooted need for further exploration of PBI chemistries for specific needs.

3.2 Introduction.

Efficient purification of hydrogen is becoming a common interest in both the industrial and energy sectors. In particular, technology which can efficiently purify, pump, and pressurize hydrogen at low to moderate flow rates is needed, but is not readily available. Of course, there are existing methods for hydrogen purification which include various combinations of mechanical compression with cryogenic cleanup, palladium membranes, pressure swing absorption, and passive membrane separators to name a few. However, these technologies are challenged by certain limitations: 1) cryogenic cleanup produces high purity hydrogen, but requires costly refrigeration equipment and is suitable for very large-scale specialty applications(1); 2) palladium membrane purification can be fairly simple in design and construction, but requires pressurization to drive the hydrogen separation process and suffers from poor utilization when purifying hydrogen from gases containing low fractions of hydrogen(2); 3) pressure swing absorption (PSA) is widely used in high volume industrial processes and relies on large, mechanical components that are subject to frequent maintenance and inherent inefficiency.(3) Such devices are not easily scaled to smaller sizes or localized generation/purification needs. Furthermore, it is important to state that all of the above processes require expensive, high maintenance, compressors.

Electrochemical pumping is not a new concept and has in fact been utilized as a diagnostic technique within the electrochemical industry for years. General Electric developed this concept in the early 1970's (4).

The use of polymer electrolyte membranes for electrochemical hydrogen compression has been demonstrated in water electrolysis (H_2 generation) devices at United Technologies Corporation, reaching 3000 psi_a (5), as well as studied in academic institutions (6). The electrochemical hydrogen pump, first developed in the 1960's and 1970's, was derived from the original proton exchange membrane fuel cell efforts. The concept is simple, requires little power, and has been shown to pump hydrogen to high pressures. In the original work, the membrane transport medium was a perfluorosulfonic

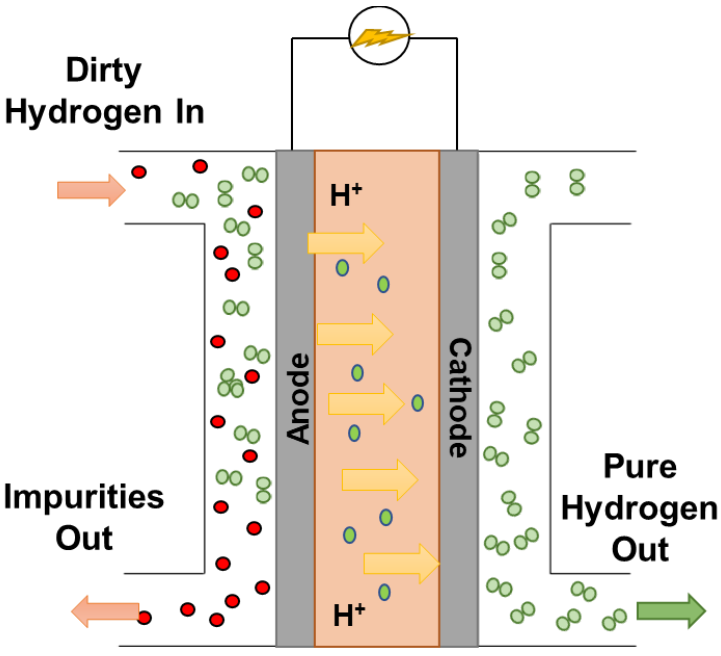

Figure 3.1: Polymer electrolyte membrane for hydrogen electrolysis

acid (PFSA) material, similar to the material used in many fuel cells today. The process is quite elegant in that like a fuel cell, molecular hydrogen enters the anode compartment, is oxidized to protons and electrons at the catalyst, and then the protons are driven through

the membrane while the electrons are driven through the electrically conductive elements of the cell.

The major difference in this cell as compared to a fuel cell is that the pump is operated in an electrolytic mode, not galvanic, meaning that power is required to "drive" the proton movement. Once the protons emerge from the membrane at the cathode, they recombine to form molecular hydrogen. Thus, hydrogen can be pumped and purified in a single step with a non-mechanical device. The pump concept builds upon the understanding of proton transport membranes. The overall chemical reaction is described by Equation 1:

Equation 1:

$$Anode: H_2 \rightarrow 2H^+ + 2e^+$$

$$Cathode: 2H^+ + 2e^- \rightarrow H_2$$

$$Total\ Reaction: H_2(anode) \rightarrow H_2(cathode)$$

The cell voltage between the anode and cathode can then be described by Equation 2. The Nernst potential, E_{Nernst}, is given by the Nernst Equation 3, where E° is the standard potential of a hydrogen reaction, R is the gas constant, T is the temperature in Kelvin, F is Faraday's constant, and p_{cathode} and p_{andode} are the partial pressures of hydrogen at the anode and cathode respectively.

Equation 2:

$$E = E_{Nernst} - E_{polarization} - E_{ohmic}$$

Equation 3:

$$E_{Nernst} = E^{\circ} - \frac{RT}{2F} \ln \frac{p_{cathode}}{p_{anode}}$$

$E_{polarization}$ is the polarization overpotential which is the sum of the polarization overpotentials at the anode and cathode. This can be described using the Butler-Volmer

equation. The polarization overpotential can be approximated at low overpotentials, Equation 4, where R is the gas constant, T is the temperature in Kelvin, F is Faraday's constant, i is the current density, and i_0 is the exchange current density.

Equation 4:

$$E_{polarization} = \frac{RTi}{2Fi_0}$$

Clearly, the proton conducting membrane properties are critical. Desirable properties include: high proton conductivity, mechanical stability, low solubility and permeability of impurity gases, and sufficient operating temperature to support tolerance to impurities (CO and H_2S) found in reformed gases. The application of the PBI membrane to electrochemical hydrogen pumping provides high proton conductivity (0.2 – 0.4 S/cm), mechanical stability, enhanced gas separation, and up to at least 180°C operation. The high operating temperature eliminates water management difficulties typically experienced with the low operating temperatures of PSFA membranes while also providing tolerance to poisonous gas species such as CO. This is a crucial quality in electrochemical hydrogen pumping as many of the common impurities being removed from the feed stream are known to poison the catalyst. As such, the PBI membrane and electrode assembly represents a significant new opportunity and paradigm shift in electrochemical hydrogen pumps as well as in advancing the science of hydrogen separation, purification, and pressurization. This concept has been evaluated and demonstrated in recent work using PBI membranes (7). The hydrogen pump was shown to operate with fairly low power requirements, and generally needed less than 100 mV when operating at 0.2-0.4 A/cm^2. This was accomplished without the critical water management commonly encountered in low

temperature, water-based membranes. The cathodic flow of hydrogen from the device was nearly identical to the theoretical Faradic flows. This suggests that the hydrogen pump could have applications as a hydrogen metering device since the hydrogen flow could be easily and accurately controlled by the current of the power source. The initial work reported devices that could operate for several thousand hours with little change in the operating parameters. This would be expected from the related work on PBI membranes for fuel cells which show outstanding long-term durability. In fuel cell applications, the ability to operate at high temperatures provides benefits for gas cleanup and durability on reformed fuels. In hydrogen pump applications, this tolerance to fuel impurities enables the hydrogen pump to purify hydrogen from hydrogen gas feeds containing such impurities. Figure 3.2 shows the operation of a PBI-based hydrogen pump operating on pure hydrogen, as well as two different synthetic reformates. The flow rates are nearly unaffected by the composition of the gas feed at the various operating conditions (the data points are superimposed for the different gases). The data demonstrates that the pump was capable of operating at high CO levels (1% in this work) and extracting hydrogen from dilute feed streams (<40% hydrogen). Additionally, the hydrogen pump was capable to producing hydrogen with purities greater than 99%, with the final purity dependent on operating conditions. This device could play a prominent role for both the current industrial hydrogen users, as well as in a future economy that is more heavily reliant on hydrogen as an energy carrier.

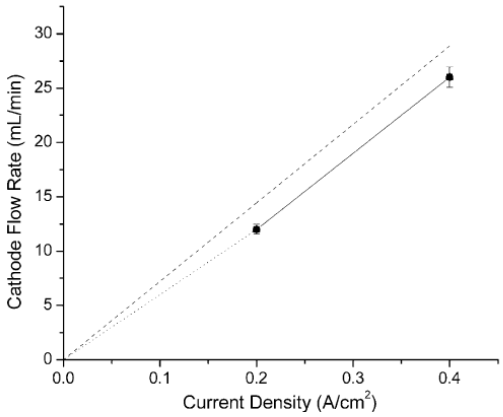

Figure 3.2: The cathodic flow rates of a hydrogen pump operated at 160 ^{O}C and 0% relative humidity and fueled by pure hydrogen (unfilled squares), a reformate gas comprised of 35.8% H_2, 11.9% CO_2, 1906 ppm CO, and 52.11% N_2 (filled circles), and a reformate gas comprised of 69.17% H_2, 29.8% CO_2, and 1.03% CO (filled triangles). The values are nearly identical, and thus, the symbols appear superimposed. The dotted line represents the theoretical flow rate at 100% efficiency.(7)

The growing industrial demand for a reliable supply of hydrogen coupled with the need for more sustainable business/energy practices provides a clear market entry point for the ability to efficiently capture, recycle, store, and transport hydrogen. EHS can be viewed as an enabling technology in these markets. EHS was first reported by Maget(4) in the 1970's while developing solid polymer electrolyte chemical processes. It was found that a proton oxidized at the anode would recombine at the cathode to form "new" molecular hydrogen after the proton had been driven across the membrane with an applied voltage. Until recently, however, this process gained little exposure beyond academic interests but should be considered as a potential candidate to meet current industrial needs.

High-temperature PEMs (HT-PEMs) are advantageous over low-temperature PEMs (LT-PEMs) in EHS applications due to the harsh working conditions of the device. LT-PEMs are highly susceptible to catalyst poisoning, diminishing the efficacy of the device to separate hydrogen from feed streams containing carbon monoxide, hydrogen

sulfide, ammonia, etc. At high temperatures the adsorption of these molecules on platinum is more labile greatly reducing the adsorbed amount at any given time. Additionally, LT-PEMs require large amounts of water to maintain proton conductivity. This can lead to flooding of the flow fields and membrane electrode assemblies (MEAs) reducing the active area, as well as incorporating extensive amounts of water vapor in the exit stream.

PBI gel membranes rely on an acid electrolyte for proton conductivity which afford working temperatures greater than 100 °C, eliminating the problems with LT-PEMs, while displaying exemplary performance in fuel cells attributed to their inherently high conductivities. These membrane materials possess the needed qualities for efficient EHS devices.

3.3 Experimental.

3.3.1 Materials.

3,3',4,4'-Tetraaminobiphenyl (TAB, polymer grade, ~97.5%) was donated by BASF Fuel Cell, Inc. and used as received. Isophthalic acid (IPA, >99% purity) and terephthalic acid (TPA, >99% purity) were purchased from Amoco and used as received. Celtec-P© and electrode materials were provided by BASF and used as received unless noted otherwise. Polyphosphoric acid (115%) was supplied from FMC Corporation and used as received. Reformate test gas (30% H_2, 3% CO, 67% N_2 – mol %) were mixed by AirGas and used as received.

3.3.2 Polymer Synthesis and Membrane Fabrication.

A typical polymerization consisted of 64.28 g tetraaminobiphenyl (TAB, 300 mmol), 43.62 g isophthalic acid (IPA, 262.5 mmol), and 6.23g terephthalic acid (TPA, 37.5

mmol) added to 1050 g polyphosphoric acid, mixed with an overhead stirrer and purged with dry nitrogen. The contents were heated in a high temperature silicone oil bath, and the temperature was controlled by a programmable temperature controller with ramp and soak features. In a typical polymerization, the final reaction temperature was approximately 195 °C and held for 12 hours. Once the reaction was completed, determined by visual inspection of viscosity, the polymer solution was cast onto clear glass plates using a doctor blade with a controlled gate thickness of 15 mils. The cast solution was hydrolyzed into membranes in a humidity chamber regulated to 55% R.H. at 25 °C.

3.3.3 Post-Membrane Formation Crosslinking.

Membranes were placed into DI water baths, and the water was replaced every 8 hours. Once all the PA was removed from the PBI gel membranes, monitored by pH strips, they were allowed to soak in a bath of 0.0523 M solution of α,α'-dichloro-p-xylene (DCX) or 4,4'-bis(chloromethyl)biphenyl (DCB) in methanol or N,N'-dimethylacetamide (DMAc). The bath was covered, heated to 30 °C (for methanol) or 60 °C (for DMAc), and agitated with a magnetic stir bar. Crosslinking reactions were typically allowed to proceed for 6 hours. The membrane was then washed with DI water and methanol cyclically, minimum three times. The membranes were then placed into a 50 wt% PA bath for acid imbibing.

3.3.4 Membrane Composition.

The composition of phosphoric acid-doped PBI membranes was determined by measuring the relative amounts of polymer solids, water, and acid in the membranes. The phosphoric acid (PA) content of a membrane was determined by titrating a membrane

sample with standardized sodium hydroxide solution (0.10 M) using a Metrohm 716 DMS Titrino auto-titrator. Once titrated, the sample was thoroughly washed with DI water and dried at reduced pressures at 120 °C overnight. The dried sample was then weighed to determine the polymer solids content of the membrane.

Using **equations 1 and 2**, the polymer weight percentage and phosphoric acid weight percentage can be determined, respectively;

$$Polymer\ \ w/w\ \ \% = \frac{W_{dry}}{W_{sample}} \cdot 100 \qquad (1)$$

$$Acid\, w/w\ \ \% = \frac{M_{acid} \cdot V_{NaOH} \cdot c_{NaOH}}{W_{sample}} \qquad (2)$$

where W_{sample} is the weight of the sample before titration, W_{dry} is the weight of final dried sample after titration, M_{acid} is the molecular weight of phosphoric acid, and V_{NaOH} and c_{NaOH} are the volume and concentration of the sodium hydroxide solution required to neutralize the phosphoric acid to the first equivalence point.

The number of moles of phosphoric acid per mole of PBI repeat unit (or the PA doping levels, X) were calculated from the equation:

$$X = \frac{V_{NaOH} \cdot c_{NaOH}}{W_{dry} \Big/ M_{polymer}} \qquad (3)$$

where V_{NaOH} and c_{NaOH} are the volume and concentration of the sodium hydroxide solution required to neutralize the phosphoric acid to the first equivalence point, W_{dry} is the final weight of the dried sample after titration, and $M_{polymer}$ is the molecular weight of the polymer repeat unit.

3.3.5 Compression Creep and Creep Recovery.

The compression creep and creep recovery method was used to study the time-dependent creep behavior of the prepared membranes in a TA RSA III dynamic mechanical analyzer using its built-in functionality for creep testing. A typical experiment consisted of a 20-hour creep phase followed by a 3-hour recovery phase. During the creep phase, a constant compressive force equivalent to a stress level of 0.1 MPa was applied, and this force was removed at the start of the recovery phase. All experiments were carried out at 180 ± 0.5 °C in a temperature-controlled oven with dry air circulation. The creep test was repeated 2-4 times for each gel membrane.

3.3.6 Burst Testing.

Membrane failure at maximum differential pressure was evaluated through a homemade device. A circular piece of membrane 8 cm in diameter was cut out and placed between two stainless steel plates with a Viton© O-ring to ensure a good seal, and compressed to 1.13 N·m. The lower steel plate contained a nitrogen inlet and a pressure release ball valve, while the upper plate was fitted with two exhaust ports open to atmospheric pressure. The nitrogen inlet was fitted to a standard nitrogen cylinder with a max 200 psi regulator and 2 psi incremental readings. Pressure applied to the membrane

was adjusted by hand steadily, ~ 5 psi per 10 seconds. Membrane failure was observed when nitrogen was freely flowing from the upper exhaust ports.

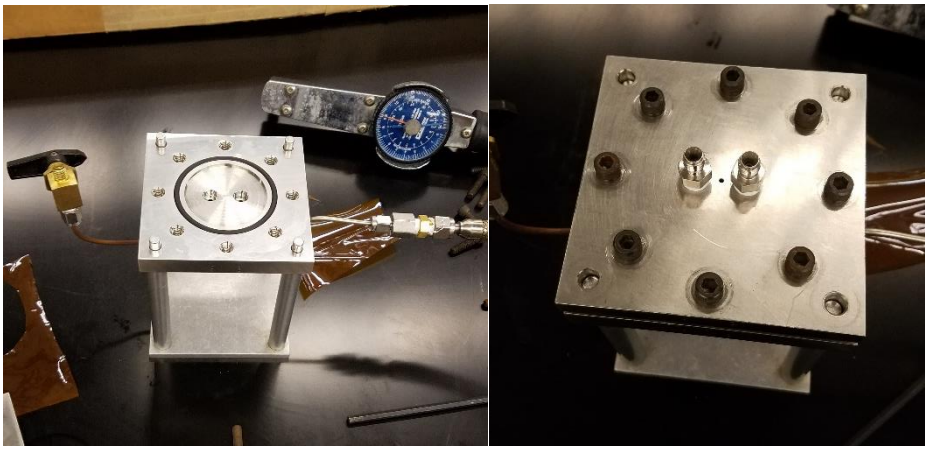

Figure 3.3 Homemade burst testing apparatus

3.3.7 Proton Conductivity.

Proton conductivities of the membrane were measured by a four-probe electrochemical impedance spectroscopy method using a Zahner IM6e electrochemical workstation over the frequency range from 1 Hz to 100 kHz with an amplitude of 5 mV. A two-component model with an ohmic resistance in parallel with a capacitor was employed to fit the experimental data. The conductivities of the membrane at different temperatures were calculated from the membrane resistance obtained from the model simulation with the following equation:

$$\sigma = \frac{d}{l \cdot w \cdot R_m} \qquad (4)$$

Where d is the distance between the two inner probes, l is the thickness of the membrane, w is the width of the membrane, and R_m is the ohmic resistance determined by the model fitting. Membrane samples underwent two heating ramps to 180 °C. Conductivity data reported was recorded on the second heat ramp, after water was removed from the membrane during the first heating cycle.

3.3.8 Membrane Electrode Assembly (MEA) Fabrication and EHS.

The gas diffusion electrodes (GDE, acquired from BASF Fuel Cell, Inc) with a platinum loading of 1.0 mg/cm^2 were used for this study. The MEA was fabricated by hot pressing a piece of membrane between two Kapton framed electrodes. MEAs were then assembled into single cell fuel cell test equipment. The gas flow plates used were constructed from graphite with triple serpentine gas channels. Stainless steel end plates with attached heaters were used to clamp the graphite flow plates. A commercial fuel cell testing station (Fuel Cell Technology, Inc.) was used for fuel testing and is capable electronically controlling temperature, back pressure, gas flows, and designing test sequences. It also has the ability to measure cell resistance while under test.

3.4 Results and Discussion.

3.4.1 Ex-Situ Results.

Table 3.1: Notable ex-situ membrane results

Membrane	Solid Content (%)	Acid Content (%)	I.V. (dL/g)[a]	σ (mS/cm) at 160 °C	σ (mS/cm) at 180°C	Creep Compliance (1/Pa)	Burst Test (psi)
Celtec-P	5	60	3-5	212	213	9.42	80
Celtec-P X-link[1]	6.84	68.8	3-5	224	259	3.78	79
Celtec-P X-link[2]	6.4	73.5	3-5	128	130	4.05	124
Celtec-P X-link[3]	*	*	3-5	243	280	2.75	92
Celtec-P X-link[4]	12	66	3-5	191	211	2.45	125
Celtec-P X-link[5]	6	66.4	3-5	*	*	3.24	82
***m/p-PBI* (IPA:TPA):TAB (7:1):1 10 wt%**	18	64	1.77	122	130	1.685	93
m-PBI 9 wt%	14.4	63.3	1.49	151	161	1.5	22
***m/p* X-link[4]**	19.4	57.3	1.5	181	195	1.587	*

[1]Crosslinking done with α,α'-Dichloro-p-xylene (0.0523 M) in methanol for 6 hours
[2]Crosslinking done with 4,4'-Bis(chloromethyl)biphenyl (0.0523 M) in methanol for 6 hours
[3]Crosslinking done with α,α'-Dichloro-p-xylene (0.0523 M) in DMAc for 6 hours
[4]Crosslinking done with 4,4'-Bis(chloromethyl)biphenyl (0.0523 M) in DMAc for 6 hours
[5]Crosslinking done with Paraformaldehyde (1 wt %) in PA at 140 °C for 1 hour
[a]I.V. measured prior to crosslinking
*In progress

BASF Celtec-P© was used as the benchmark membrane material for EHS applications. Testing was done on membranes supplied by BASF BNB, GmbH produced by Trigona. Celtec-P© demonstrates superior performance in-terms of power efficiency. This result was not surprising due to its low in-cell resistance qualities. When considering pumping pure hydrogen across a membrane, the voltage directly relates to Ohm's Law (V = IR) where the resistance is that of the total cell. This relationship, however, starts to breakdown when multi-component gas streams are fed to the device and mass transport limitations arise.

Typically, ex-situ membrane conductivities are a good indication of in-cell resistance. These can be used to screen new materials estimating their potential performance under test. It is important to note, that ex-situ conductivity is not the only factor of cell resistance but is also greatly dependent on the membrane/electrode interface. **Scheme 3.1** shows the post-membrane formation crosslinking modification conducted on various PBI membranes. All membranes tested exhibited adequate ex-situ conductivities and therefore advanced for further testing. Interestingly, crosslinking under these methods does not greatly impede proton conductivity and in some instances even augments conductivity.

As EHS applications cover a broad scope of conditions, it became imperative to determine possible membrane failure modes that could result in decreased performance or irrecoverable drops in power efficiency. These conditions include the possibility of subjecting the PEMs to a differential pressure during operation. To distinguish membrane candidates two ex-situ tests were developed to give insight of undesired cell performance, i.e. creep compliance using a dynamic mechanical analyzer and burst testing. The creep

compliance, defined as the rate of strain to stress at a certain time, is used to evaluate the membranes' resistance to flow, and was measured by applying a static load to each membrane while measuring its displacement over time.

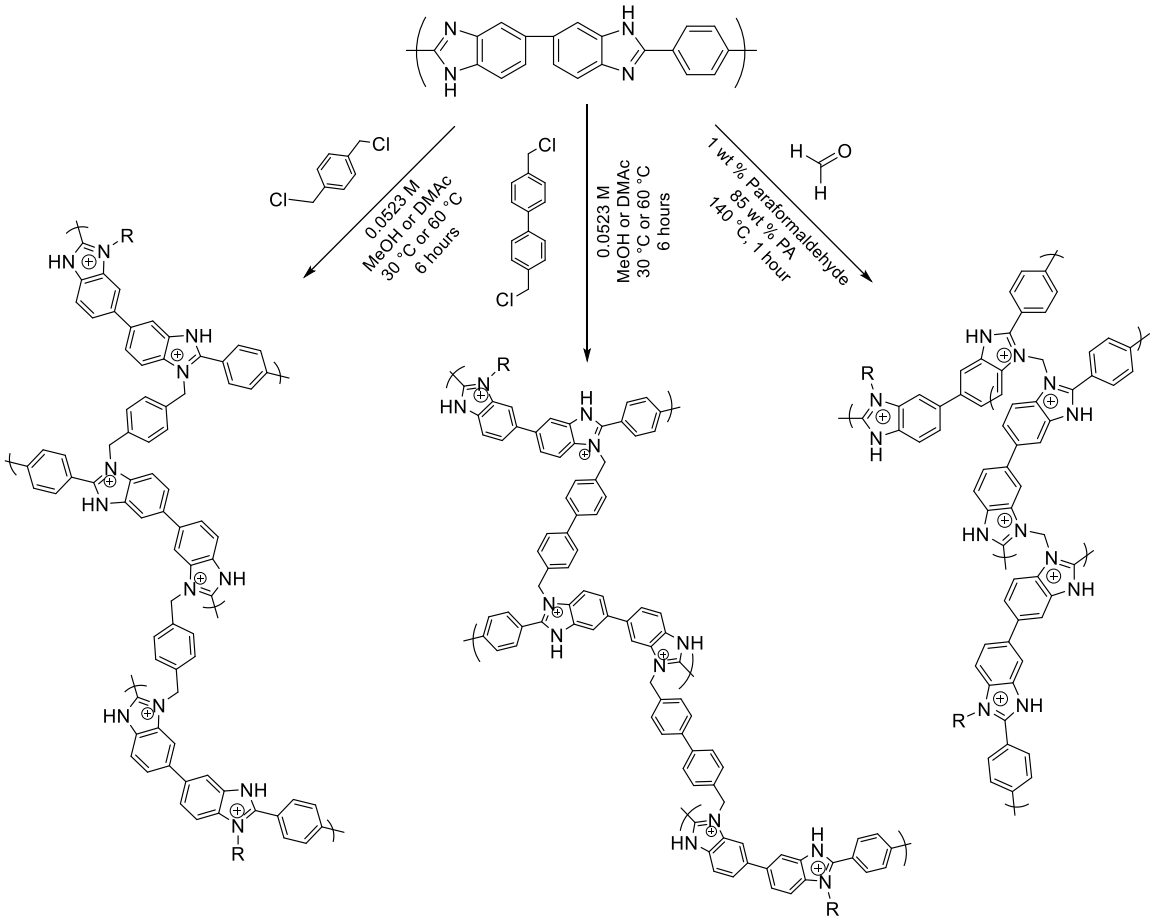

Scheme 3.1 Post-membrane formation crosslinking reaction schemes.

The creep compliance data for the membranes in **Table 3.1** is shown in **Figure 3.4**. The compression of the membrane with a static load over time gives a relative understanding of how a membrane responds to the mechanical stress applied from cell fabrication and under certain operating conditions. This is also a good indication of membrane expected lifetime when experiencing a differential pressure. Burst testing was done by applying a

steadily increasing differential pressure across the membrane under test and reporting the final failure pressure. It is important to note that this test is likely not indicative of the long-term operating conditions the membrane can withstand but is applicable in providing a relative ranking of membrane candidates for differential pressure applications.

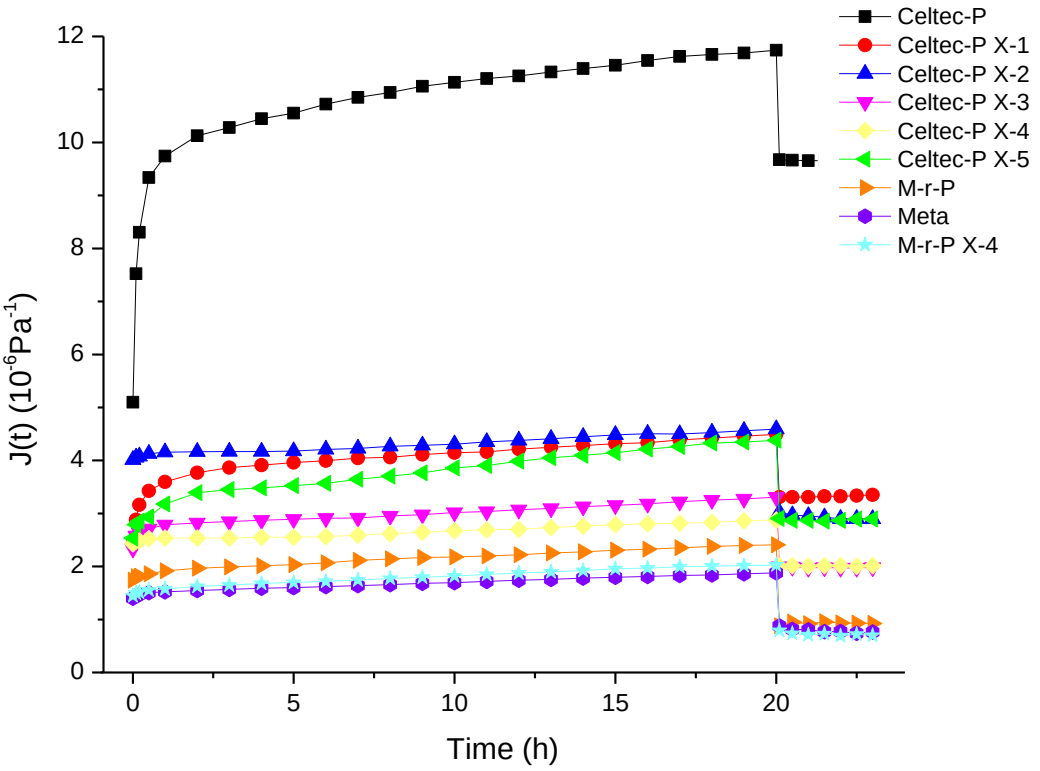

Figure 3.4 DMA results of selected membranes.

p-PBI type membranes show an obvious increase in conductivity over chemistries incorporating *meta* character into the polymer backbone. However, to be considered as a potential membrane for EHS applications in differential pressure operation, membranes must undergo some post-modification crosslink strategy to improve structural integrity; after all, they work pretty well in ΔP=0 conditions.(8-11) From the results shown in **Table 3.1,** it was found that crosslinking the PBI membranes in N,N'-dimethylacetamide instead

of methanol afforded the highest improvement in mechanical properties with either of the bischloromethyl type crosslink chemistries.(12) Furthermore, the larger DCB crosslinker decreased both the creep compliance and increased the pressure at burst of the membranes over the smaller DCX crosslinker. However, this added mechanical strength of DCB over DCX is achieved at the cost of membrane proton conductivity. Comparatively, the DCX crosslinker showed negligible decreases in proton conductivity.

DCX and DCB crosslinking techniques require the membrane to be washed of the imbibed electrolyte (phosphoric acid) before undergoing the crosslinking reaction, generating acidic waste water that must be handled. This will inevitably increase the cost of manufacturing membranes on an industrial scale. The organic solvents needed for the reaction also pose more handling risks and extra costs. These aspects must be considered when designing a viable membrane for widespread use in a certain application. Two approaches were considered for reducing the membrane cost basis while still improving performance in EHS applications: [1] using a crosslinker that is soluble and reactive in phosphoric acid and [2] improving the intrinsic mechanical properties of the membrane with the polymer backbone chemistry.

Formaldehyde is soluble in phosphoric acid at small concentrations and is reactive with the imidazole nitrogens at elevated temperatures in acidic conditions. It provides a single bridging carbon between two chains (or two segments of a chain). For easier handling, paraformaldehyde (a solid) can be used to generate formaldehyde in-situ as the water/phosphoric acid solvent breaks down the polymeric form into its monomeric form. This technique allows PBI membranes to be crosslinked without having to remove the imbibed phosphoric acid from the as cast film but requires reaction temperatures of at least

140 °C. Results of membrane crosslinking using paraformaldehyde are presented in **Table 3.1** and **Figure 3.4** (Celtec-P X-link[5]) and show minimal increases in the desired mechanical properties. The pressure at burst is similar to that of uncrosslinked Celtec-P©. The creep compliance marginally improved and the creep rate was still high (slope of the line in **Figure 3.4**). EHS performance of this membrane will not be discussed further in the next section because it was similar to Celtec-P in regard to failure with differential pressure and had slightly higher power requirements.

It has also been shown that the polymer chemistry has an integral role in the mechanical properties of the membrane. The chemistry dictates the total amount of polymer content that can be achieved in the final film and the structure morphology of the chains.(13) *Para* oriented PBI polymers are more rigid in nature and provide increased mechanical properties at equivalent solids content of polymer incorporated in the membrane compared to their *meta* counterparts. However, this rigidity of the chains is also responsible for their low solubilities, hence, the lower polymer content that can be attained in *p*-PBI membranes. Although *meta* oriented chains provide marginal decreases in creep compliance compared to the *para*-oriented isomer, *m*-PBI has greatly enhanced solubility properties that enable drastically higher polymer concentrations in the casting solution. For this reason, *m*-PBI membranes can ultimately achieve better creep properties over *p*-PBI. To capitalize on this phenomenon a copolymer membrane was designed incorporating both *meta* and *para* oriented repeat units into the polymer backbone. It was found that a copolymer comprising of a 7:1 ratio of *meta* to *para* repeat units produced a membrane with exceptional mechanical properties without severely impacting the ionic conductivity. It is important to note that this membrane can be produced without further processing

requirements and is directly scalable with current infrastructure but is also a candidate for further post-modification crosslinking due to the flexibility of the developed crosslinking technique.

These results indicate possible routes to increase durability of PEMs for operating under differential pressure conditions; 1.) higher solids content membranes are more resistant to flow suggesting longer lifetimes under mechanical stresses, however, that relationship does not always correspond to burst pressure and 2.) crosslinking membranes enhances creep compliance and improves membrane utility to operate under conditions of differential pressure.

3.4.2 In-Situ Results.

Membrane materials were further evaluated by in-cell performance under various conditions. MEAs were subjected to feed streams of pure hydrogen, and a mixed gas consisting of 30, 3, and 70 mol % of H_2, CO, and N_2, respectively. These were tested at various temperatures, backpressures, and humidification. Long-term durability studies were conducted on chosen membranes where they were operated at steady-state conditions with a 30 psi differential pressure on the anode.

3.4.2.1 *p*-PBI Type Membranes.

Celtec-P© has shown to be an effective membrane for EHS applications that do not require harsh conditions. It maintains low in-cell resistance under varying current loads and temperatures. This can be seen in **Figure 3.5**, where even operating at high current densities, 1 $A \cdot cm^{-2}$, the maximum potential barely exceeds 140 mV. Surprisingly, the cell

voltage increased with increasing temperature, opposite to the expected result as predicted from the conductivity trends. The cell voltage dependence on temperature was repeatable with multiple temperature cycles, and with multiple MEAs. At this time, we speculate that the membrane deforms at higher temperatures and partially blocks gas channels in the electrode structure. This could contribute to higher cell resistance and thus, higher operating voltages. Additionally, a small change in % RH displays noticeable changes in the voltage response, but without any clear trend.

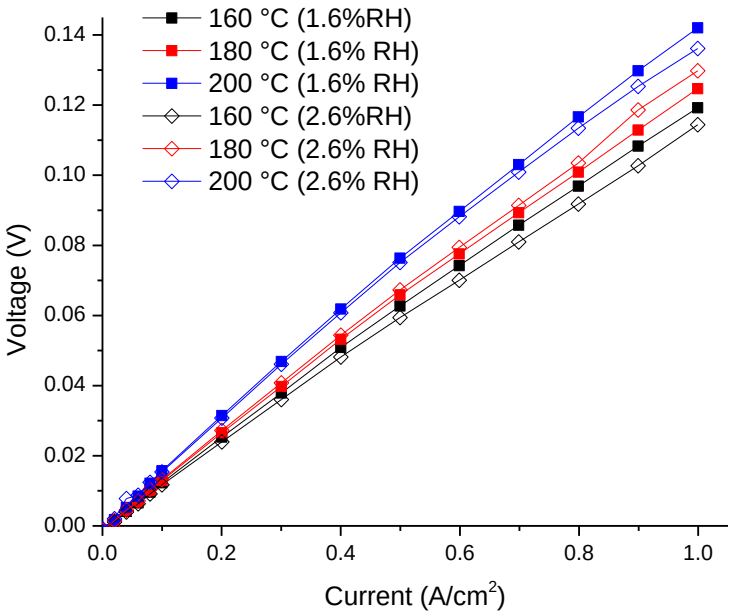

Figure 3.5 Celtec-P© performance in an EHS cell with hydrogen as the test gas, 1.25 stoich. (50 SCCM minimum). Water bottle temperature adjusted to match desired % RH.

Further analysis of Celtec-P© was conducted using a reformate gas stream consisting of only 30 mol % hydrogen and 3 mol % CO (balanced with nitrogen). With very little hydrogen and a large amount of catalyst poisoning CO, this is a relatively harsh operating condition for most PEMs.

The cell performance for Celtec-P© at three different temperatures is shown in **Figure 3.6**. Although cell performance is low at 160 °C, and showed significant poisoning effects at low current densities, increasing the cell temperature drastically improved power efficiencies. This demonstrates the substantial impact of CO catalyst poisoning at reducing the active area at the anode. Additionally, at high current densities there appears to be suggestions of mass transport limitations observed by the increasing rate of voltage change (non-linearity). This is most likely the result both catalyst poisoning and the modest amount of overall hydrogen in the test gas.

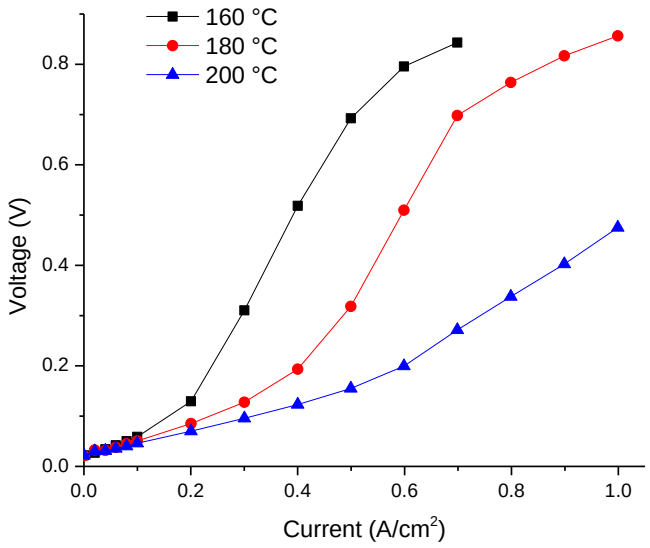

Figure 3.6 Celtec-P© performance in an EHS cell. Test gas is reformate (30 mol % H_2, 3 mol % CO, and 67 mol % N_2). 1.25 stoich. Minimum hydrogen flow was 200 SCCMs and water bottle temperature was held at 65 °C, with 1.5 bar absolute on both anode and cathode.

Further tests were conducted on Celtec-P© to evaluate its properties and performance when subjected to EHS applications with differential pressures. Proposed EHS applications have vastly different specifications including operating under pressure from the feed stream or pumping hydrogen to higher pressures

(EHS hydrogen compression), both resulting in the need for a membrane with resistance to pressure failures.

Using pure hydrogen as the test gas, back pressure at the anode was cycled from 0 to 15 to 30 psi and returned back to 0 psi in a 24-hour period. Polarization curves were taken at each pressure after the cell reached a stable voltage, as shown in **Figure 3.7**. This cycle was repeated for three days and on the fourth day the membrane underwent critical failure. Looking at only data from day one, from 0 psi to 15 psi Celtec-P© performance followed the Nernst equation as expected with a decrease in voltage, dropping from ~0.043 V to ~0.036 V at 0.4 $A \cdot cm^{-2}$. However, upon increasing the anode back pressure to 30 psi, a reverse trend is observed where the voltage was found to increase to 0.043 V at the same current density compared earlier. Upon completion of the first cycle, back to 0 psi anode back pressure, an irrecoverable performance loss, increase in voltage, was recorded (0.059 V at 0.4 $A \cdot cm^{-2}$). Furthermore, as the cycles were repeated daily noticeable voltage increases were found at all pressures. On day 4 the MEA was unable to hold a steady pressure due to a critical failure in the membrane. This result most likely coincides with the low mechanical properties of the *p*-PBI membrane, more specifically its low resistance to creep.

Pressure cycling can create added stress on the membrane due to the constant compression and relaxation of the MEA. This can also lead to an increase in interfacial resistance between the membrane and electrode. A steady-state test was used to fully examine Celtec-P© based MEAs operating under increased differential pressures, as shown in **Figure 3.8**. The MEA was run in EHS mode under constant conditions: 160 °C cell temperature, humidification (45 °C water bottle temperature), 50 SCCM H_2 feed stream,

and 0.2 A/cm^2 current load with 30 psi back pressure on only the anode. Critical failure of the membrane occurred after approximately 130 hours of operation with a steady increase in voltage throughout the entire test.

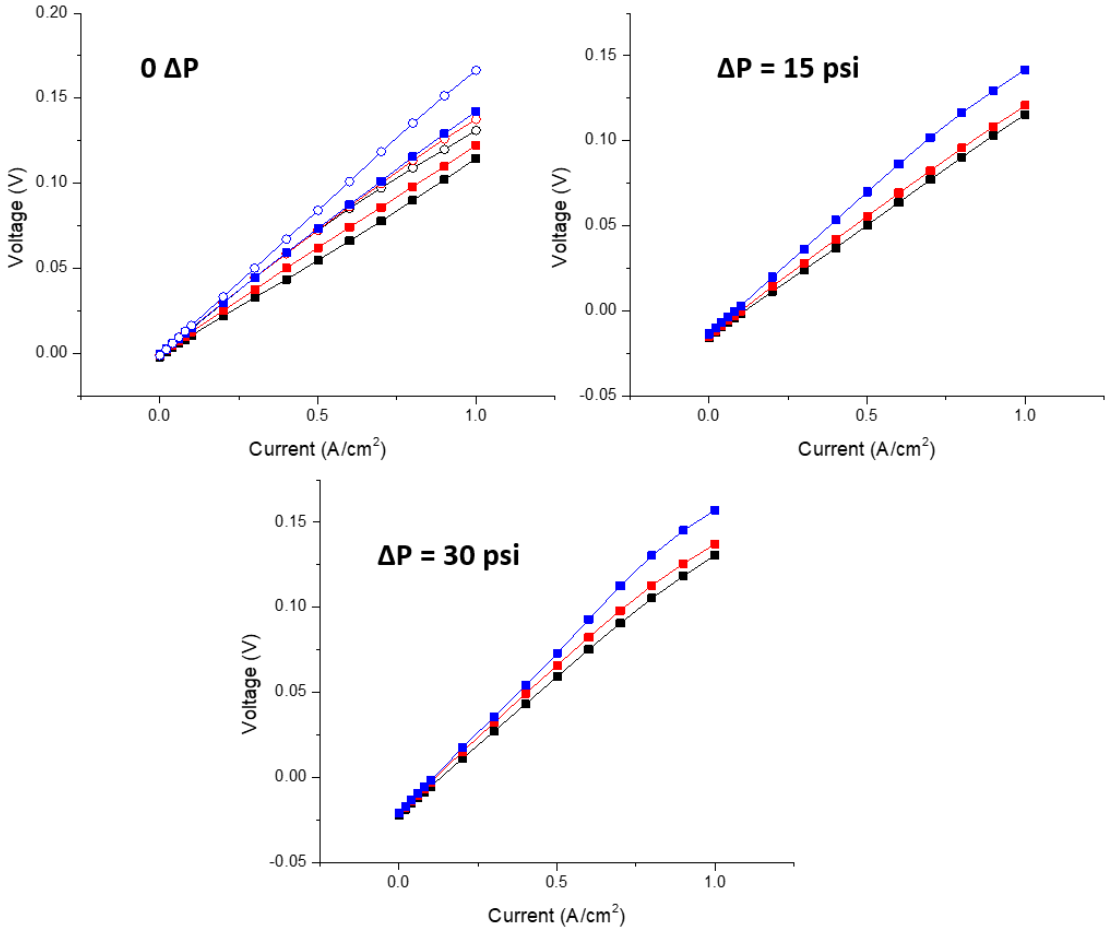

Figure 3.7 Celtec-P under EHS conditions. Test gas is pure hydrogen, 1.5 stoich. Cell temperature is 160 °C with constant 45 °C water bottle for humidification (1.6 % RH). Pressure was cycled as follows: 0 psi – 15 psi – 30 psi – 0 psi, once a day for 3 days. Black lines correspond to day 1, red is day 2, and blue is day 3. Open circles correspond to the polarization curve taken at 0 psi back pressure upon completion of the cycle.

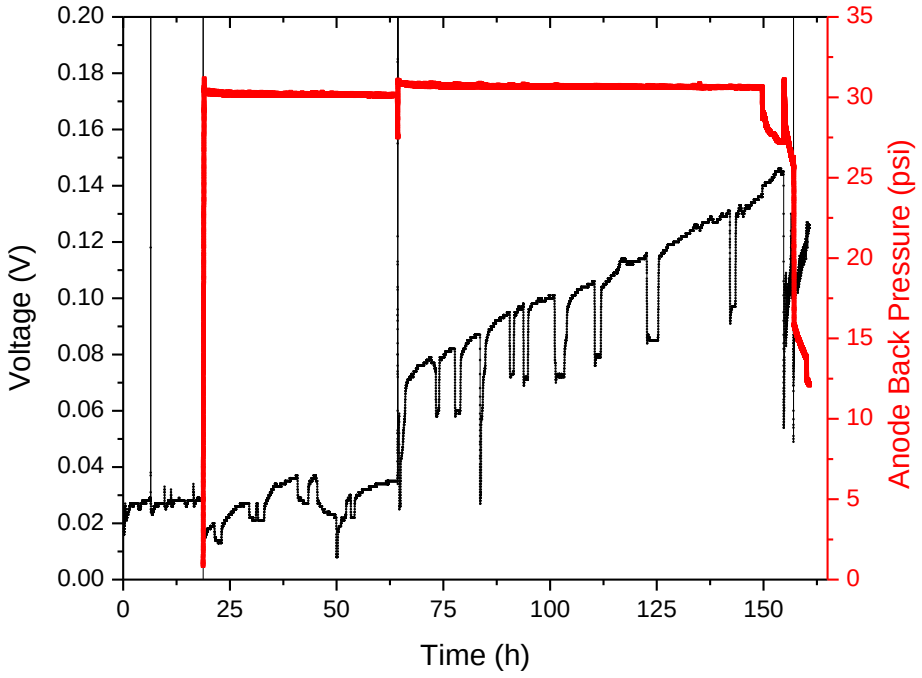

Figure 3.8 Long-term durability of Celtec-P© under a differential pressure of 30 psi on the anode at 160 °C, 0.2 A/cm^2.

Crosslinking of Celtec-P© showed promising ex-situ results with increased creep compliance and higher pressures at burst. Celtec-P© crosslinked with paraformaldehyde was chosen due to the industrial feasibility of the process. Since the membranes sensitivity to pressure became a key concern a quick screening test was developed where polarization curves were taken at 160 and 180 °C under 0 Δp, then repeated with a 30 psi back pressure on the anode, as shown in **Figure 3.9.**

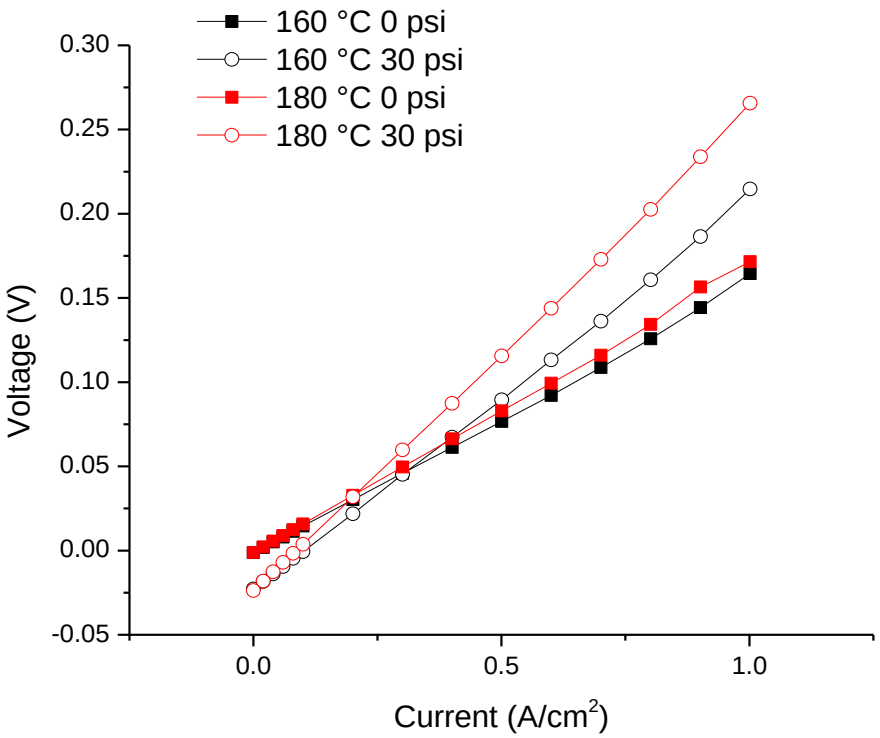

Figure 3.9 Celtec-P crosslinked with paraformaldehyde under EHS conditions. Pure H_2 test gas, 1.5 stoich. (minimum of 50 SCCM), and constant 45 °C water bottle temperature for humidification.

Celtec-P© crosslinked with paraformaldehyde showed improvements in creep compliance through ex-situ DMA testing but only showed slight improvements in failure at burst. Initial cell testing under Δp conditions does not give the indication that this modification is suitable for such applications, at least at these crosslinking concentrations (1 wt %).

3.4.2.2 Meta/Para PBI Membranes.

Meta/para (*m/p*) PBI gel membranes are comprised of a novel copolymer series that is still under investigation. Introducing the more soluble *meta*-PBI repeat unit into the less soluble *para*-PBI, in PPA, results in copolymer/PPA solutions having processable viscosities with much higher polymer content. Ex-situ results here and in prior research depicts a strong correlation to membrane solids content and its mechanical properties. It was envisioned that this mechanical enhancement would lead to a more pressure resistant membrane.

M/p based MEAs were evaluated through the same testing protocols as Celtec-P©. Pumping pure hydrogen was first investigated with varying cell temperatures and % RH. **Figure 3.10** shows that, *M/p* membranes followed the expected trend of decreasing voltage with increasing temperature, in contrast to the Celtec-P© membranes. However, the overall voltage was still higher in *m/p* membranes which translates to lower power efficiencies. This is likely due to the difference in conductivity between the *m/p* membranes and Celtec-P© membranes. The affects of two different RH levels (1.6 and 2.6 %) were also tested. At each temperature tested, the higher RH showed slightly lower voltages, which is generally believed to be from lowering interfacial resistances in the MEA and should be further investigated.

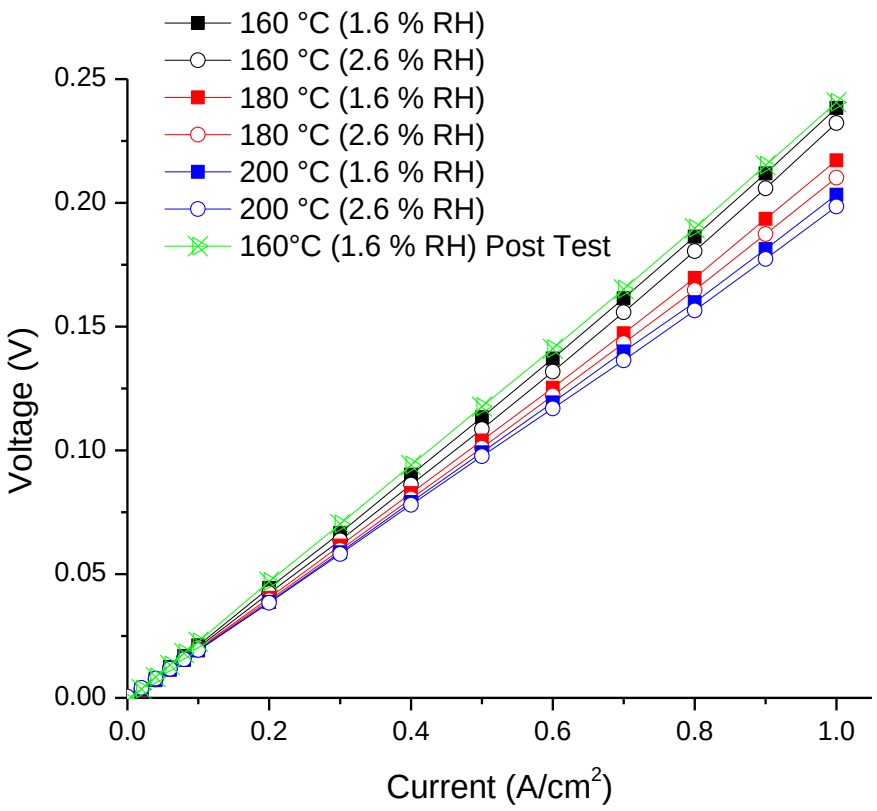

Figure 3.10 *M/p* PBI gel membrane under EHS conditions using pure hydrogen. Closed symbol = 1.6 % RH and open symbols = 2.6 % RH.

Polarization curves were subsequently taken at different anode back pressures to probe the MEA stability under differential pressure conditions. These results show that m-r-p membranes are also susceptible to a decrease in performance over time, albeit, at a slower rate. The comparison between m-r-p and Celtec-P© membranes can be seen in **Figure 3.11**, where results are both shown at day 1 and day 3. It is important to recall that Celtec-P© had a critical failure after 3 days under these testing conditions, where *m/p* was capable of running 10 days without signs of failure.

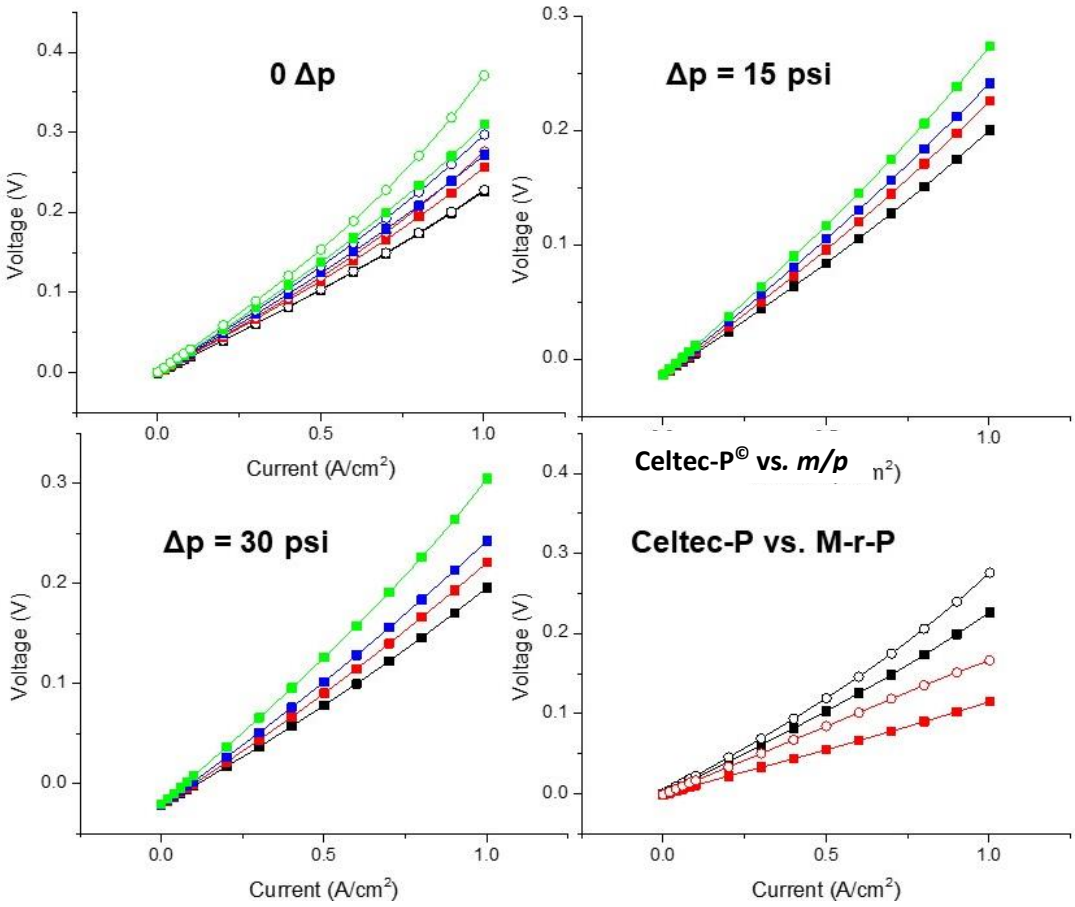

Figure 3.11 *M/p* based MEAs with the same pressure cycling previously shown on Celtec-P© (0 psi – 15 psi – 30 psi – 0 psi using pure hydrogen). Black lines represent day 1, red day 3, blue day 5, and green day 10. At 0 Δp filled in squares represent polarization curves at the beginning of the day and open circles are those at the end of the day. The graph in the bottom right (m-r-p black lines, Celtec-P© red lines) shows no back-pressure results at the beginning of the test (filled in squares) and no pressure at the end of 3 days (open circles).

EHS performance of m-r-p membranes with mixed gases show promising results in comparison to Celtec-P©. **Figure 3.12** shows that at low current densities (< 0.4 A/cm^2) the performance is nearly identical. This similarity in performance suggests that the major contributor to power inefficiencies is the anodic overpotential stemming from the large

amounts of catalyst poisoning CO in the feed stream and membrane resistance isn't a prominent concern until there is a high demand on the system (high current densities).

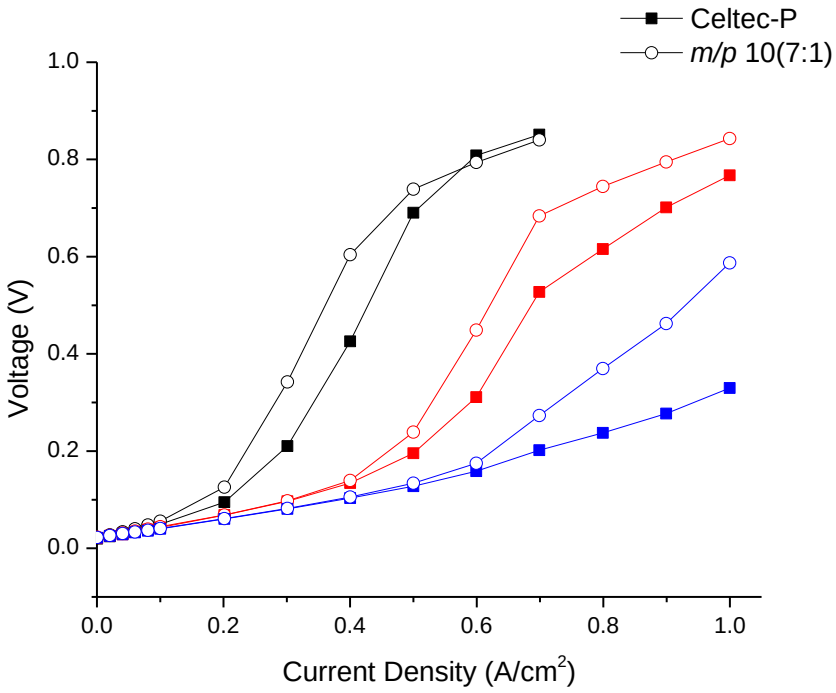

Figure 3.12 *M/p* PBI membranes compared to Celtec-P© with a reformate feed stream of 30, 3, and 67 mol % of H_2, CO, N_2 respectively. Black lines are at 160 °C, red 180 °C, and blue 200 °C

A *m/p* 10(7:1) (*m/p*-X) PBI membrane was crosslinked using DCB in N,N'-dimethylacetamide (refer to **Table 3.1**, X-link[4]) and tested under similar conditions. As mentioned previously, membrane cross-linking may enhance membrane mechanical stability allowing for longer lifetimes, especially under high differential pressure operation. **Figure 3.13** displays *m/p*-X PBI performance in EHS mode against pure hydrogen. As expected from the differences in ionic conductivity, the cell resistance was larger than Celtec-P©, however, the tests showed good linearity and reproducibility. Also, the expected trend of the relationship between temperature and performance was followed. Performance

for the crosslinked *m/p* PBI membrane was slightly lower (20 mV difference at 0.4 A/cm^2) than the non-crosslinked *m/p* 10(7:1) membrane. The crosslinked membrane had a surprisingly higher conductivity than its non-crosslinked counterpart (195 vs. 130 mS/cm at 180 °C), suggesting a better in cell performance. Due to the toughness of the membrane, it is likely that the interfacial resistance between the membrane and the electrode could be higher. This should be of interest in future work because the increased overpotential could be mitigated through MEA fabrication (hot press times, temperatures, or electrode pre-treatments) to take advantage of the improved mechanical properties *and* higher conductivities.

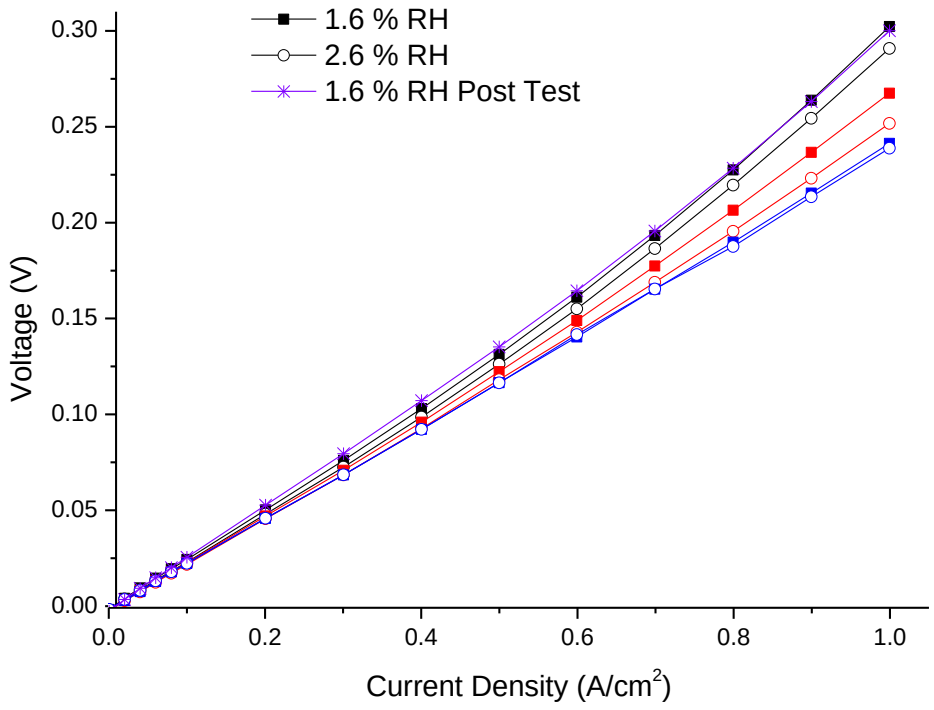

Figure 3.13 *M/p*-X PBI membranes under EHS conditions with pure H_2 as the feed stream. Black lines are 160 °C, red 180 °C, and blue 200 °C. Water bottle temperatures were adjusted to reach desired % RH and allowed to equilibrate.

Similarly, when testing *m/p*-X PBI membranes with the same mixed gas feed stream as Celtec-P© and *m/p* 10(7:1) PBI membranes, lower performance was observed (more power is needed), as shown in **Figure 3.14**. At low current densities this difference was not large but displayed a larger effect at high currents. Again, when considering the ex-situ membrane measurements, *m/p*-X PBI membranes had conductivities similar to *m/p* 10(7:1) PBI membranes, thus, this difference in performance may be the result of a poor interface between the electrode and membrane.

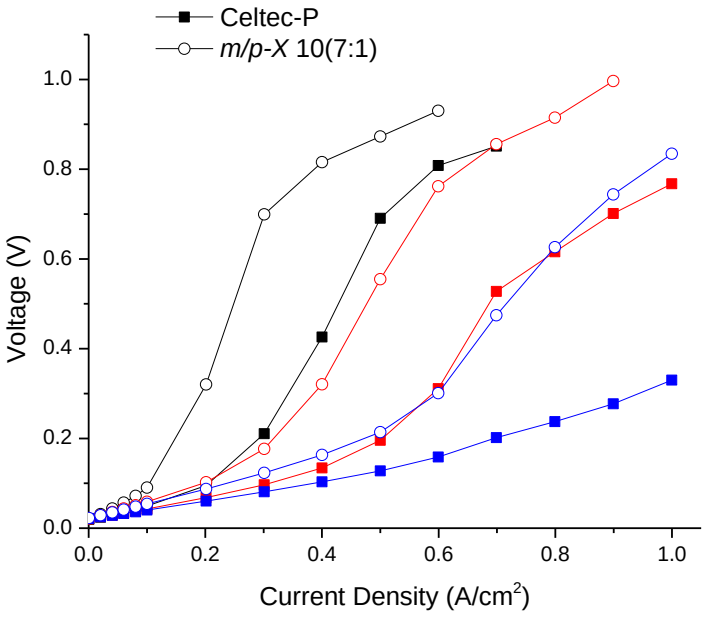

Figure 3.14 *m/p*-X in EHS mode, Celtec-P© for comparison, with reformate test gas comprised of 30, 3, and 67 mol % H_2, CO, and N_2 respectively. Black lines correspond to 160 °C, red 180 °C, and blue 200 °C. Water bottle temperature was maintained at 45 °C with 1.5 stoich gas flows according to H_2.

Figure 3.15 shows the *m/p* 10(7:1) non-crosslinked PBI membrane performance under a differential pressure of 30 psi on the anode. The membrane was capable of sustaining this mechanical load for over 3,500 hours before the test was ended (not due to membrane

failure), approximately 30 times longer than Celtec-P©. The first 1,000 hours, running with pure hydrogen, showed a negligible increase in voltage from mechanical deformation. Conditions were changed approximately every 500 hours; carbon monoxide content (1 mol

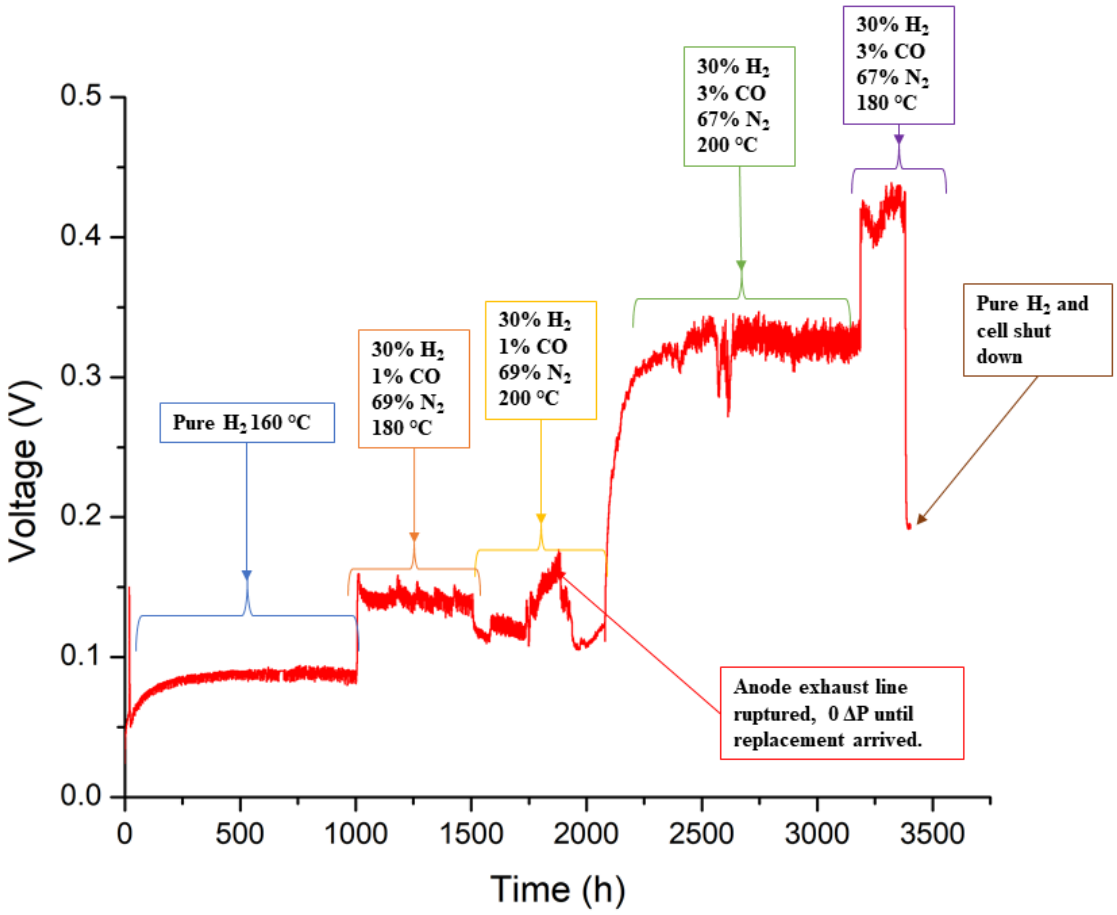

Figure 3.15 Long-term EHS performance of *m/p* PBI 10(7:1) under various conditions. Hydrogen stoichiometry was kept at a constant of 1.25 and a differential pressure of 30 psi was applied to the anode (except as noted in the red box).

- 3 mol %) and temperature (180 – 200 °C). The EHS performance was dramatically affected by the increase in CO content, as expected, considering its ability to bind to and poison the platinum catalyst. Increasing the temperature minimizes CO poisoning but can hasten mechanical deformation of the membrane. This was most evident by the differences in voltage observed on pure hydrogen at the beginning of the test (~80 mV at 160 °C) and

at the end of the test (~190 mV at 180 °C). However, even at 200 °C for approximately 1,500 hours the potential increase overtime was relatively low. This metric should be studied under steady-state conditions for a full understanding of the voltage contributions from mechanical deformation.

3.5 Conclusion.

Membranes were tested and evaluated to a benchmark set by Celtec-P©. To date, *m/p* copolymer membranes offer a unique alternative to the conventional *p*-PBI (Celtec-P©). It was found that Celtec-P©, as expected from its high ionic conductivities, had the best performance under standard operating conditions (160 °C with no back pressure). However, these *p*-PBI membranes have low polymer content which has been shown to be directly correlated with their low creep resistance. This physical properties become pronounced when membranes are subjected to more harsh operating conditions, i.e. increased temperature to mitigate catalyst poisons and differential pressures for more robust applications, where membrane performance losses and critical failure are evident. *p*-PBI membranes were crosslinked and showed increased mechanical properties, i.e. creep compliance at pressure at burst, and maintain high ionic conductivities. These new crosslinked *p*-PBI membranes should be further investigated as their *ex-situ* properties suggest they are viable options for EHS applications. Higher polymer solids membranes, *m/p*-PBI 10(7:1), were also studied for the efficacy in EHS applications. *m/p*-PBI membranes display increased mechanical properties over *p*-PBI membranes which was also evident in their long-term performance and stability under differential pressures. *m/p*-PBI membranes were also crosslinked which further improved mechanical stability and increased ionic conductivities. When using mixed gas feed streams with low hydrogen

content and high concentration of gases that acts as poisons to the platinum catalyst, it was found that higher temperatures (>160 °C) are required as it substantially improves catalyst and overall performance. However, the combination of higher temperatures and differential pressure operations will require improvements in membrane stability.

3.6 References.

1. H. C. Rowles, D. M. Nicholas, H. L. Vines and M. F. Hilton, *Energy Prog.; (United States)*, Medium: X; Size: Pages: 25 (1986).
2. J. Shu, B. P. A. Grandjean, A. V. Neste and S. Kaliaguine1, *The Canadian Journal of Chemical Engineering*, **69**, 1036 (1991).
3. P. Li, Z. Wang, Z. Qiao, Y. Liu, X. Cao, W. Li, J. Wang and S. Wang, *Journal of Membrane Science*, **495**, 130 (2015).
4. H. J. R. Maget, Process for Gas Purification, U.S. Patent 3489670, in (Jan. 13,1970).
5. J. F. McElroy, in *Energy Conversion Engineering Conference*, p. 1631, Proceedings of the 24th Intersociety, Washington, DC, USA (Aug. 1989).
6. B. Rohland, K. Eberle, R. Strobel, J. Scholta and J. Garche, *Electrochem. Acta.*, **43**, 3841 (1998).
7. K. A. Perry, G. A. Eisman and B. C. Benicewicz, *J. Power Sources*, **177**, 478 (2008).
8. Q. Li, J. O. Jensen, R. F. Savinell and N. J. Bjerrum, *Progress in Polymer Science*, **34**, 449 (2009).
9. L. Qiao, H. Zhang, M. Li, Z. Yuan, Y. Zhao and X. Li, *Journal of Materials Chemistry A*, **5**, 25555 (2017).
10. I. B. Valtcheva, P. Marchetti and A. G. Livingston, *Journal of Membrane Science*, **493**, 568 (2015).
11. J. Yang, H. Jiang, L. Gao, J. Wang, Y. Xu and R. He, *International Journal of Hydrogen Energy*, **43**, 3299 (2018).
12. M. Razali, C. Didaskalou, J. F. Kim, M. Babaei, E. Drioli, Y. M. Lee and G. Szekely, *ACS Applied Materials & Interfaces*, **9**, 11279 (2017).
13. X. M. Chen, G. Q. Qian, M. A. Molleo, B. C. Benicewicz and H. J. Ploehn, *Journal of Polymer Science Part B-Polymer Physics*, **53**, 1527 (2015).

3.7 Performance Summary.

Table 3.2: Membrane EHS performance and power consumption under various conditions.

EHS Performance		Celtec-P		m-r-p (7:1)		m-r-p (7:1) X-link 4		Celtec-P X-link 5		
	Current Density (A/cm^2)	Voltage (mV)	Power (mW/cm^2)	Voltage (mV)	Power (mW/cm^2)	Voltage (mV)	Power (mW/cm^2)	Voltage (mV)	Power (mW/cm^2)	
100% H_2 160°C	0.2	25	5	41	8	50	10	30	6	10 cm^2 cell
	0.4	51	20	83	33	103	41	61	24	minimum 50ml/min
	0.6	74	45	125	75	161	97	92	55	stoic 1.5
100% H_2 180°C	0.2	27	5	37	7	47	9	33	7	RH 1.6%
	0.4	53	21	76	30	96	38	66	27	No P on both side
	0.6	78	47	115	69	149	89	99	60	
100% H_2 200°C	0.2	31	6	35	7	46	9	-	-	
	0.4	62	25	72	29	92	37	-	-	
	0.6	90	54	109	65	140	84	-	-	
30% H_2 3% CO 160°C	0.2	95	19	126	25	320	64	-	-	10 cm^2 cell
	0.4	426	170	604	242	816	326	-	-	minimum 200ml/min
	0.6	808	485	794	476	930	558	-	-	stoic 1.25
30% H_2 3% CO 180°C	0.2	68	14	69	14	102	20	-	-	Water Bottle 65°C
	0.4	134	54	140	56	321	128	-	-	Anode 7.5 psi
	0.6	311	187	449	269	762	457	-	-	Cathode 7.5 psi
30% H_2 3% CO 200°C	0.2	60	12	61	12	87	17	-	-	
	0.4	103	41	105	42	163	65	-	-	
	0.6	159	95	175	105	301	181	-	-	
30% H_2 3% CO 160°C	0.4	730	292	722	289	844	338	-	-	10 cm^2 cell
	0.6	824	495	802	481	954	572	-	-	no minimum flow rate
30% H_2 3% CO 180°C	0.4	186	74	285	114	598	239	-	-	**80% H_2 seperation**
	0.6	390	234	603	362	789	473	-	-	Water Bottle 65°C
30% H_2 3% CO 200°C	0.4	117	47	125	50	202	81	-	-	Anode 7.5 psi
	0.6	169	101	214	129	364	218	-	-	Cathode 7.5 psi

CHAPTER 4

SULFONATED MEMBRANES FOR SO_2 DEPOLARIZED ELECTROLYZERS

4.1 Abstract.

The hybrid sulfur cycle has been investigated as a means to produce CO_2-free hydrogen efficiently on a large scale through the decomposition of H_2SO_4 to SO_2, O_2, and H_2O, and then electrochemically oxidizing SO_2 back to H_2SO_4 with the cogeneration of H_2. The net effect is the production of hydrogen and oxygen from water. Recently, sulfonated polybenzimidazoles (s-PBI) have been investigated as a replacement for Nafion due to the lower cost in membrane fabrication and the ability to offer increased process efficiency through the generation of higher acid concentrations at lower potentials. Here, we measure the acid concentrations and individual potential contributions towards the overall operating voltage observed in the SO_2-depolarized-electrolyzer. We then determine model parameters necessary to predict voltage losses in a cell over a wide range of operating temperatures, pressures, currents and reactant flow rates.

4.2 Introduction.

Currently, the main production of hydrogen is through the steam reformate process involving fossil fuels. In order to develop a hydrogen based society the increased demand for hydrogen must be accommodated and preferably done so without the need of fossil fuels. The hydrogen production program at the U. S. Department of Energy is examining an array of distributed and centralized hydrogen facilities that could contribute to the hydrogen generation infrastructure(1). Thermochemical cycles are being considered for large scale, centralized facilities due to their potential for high efficiencies at low costs. These cycles involve a series of chemical reactions that result in the splitting of water at much lower temperatures (~500-1000°C) than direct thermal dissociation (>2500°C) and at much higher efficiencies than direct water electrolysis(2). Chemical species in these

reactions are recycled resulting in the consumption of only heat and water to produce hydrogen and oxygen. Although there are hundreds of possible thermochemical cycles, the hybrid-sulfur (HyS) process is the only all-fluid, two step thermochemical cycle(3-6). The high temperature step (850-950°C) involves the decomposition of H_2SO_4 to produce oxygen and sulfur dioxide via the following reaction:

$$H_2SO_4 \rightarrow SO_2 + \frac{1}{2} O_2 + H_2O \qquad (1)$$

The SO_2 is separated, cooled, and sent to the SO_2-depolarized electrolyzer (SDE). The resulting reactions at the anode and cathode, respectively, are:

$$SO_2 + 2H_2O \rightarrow H_2SO_4 + 2H^+ + 2e^- \quad U^0_{SO2} = 0.158 \text{ V vs. SHE} \qquad (2)$$

$$2H^+ + 2e^- \rightarrow H_2 \quad U^0_{H2} = 0 \text{ V vs. SHE} \qquad (3)$$

The overall reaction in the electrolyzer is then:

$$SO_2 + 2\,H_2O \rightarrow H_2SO_4 + H_2 \qquad (4)$$

Leaving the total net reaction for the entire thermochemical process:

$$2\,H_2O \rightarrow O_2 + 2\,H_2 \qquad (5)$$

Considerable progress was made in the last decade in lowering the operating voltage and increasing the current density of the SDE by moving from a microporous rubber diaphragm separator used by Westinghouse (7) to a perfluorinated sulfonic acid membrane (e.g., Dupont's Nafion®) (8-12). For example, Westinghouse was only able to lower the cell voltage to 1.0 V at 400 mA/cm^2, where more recent work reported 500 mA/cm^2 at 0.71 V and 1.2 A/cm^2 at 1.0 V using Nafion 212 (N212). However, to achieve

overall process efficiency, concentrated sulfuric acid as well as low cell voltage at high current densities is necessary. The key issue when using membranes like Nafion that rely on water for their proton conductivity is that high acid concentrations dehydrate the membrane and dramatically increase membrane resistance. In previous work(10-12), the water needed for reaction 5 was controlled by varying the pressure differential across the cell, which in turn affected both the cell voltage and acid concentration.

Figure 4.1 illustrates the tradeoff between these two performance metrics. When there is no differential pressure ($\Delta P = 0$) across Nafion, minimal water crosses from the cathode to the anode, resulting in high acid concentrations that exceed 7 M and high cell voltages (0.90 V at 80°C and 500 mA/cm^2). When a differential pressure is created (ΔP = 600 kPa) additional water crosses over the membrane, lowering the cell voltage at 0.5 A/cm^2 from 0.9 V to 0.72 V through an increase in the membrane conductivity. However, this additional water results in a decrease in the acid concentration to 4.5 M at the anode. In contrast, sulfuric acid-doped polybenzimidazole (s-PBI) membranes represent an alternative to membranes like Nafion because they do not rely on water for their proton conductivity. **Figure 4.1** also shows the voltage and acid concentration for an SDE with sulfonated polybenzimidazole (s-PBI) operated at 110°C and 500 mA/cm^2. Here we achieved 0.68 V with an acid concentration of 7.0 M. The acid concentration was varied by adjusting the water fed to the cell, which had little effect on the cell voltage. Consequently, these two performance metrics can be varied independently.

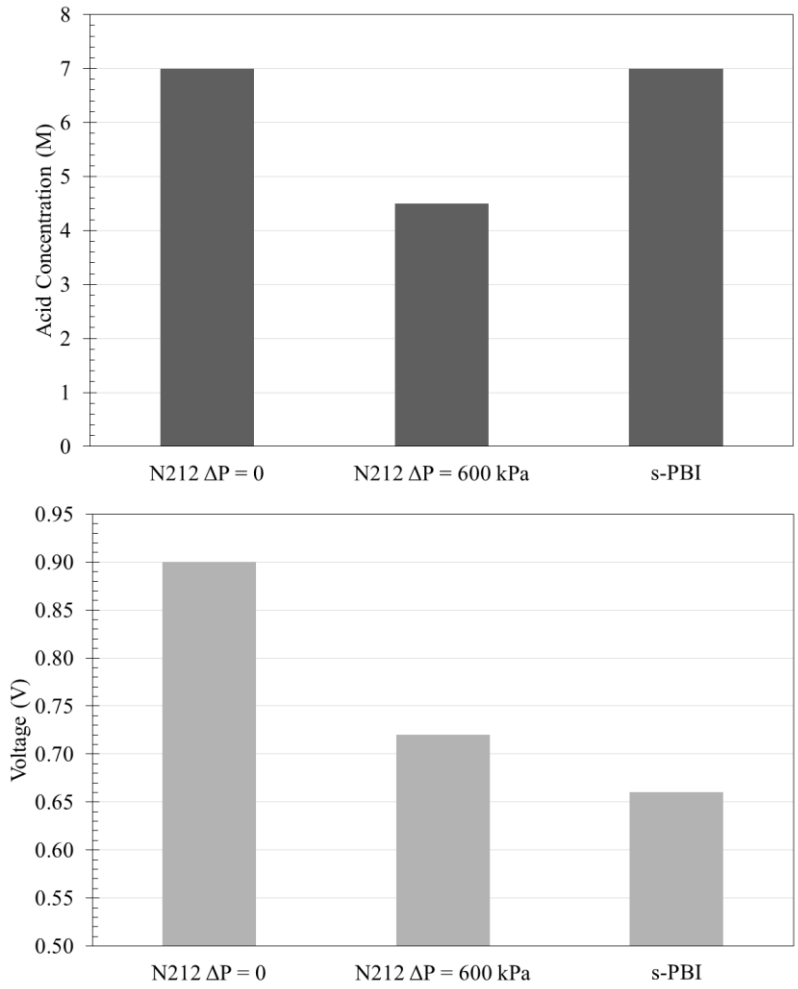

Figure 4.1 The sulfuric acid concentration (top) and the cell voltage at 0.5 A/cm^2 (bottom) for Nafion at 80 °C at two differential pressures (ΔP)(11) and s-PBI at 110 °C.

Therefore, polybenzimidazole (PBI) membranes offer the possibility of operating at high acid concentrations and/or elevated temperatures to minimize voltage losses (e.g., kinetic and ohmic resistances) (4, 13-15). PBIs are a class of aromatic heterocyclic polymers that exhibit high thermal and chemical stabilities and tailorable chemistries for different applications. PBI membranes have exceptional performance characteristics in various electrochemical devices due to their high ionic conductivity when imbibed with various acid electrolytes.(16-21) To date, a large variety of PBI polymers have been

synthesized and studied, and a sulfonated polybenzimidazole (s-PBI) was selected for use in SDE applications due to its stability in concentrated sulfuric acid environments, even at elevated temperatures, which are present in the SO_2 depolarized electrolyzer (SDE).(13) These inherent attributes of s-PBI have sparked an increased interest in utilizing PBI for SDE applications.(20, 22-24). Recent literature has focused on using different blends of PBI with highly sulfonated polymers (80 wt%, measured by EDX)(20, 24) during membrane preparation, partially fluorinated PBI(22, 24), and crosslinked PBI(23). However, these SDEs were operated with liquid water in the cathode, relying on water crossover to provide the water for Reaction 2 at the anode. No attempt was made to decouple the cell voltage and acid concentration produced in the anode.

Here, we report the synthesis and membrane properties of sulfonated PBI (s-PBI) and analyze the voltage losses and acid concentration from an SDE operated using these membranes under a range of operating conditions. Namely, the current density was varied from 0.1 to 1.2 A/cm^2, the temperature from 75 to 122°C, and the water stoichiometry from 4 to 18. From these data, kinetic parameters and membrane conductivity were obtained to better understand and quantify the individual potential contributions to the cell voltage. These model parameters will enable the prediction of voltage losses in a cell over a wide range of operating temperatures, pressures, currents and reactant flow rates.

4.3 Experimental.

4.3.1 Materials.

3,3',4,4'-Tetraaminobiphenyl (TAB, polymer grade, ~97.5%) was donated by BASF Fuel Cell, Inc. and used as received. Mono-sodium-2-sulfoterepthalate (>98 %

purity) was purchased from TCI Chemicals and used as received. Polyphosphoric acid (PPA) 115% was supplied from FMC Corporation and used as received.

4.3.2 Polymer Synthesis and Membrane Formation.

S-PBI was synthesized, as seen in Figure 2, with a pre-sulfonated monomer, mono-sodium-2-sulfoterephthalate, to ensure 100 percent sulfonation of the synthesized polymer.(25) In a typical reaction, 2.226 g of mono-sodium-2-sulfoterephthalate was combined with 1.778 g 3,3',4,4'-tetraaminobiphenyl and 96 g of PPA in a 3-necked resin kettle equipped with nitrogen flow and an overhead mechanical stirrer. The solutions were heated to 195 °C via a ramp and soak method and allowed to sit at that temperature for 30 – 40 hours. The solutions were then held at 220 °C for at least one hour before casting into films. The stir-rate and the temperature were monitored and controlled during the polymerization. Upon reaching an optimal casting viscosity, which was judged visually, the polymer solutions were poured onto a heated glass plate. Using a doctor's blade, the s-PBI solutions were drawn across the plates to a uniform thickness of 15 mils (381 microns). The glass plates containing the cast solution were immediately placed into a humidity-controlled chamber at 55% ± 5% relative humidity (RH), 25 °C ± 2 °C. This method was used to drive the formation of gel membranes through the sol-gel process. Complete hydrolysis of the membranes occurred in under 24 hours. The final gel thickness was approximately 300-500 microns. The hydrolyzed polymer membranes with an area of at least 80 cm^2 directly cast from PPA solution were soaked in a de-ionized water bath for phosphoric acid removal, and the water bath pH was monitored to ensure complete phosphoric acid removal. The PBI membranes were then immersed in a 30-50 wt% H_2SO_4 bath at various temperatures for the imbibing procedure.

4.3.3 Membrane Composition.

The composition of sulfuric acid-doped PBI membranes was determined by measuring the relative amounts of polymer solids, water, and acid in the membranes. The sulfuric acid (SA) content of a membrane was determined by titrating a membrane sample with standardized sodium hydroxide solution (0.10 M) using a Metrohm 716 DMS Titrino auto-titrator. Once titrated, the sample was thoroughly washed with DI water and dried at reduced pressures at 120 °C overnight. The dried sample was then weighed to determine the polymer solids content of the membrane.

Using **equations 1 and 2**, the polymer weight percentage and sulfuric acid weight percentage can be determined, respectively;

$$Polymer\ \ w/w\ \ \% = \frac{W_{dry}}{W_{sample}} \cdot 100 \qquad (1)$$

$$Acid\ w/w\ \ \% = \frac{M_{acid} \cdot V_{NaOH} \cdot c_{NaOH}}{2 \cdot W_{sample}} \qquad (2)$$

where W_{sample} is the weight of the sample before titration, W_{dry} is the weight of final dried sample after titration, M_{acid} is the molecular weight of sulfuric acid, and V_{NaOH} and c_{NaOH} are the volume and concentration of the sodium hydroxide solution required to neutralize the sulfuric acid to the first equivalence point. Due to the strong acidity of both protons of sulfuric acid (pka of -3 and 1.99 respectively), when titrating with a relatively weak base only one equivalence point is measured and is indicative of the titration of both protons of sulfuric acid.

The number of moles of sulfuric acid per mole of PBI repeat unit (or the SA doping levels, X) were calculated from the equation:

$$X = \frac{V_{NaOH} \cdot \frac{c_{NaOH}}{2}}{W_{dry} / M_{polymer}} \qquad (3)$$

where V_{NaOH} and c_{NaOH} are the volume and concentration of the sodium hydroxide solution required to neutralize the sulfuric acid to the first equivalence point, W_{dry} is the final weight of the dried sample after titration, and $M_{polymer}$ is the molecular weight of the polymer repeat unit.

4.3.4 Proton Conductivity.

Proton conductivities of the membrane were measured by a four-probe electrochemical impedance spectroscopy method using a Zahner IM6e electrochemical workstation over the frequency range from 1 Hz to 100 kHz with an amplitude of 5 mV. A two-component model with an ohmic resistance in parallel with a capacitor was employed to fit the experimental data. The conductivities of the membrane at different temperatures were calculated from the membrane resistance obtained from the model simulation with the following equation:

$$\sigma = \frac{d}{l \cdot w \cdot R_m} \qquad (4)$$

Where d is the distance between the two inner probes, l is the thickness of the membrane, w is the width of the membrane, and R_m is the ohmic resistance determined by the model fitting. Membrane samples underwent two heating ramps to 120 °C. Conductivity data reported was recorded on the second heat ramp, after water was removed from the membrane during the first heating cycle.

4.3.5 Membrane Electrode Assembly (MEA) Fabrication.

Sub-gasked MEAs were assembled with Kapton frames that were thermally adhered to gas diffusion electrodes (GDEs) supplied by BASF Fuel Cell GmbH with 1.0 mg/cm^2 platinum loading. The membrane was placed between two sub-gasketed electrodes and hot-pressed at 140 °C for 50-60 seconds using 2.0x10^{4}N (4500 lbs) of force. Shim stock was used to reliably reach a target compression of 20% of the MEA thickness.(25)

4.3.6 SO_2 Depolarized Electrolyzer Operation.

The electrolyzer operation and acid-concentration measurements are similar to previous works(13). The exception is that water to humidify the SO_2 stream was directly injected into the feed stream at the entrance to the electrolyzer using a micropump rather than using a humidification bottle. The procedure enabled the water feed stream to be more accurately controlled. For all data reported here, the catalyst loading was 1.0 mg Pt/cm^2 and SO_2 was fed in significant excess (5-10% single-pass conversion) to neglect concentration variations.

High frequency resistance (HFR) measurements were used to determine the membrane resistance for each MEA tested. Approximately 20 membranes were cut from two separate sheets and were tested and used to determine the trend in membrane resistance as a function of temperature, pressure, and current density.

When testing 10 cm^2 MEAs, the contents of the anode exit stream were collected in an airtight container pressurized and heated to the same conditions present in the electrolyzer to ensure that no water condensed out of the vapor phase and diluted the resulting acid. When collecting acid, the operating conditions were held constant for between 5 and 30 minutes until approximately 20 mL of liquid was obtained. A few membranes were held for much longer periods (~12 hr) in order to confirm that the acid concentration obtained from the 20 mL sample was representative of the operating conditions, as well as to ensure that water was accounted for, and not absorbing into or diffusing through the membrane.

4.4 Results and Discussion.

4.4.1 Membrane Properties.

The synthesis of s-PBI polymer was conducted with a pre-sulfonated monomer. This method of polymerization offers two advantages over post-sulfonation techniques: [1] precise and quantifiable sulfonation of the membrane and [2] chemical stability of the sulfonate functional group. Sulfonation is a common "blocking" technique of aromatic rings used in organic chemistry because it is the only reversible electrophilic aromatic substitution reaction. The sulfonate group is easily placed onto the ring in concentrated sulfuric acid and just as easily removed in dilute sulfuric acid with elevated temperatures; essentially an "easy on, easy off" strategy. Thus, when post-sulfonating the polymer, the sulfonate will be more inclined to react with the more activated position on the ring. However, by pre-sulfonating the monomer the sulfonate group will be attached to a deactivated ring position of the polymer, stabilizing the functionality against easy removal. To demonstrate this, computational studies were performed on a *p*-PBI repeat unit to

determine the most likely site for an EAS reaction by predicting the protonated regioisomer with the lowest standard free energy. This was achieved by calculating the CH group with the highest proton affinity estimated by PM3/COSMO method utilizing the MOPAC program.(26)

The computational studies revealed the most likely position of sulfonation on the polymer backbone via a post-polymerization technique. The most activated positions are indicated in **Figure 4.2** by green circles (< 1 kcal mol^{-1} free energy) and red circles (< 3 kcal mol^{-1} free energy), and all positions are located on the 3,3',4,4'-tetraaminobiphenyl portion of the repeat unit. Sulfonating these positions would fall into the "easy on, easy off" regime and are likely unstable in typical operating conditions of sulfuric acid based electrochemical devices. Whereas, by pre-sulfonating the diacid in the reaction, functionality can be placed onto a deactivated position of the polymer repeat unit, increasing the chemical stability.

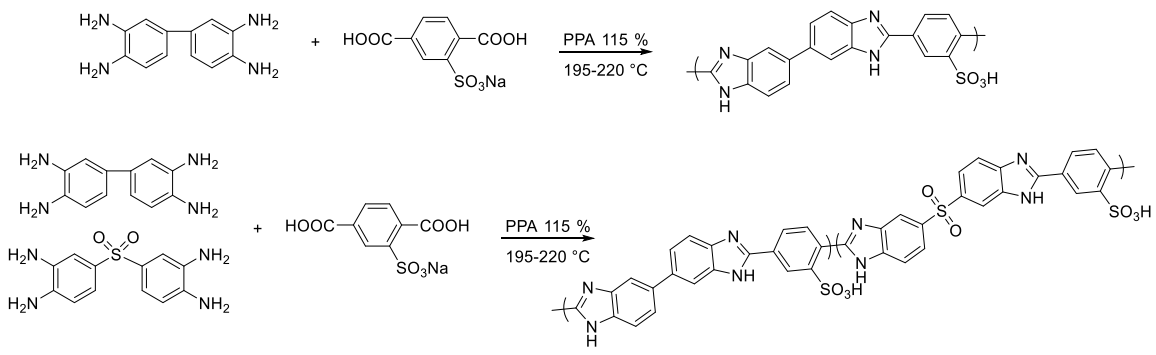

Scheme 4.1 Synthesis of s-PBI homopolymer and random copolymer with S-TAB.

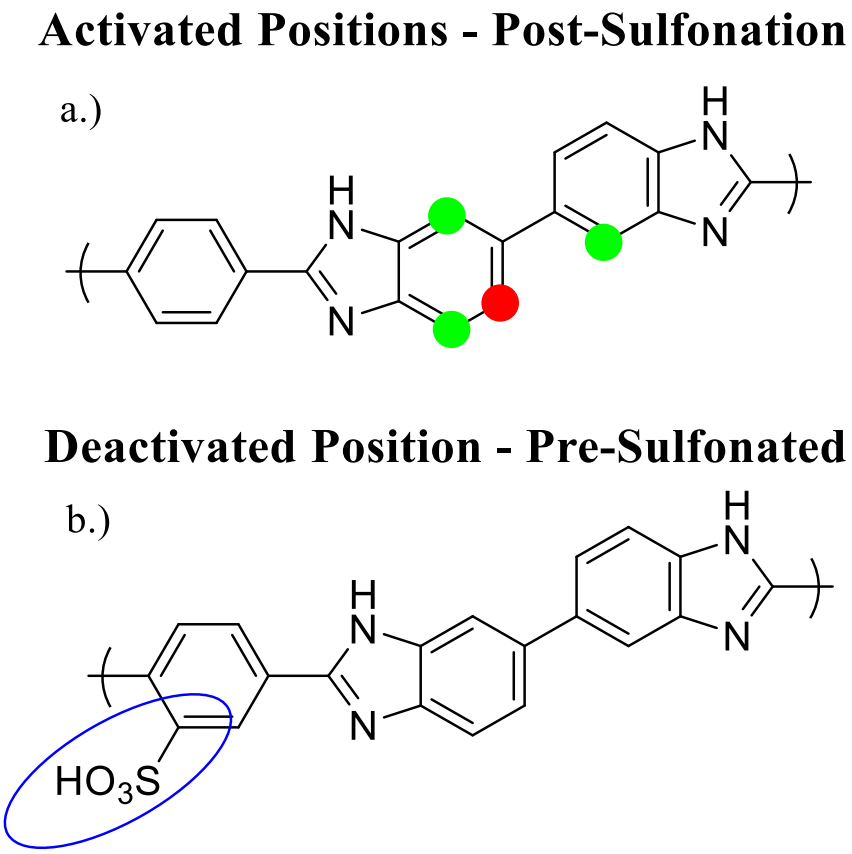

Figure 4.2 a.) Predicted regioselectivity of an EAS reaction on a *p*-PBI r.u. Green circles represent areas sites with free energies below 1 kcal mol^{-1} and red circles indicate free energies below 3 kcal mol^{-1}. b.) Location of the sulfonate group via the pre-sulfonation technique.

Pre-sulfonated monomers used for polymerizing a sulfonated PBI polymer, **Scheme 4.1**, resulted in gel membranes stable in 9.0 [M] sulfuric acid for > 3 years. Membranes were also found to be stable in the same solution at temperatures of 100 °C for extended periods of time. This attribute is not found in post-sulfonated or non-sulfonated membranes.

Table 4.1 s-PBI variants and acid loading technique on membrane composition and conductivity

Notebook #	Membrane	I.V. (dL/g)	Acid Bath Treatment	Polymer wt %	SA wt %	σ at 120 °C (Run 2*) (mS/cm)
AP1-129	s-PBI	1.30	50 wt % RT SA Bath	10.2	49.4	87
AP1-148 A	s-PBI	1.40	50 wt % RT SA Bath	10.6	40.5	91
AP1-148 B	s-PBI	1.40	50 wt % 80 °C SA Bath	19.8	42.2	27
AP1-158 A	s-PBI with 10% sulfo-tab (7 wt % Monomer Charge)	1.44	50 wt % RT SA Bath	6.3	67.5	N/A*
AP1-158 B	s-PBI with 10% sulfo-tab (7 wt % Monomer Charge)	1.44	50 wt % 80 °C SA Bath	12.3	40.8	N/A*
AP1-196 A	s-PBI	1.70	50 wt % RT SA Bath	9.6	45.6	93
AP1-196 B	s-PBI	1.70	30 wt % RT SA Bath	12.6	19.2	79
AP1-200	s-PBI	1.53	30 wt % Heated SA Bath	11	10.3	129
AP1-217	s-PBI with 10 % Sulfo-Tab Crosslinked (7 wt % Monomer Charge)**	1.44	50 wt % RT SA Bath	15	37.8	98
AP1-225	s-PBI Crosslinked	1.32	50 wt % RT SA Bath	10.6	33	145

* - Run 2 conductivities are considered anhydrous, conducted immediately following a previous temperature ramp.
N/A* - Membrane decomposed in conductivity cell before measurement completed
** - Crosslinked AP1-158 Membrane

The homopolymer of s-PBI was synthesized and acid exchanged in various conditions. **Figure 4.3** shows the conductivities of the various membranes from room temperature to 140 °C. The maximum conductivity, at 120 °C, was achieved in a heated 30 wt % sulfuric acid bath, 129 mS/cm. Room temperature baths of 50 and 30 wt % sulfuric acid gave conductivity values of 87-93 mS/cm and 79 mS/cm, respectively. The worst conductivity was a result of a heated 80 °C sulfuric acid bath, 27 mS/cm. At this temperature and acid concentration, sulfonation and sulfonation induced crosslinking reactions may occur, as seen by the dramatic increase in polymer content of the membrane.

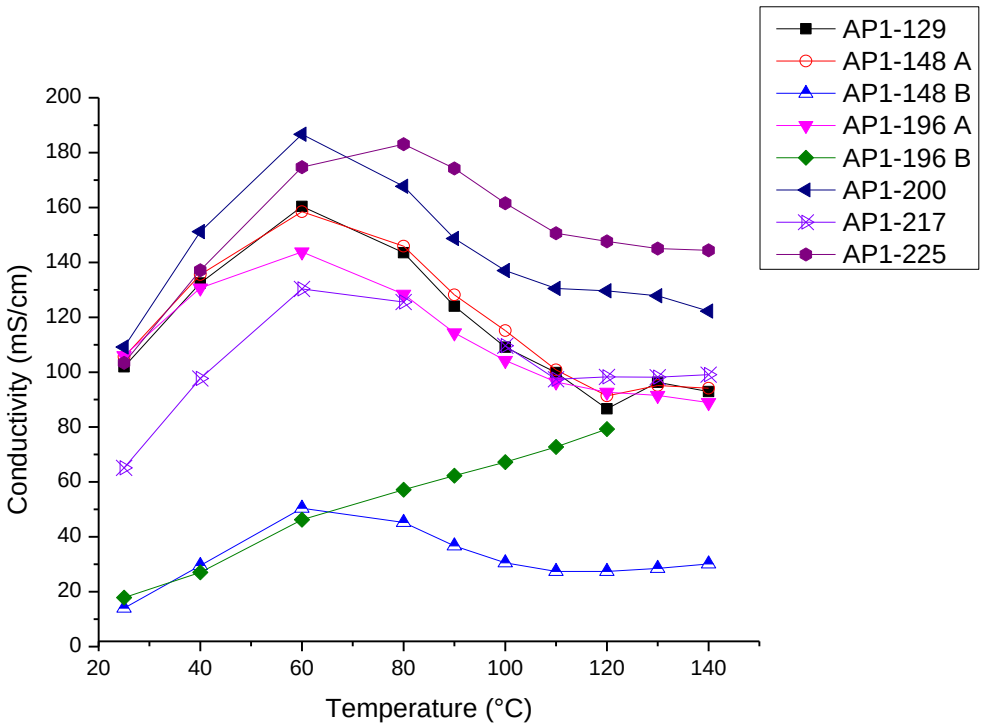

Figure 4.3 Anhydrous conductivities of sulfonated PBIs from room temperature to 140 °C.

An attempt to increase the mechanical stability of the membrane while maintaining high chemical resistance was done by adding increased polymer solids and sulfur content with a more flexible sulfone linkage, AP1-158 in **Table 4.1**. This polymer was achieved via a random copolymerization of mono-sodium-2-sulfoterephthalate, 3,3',4,4'-tetraaminobiphenyl (TAB), and 4,4'-sulfonylbis-1,2-benzenediamine (S-TAB); where TAB and S-TAB were used in a 9:1 ratio. Interestingly, even though the casting solution was more concentrated, i.e., higher solubility, when the membrane was acid exchanged with sulfuric acid the polymer content was less than that of the homopolymer of s-PBI. This result can be rationalized by the greatly increased acid uptake of the membrane, 67.5%. Furthermore, when the membrane was imbibed in a heated solution of sulfuric acid,

slight deterioration was observed. These membranes were also unable to complete a full conductivity test due to decomposition at elevated temperatures.

A crosslinking reaction was proposed to increase chemical stability of the membrane where N-alkylation reactions were conducted with a difunctional methyl-chloride compound, *α,α'*-dichloro-*p*-xylenes. AP1-158, which decomposed during conductivity testing, was selected as a candidate for this new reaction. Crosslinking increased the polymer solids content and not only improved chemical stability, and maintained structure throughout the conductivity test, but also increased the ionic conductivity over the homopolymer of s-PBI under the same acid imbibing conditions, 98 mS/cm. With these results, the same crosslinking technique was applied to s-PBI. Interestingly, there was minimal change in the membrane composition except a reduced loading of sulfuric acid. However, this membrane achieved the highest conductivity recorded under these conditions (RT 50 wt % SA bath), 145 mS/cm.

4.4.2 Electrolyzer Performance.

The electrolyzer cell voltage is the sum of the equilibrium potential, the potential rise due to the ohmic resistance of the membrane, the cathodic overpotential, and the anodic overpotential as expressed in the following equation:

$$V = U_{eq} + iR_A + \eta_a + \eta_c \qquad (5)$$

The cathodic overpotential of the electrolyzer is due to kinetic losses in the production of hydrogen at the cathode. Due to the fast nature of the reaction, the cathodic overpotential was assumed to be negligible and set to zero for all conditions shown here.

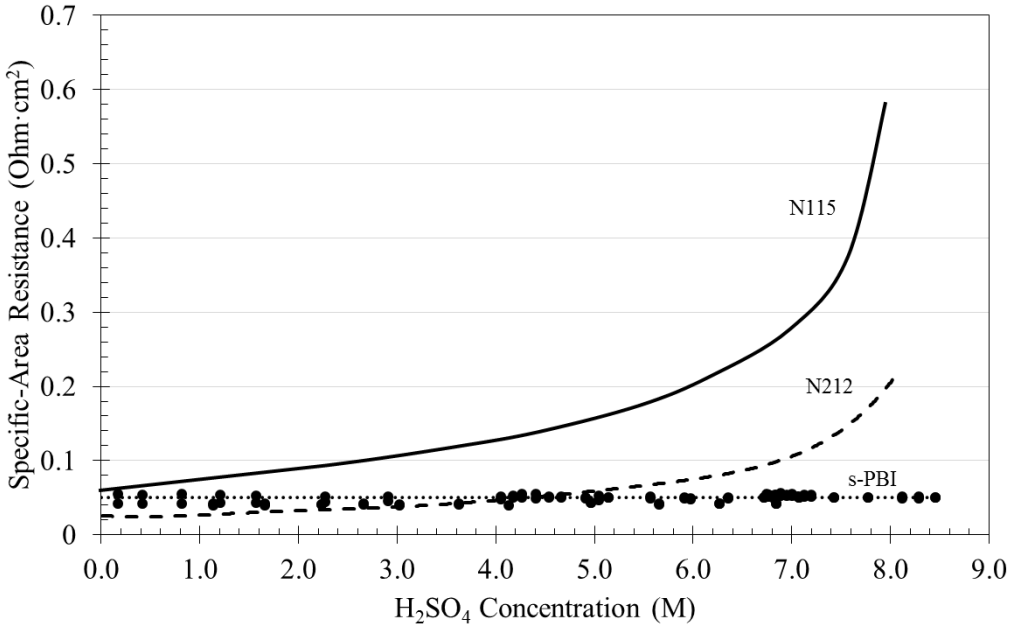

Figure 4.4 Specific area resistance as a function of sulfuric acid concentration for s-PBI obtained from multiple membranes compared to Nafion 115 and Nafion 212. ΔP = 600 kPa for the Nafion membranes, and no pressure differential used for s-PBI.

Figure 4.4 shows the membrane resistance as a function of acid concentration. The data for Nafion was obtained from previous works.(8, 11, 12) The data for s-PBI were collected during 18 different tests on different membranes with the temperature ranging from 70°C to 125°C. As seen here, as the acid concentration produced in the SDE with a Nafion membrane increased, the specific area resistance increased due to a decrease in the water content in the Nafion membrane.(8, 9, 11, 12) However, an increase in acid concentration at the anode in the SDE operated with s-PBI showed no adverse effect on membrane resistance because the conductivity of s-PBI is not dependent on water to

facilitate proton conduction. Also, due to the decoupling of acid concentration and membrane resistance, a pressure differential is not needed for SDE operation with s-PBI in order to maintain conductivities for efficient operation, allowing for operation at atmospheric pressure which is not an option with many SDE examples in the literature that utilize a Nafion membrane.(3, 6, 27-30) From this figure, the average specific area resistance, R_A, was 0.05 Ohm·cm^2 for s-PBI across all temperatures and acid concentrations, as obtained via HFR measurements. This value was used to calculate the potential rise due to the ohmic resistance in the membrane, iR_A.

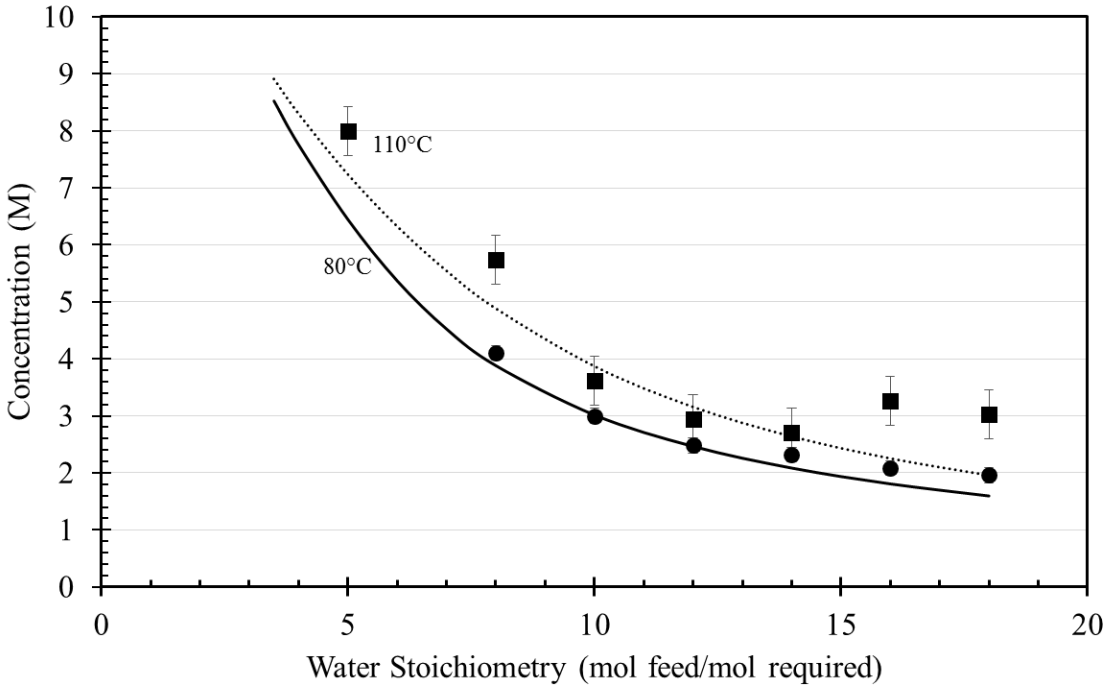

Figure 4.5 Sulfuric-acid concentrations produced in the cell at 0.5 A/cm^2 and either 80 (circles) or 110°C (squares) as a function of water stoichiometry. The water stoichiometry refers to the ratio of the moles of water fed to the cathode to that required via Eqn. 4 at a given current. The lines are the acid concentrations predicted from the Mixed Solvent Electrolyte Thermodynamics Framework (MSE) package in the OLI Systems, Inc. electrolyte software.

Figure 4.5 shows the sulfuric-acid concentration produced in the cell at 0.5 A/cm^2 and either 80°C or 110°C as a function of water stoichiometry. According to Eqn. 4, 2 moles of water are required for every mole of SO_2 consumed. Therefore, water stoichiometry refers to the ratio of the moles of water fed to the cathode to that required via Eqn. 4 at a given current. For example, 5 A are passed at 0.5 A/cm^2 for a 10 cm^2 MEA, which requires 51.8 μmol/s of water. Water stoichiometry of 10 means 518 μmol/s of water were fed. Increasing the water stoichiometry increases the excess of water and decreases the overall acid concentration in the exit stream. Also shown in Fig. 4 are the model predictions generated from the Mixed Solvent Electrolyte Thermodynamics Framework (MSE) package in the OLI Systems, Inc. electrolyte software. The good agreement between the model predictions and the data confirms that the OLI electrolyte software can be used to accurately predict the sulfuric-acid concentration produced in the cell. In addition, accurate concentrations enable us to predict the equilibrium potential (U_{eq}) at different temperatures, pressures, currents, and reactant flow rates as described previously (31). The error bars represent errors due to uncertainty in the temperatures at which the acid was collected, as well as uncertainty in the pressure drop between the SDE and the pressure sensor located immediately downstream from the SDE.

Using the predicted values for U_{eq} and iR_A, the anodic overpotential can be determined from the measured cell voltage and Eqn. 5. The relationship between the current density and the anodic overpotential is assumed to follow Tafel kinetics.(9)

$$i = i_0 e^{\frac{\alpha n F \eta_a}{RT}} \qquad (6)$$

where i_0 is the exchange current density and is defined as follows:

$$i_0 = nFk \tag{7}$$

The kinetic term k is assumed to be independent of the catalyst loading and only depends on temperature via the Arrhenius relationship:

$$k = k_0 e^{\frac{-E}{RT}} \tag{8}$$

Equation 6 and 7 were used to fit the anodic overpotential calculated through Equation 5 to obtain k at several temperatures and 0.5 A/cm^2, which was in turn fit to Eqn. 8 to obtain k_0 and E of 3.06x10^8 A/cm^2 and 118 kJ/mol, respectively. Substituting the values of k_0 and E into Equation 8 and combining with Equations 7 and 6 allows for the prediction of the anodic overpotential at any temperature and current density.

Now that the individual voltage contributions can be predicted as a function of operating conditions, the individual potential contributions to the overall cell voltage can be examined. The individual potential contributions to the overall cell voltage can be displayed as a function of current density, seen in **Figure 4.6** at an operating temperature of 110 °C and a constant water feed (variable water stoichiometry). The iR_A curve is linear because R_A was found to be constant at 0.05 Ohm·cm^2 (see Fig. 3). The anodic overpotentials were predicted via Eqns. 6, and 7, and the equilibrium potentials were predicted using the OLI software in conjunction with thermodynamics examined in previous works.(31) At 0.5 A/cm^2, the cell voltage is approximately 660 mV, which consists of 290 mV from the equilibrium potential, 345 mV of anodic overpotential, and 25 mV iR_A drop due to membrane resistance.

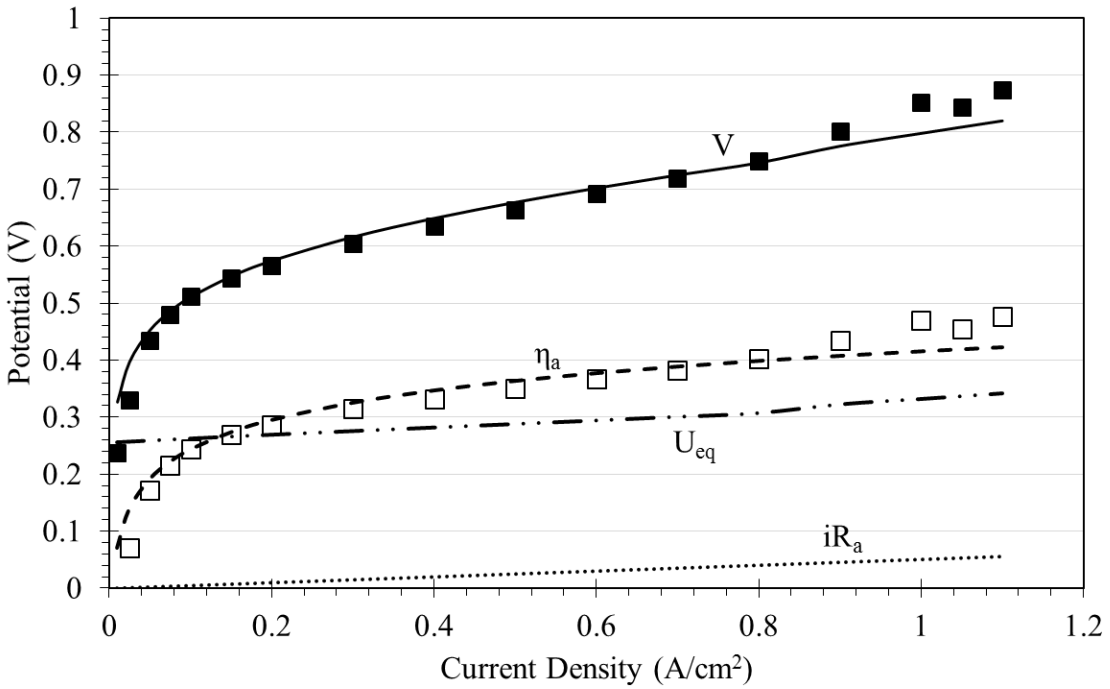

Figure 4.6 Individual potential contributions towards the overall cell voltage for the HyS electrolyzer at 110°C and a constant water feed rate of 0.45 mL/min. Lines represent model predictions and the symbols are the cell voltages (filled symbols) and anodic overpotentials (open symbols) data.

The largest contribution towards the total cell voltage at desired current densities is due to the anodic overpotential. From 0.2 to 1.0 A/cm^2, the cell voltage increases by 220 mV, with 150 mV of that coming from increased η_A. Although the membrane resistance increases with current, the small increase in iR_A is dwarfed by the increase in η_A and U_{eq}, the latter term associated with a slight increase in concentrations at higher currents due to a constant water feed for the data presented here.

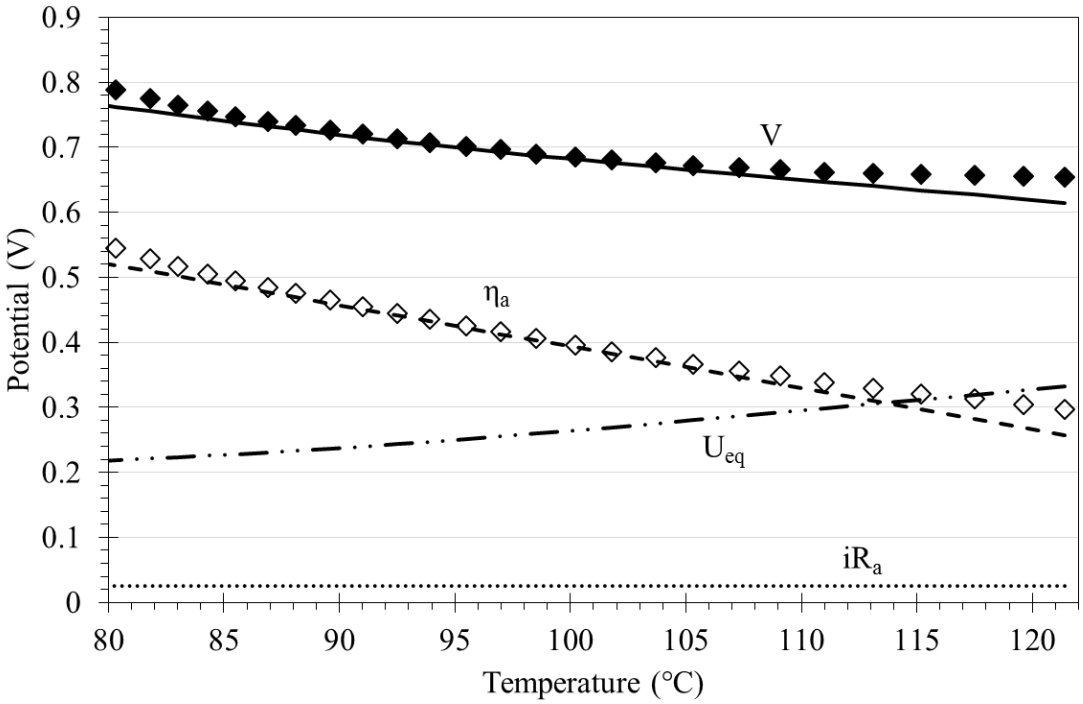

Figure 4.7 Contributions towards total operating voltage across a range of temperatures in the HyS electrolyzer at a current density of 0.5 A/cm^2 and a constant water flow rate of 0.50 mL/min. Lines represent model predictions and the symbols are the cell voltages (filled symbols) and anodic overpotentials (open symbols) data.

Figure 4.7 shows the potential contributions to the cell voltage as a function of temperature at 0.5 A/cm^2 and a constant water stoichiometry. The cell voltage decreases from 730 mV at 90°C to 650 mV at 120°C. The equilibrium potential increases over that temperature range from 240 to 320 mV due to an increase in the acid concentration from 3.3 to 6 M, which follows the relationship observed previously.(31) However, this is more than offset by a decrease in η_A from 440 mV to 300 mV coupled with the benefit of iR_A being independent of acid concentration. The effect of water stoichiometry and system pressure on cell voltage was found to only occur through its effect on the equilibrium voltage via the acid concentration. That is, higher pressures (from 1 to 3 atm) or higher water stoichiometry (from 5 to 18) decreases the acid concentration and hence decreases

the equilibrium voltage, but they do not measurably affect the membrane resistance or the anodic overpotential. Thus, the largest contribution to the overall cell potential is the anodic overpotential, which illustrates the area most deserving of future research. The model fit at 0.5 A/cm^2 and predictions at 0.25 A/cm^2 and 0.75 A/cm^2 are shown in **Figure 4.8** and is compared to experimental data at three different current densities. Overall, there is good agreement between the model predictions and data between 0.25 A/cm^2 and 0.75 A/cm^2, which confirms the validity of the physical parameters obtained in this study.

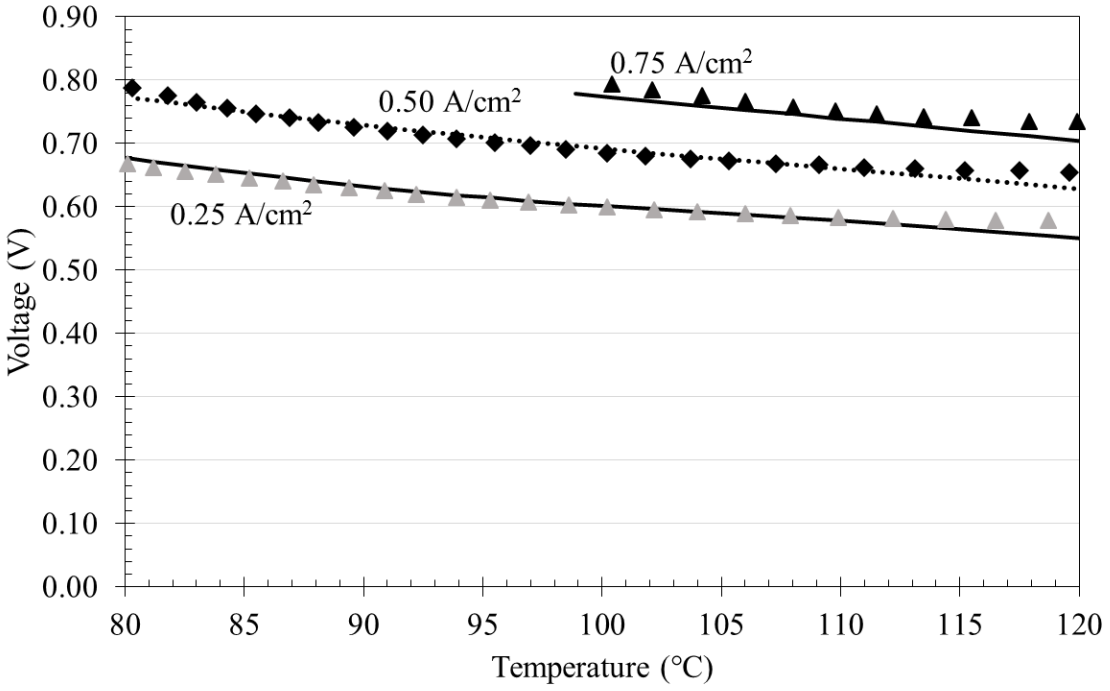

Figure 4.8 Model predictions compared to experimental data at three different current densities across a range of temperatures in the HyS electrolyzer at a constant water flow rate of 0.50 mL/min. The solid lines represent model predictions and dotted line represents the model fit at 0.5 A/cm^2 (i.e., same as the solid line in **Figure 4.7**).

4.5 Conclusion.

s-PBI and its derivatives were synthesized with pre-sulfonated monomers via the PPA Process to afford gel polymer electrolyte membranes with enhanced chemical durability. Computational studies were conducted on the polymer backbone structure indicating activated ring positions where sulfonate groups would most likely react in an electrophilic aromatic substitution, essentially an "easy-on, easy-off" strategy. This was in good agreement with experimental chemically stability tests of s-PBI synthesized from pre-sulfonated monomers where the sulfonate group was strategically placed in a more deactivated position. As a result, membranes fabricated from this technique were found to be stable in concentrated 9 [M] sulfuric acid for over three years and at elevated temperatures in the same electrolyte solution for greater than a week. Increased mechanical and chemical stability was also achieved via a n-alkylation post-membrane formation crosslinking. Furthermore, these membranes exhibited exceptional conductivities with varying degrees of acid loading, making them suitable for use in a SO_2 depolarized electrolyzer.

The contributions of the equilibrium potential, anodic overpotential, and ohmic losses due to membrane resistance have been examined for the SDE operated with s-PBI membranes at elevated temperatures. The large anodic overpotentials that exists in this system suggest a need for improved catalysts, and that kinetics would improve with the higher temperatures afforded s-PBI membranes. Also, the specific-area resistance of the membrane was independent of temperature over the range of 70-120°C and could potentially be reduced further using a crosslinked membrane affording more mechanical and chemical stability. In addition, the membrane resistance is not adversely affected by

acid concentration, which offers benefits not seen when using Nafion as the pressure and water stoichiometry only affect the overall cell voltage via the equilibrium potential. This work demonstrates that s-PBI is a viable candidate for use in a SO_2 depolarized electrolyzer since membrane resistance is independent of produced acid concentration, enabling increased round trip efficiency of sulfur species.

4.6 References.

1. U.S.DRIVE, Hydrogen Production Technical Team Roadmap, in (2013).
2. Nuclear Hydrogen Research and Development Plan, in, Department of Energy, Office of Nuclear Energy, Science and Technology (2004).
3. C. Corgnale and W. A. Summers, *Int J Hydrogen Energ*, **36**, 11604 (2011).
4. J. W. Weidner, *J Appl Electrochem*, **46**, 829 (2016).
5. C. Corgnale, S. Shimpalee, M. B. Gorensek, P. Satjaritanun, J. W. Weidner and W. A. Summers, *Int J Hydrogen Energ* (2017).
6. M. B. Gorensek and W. A. Summers, *Int J Hydrogen Energ*, **34**, 4097 (2009).
7. P. W. T. Lu, E. R. Garcia and R. L. Ammon, *J Appl Electrochem*, **11**, 347 (1981).
8. J. Staser, R. P. Ramasamy, P. Sivasubramanian and J. W. Weidner, *Electrochem Solid St*, **10**, E17 (2007).
9. J. A. Staser, M. B. Gorensek and J. W. Weidner, *J Electrochem Soc*, **157**, B952 (2010).
10. J. A. Staser, K. Norman, C. H. Fujimoto, M. A. Hickner and J. W. Weidner, *J Electrochem Soc*, **156**, B842 (2009).
11. J. A. Staser and J. W. Weidner, *J Electrochem Soc*, **156**, B16 (2009).
12. J. A. Staser and J. W. Weidner, *J Electrochem Soc*, **156**, B836 (2009).
13. J. V. Jayakumar, A. Gulledge, J. A. Staser, C. H. Kim, B. C. Benicewicz and J. W. Weidner, *Ecs Electrochem Lett*, **1**, F44 (2012).
14. T. R. Garrick, A. Gulledge, J. A. Staser, B. Benicewicz and J. W. Weidner, *Ecs Transactions*, **61**, 11 (2014).
15. T. R. Garrick, A. Gulledge, J. A. Staser, B. Benicewicz and J. W. Weidner, *ECS Transactions*, **66**, 31 (2015).
16. K. J. Fishel, A. L. Gulledge, A. T. Pingitore, J. P. Hoffman, W. P. Steckle and B. C. Benicewicz, *J Polym Sci Pol Chem*, **54**, 1795 (2016).
17. A. L. Gulledge and B. C. Benicewicz, *Abstr Pap Am Chem S*, **245** (2013).
18. A. L. Gulledge, X. M. Chen and B. C. Benicewicz, *J Polym Sci Pol Chem*, **52**, 619 (2014).
19. A. L. Gulledge, B. Gu and B. C. Benicewicz, *J Polym Sci Pol Chem*, **50**, 306 (2012).
20. P. J. Cichon, A. J. Kruger, H. M. Krieg, D. Bessarabou, K. Aniol and J. Kerres, *Int J Hydrogen Energ*, **41**, 4521 (2016).
21. L. Xiao, H. Zhang, E. Scanlon, L. S. Ramanthan, E. W. Choe, D. Rogers, T. Apple and B. C. Benicewicz, *Chem. Mater.*, **17**, 5328 (2005).
22. A. J. Kruger, P. Cichon, J. Kerres, D. Bessarabov and H. M. Krieg, *Int J Hydrogen Energ*, **40**, 3122 (2015).
23. A. J. Kruger, J. Kerres, D. Bessarabov and H. M. Krieg, *Int J Hydrogen Energ*, **40**, 8788 (2015).
24. H. Schoeman, H. M. Krieg, A. J. Kruger, A. Chromik, K. Krajinovic and J. Kerres, *Int J Hydrogen Energ*, **37**, 603 (2012).
25. J. A. Mader and B. C. Benicewicz, *Macromolecules*, **43**, 6706 (2010).
26. J. C. Kromann, J. H. Jensen, M. Kruszyk, M. Jessing and M. Jørgensen, *Chemical Science*, **9**, 660 (2018).

27. H. R. Colon-Mercado, M. C. Elvington, J. L. Steimke, T. J. Steeper, D. T. Herman, M. B. Gorensek, W. A. Summers and D. T. Hobbs, *Acs Sym Ser*, **1046**, 141 (2010).
28. M. B. Gorensek, W. A. Summers, E. J. Lahoda, C. O. Bolthrunis and R. Greyvenstein, *Proceedings of the 4th International Topical Meeting on High Temperature Reactor Technology - 2008, Vol 2*, 531 (2009).
29. W. A. Summers and M. B. Gorensek, *Chem Eng Prog*, **101**, 4 (2005).
30. W. A. Summers, J. L. Steimke, D. T. Hobbs, H. R. Colon-Mercado and M. B. Gorensek, *Proceedings of the 4th International Topical Meeting on High Temperature Reactor Technology - 2008, Vol 2*, 527 (2009).
31. M. B. Gorensek, J. A. Staser, T. G. Stanford and J. W. Weidner, *Int J Hydrogen Energ*, **34**, 6089 (2009).

CHAPTER 5

ADVANCED MEMBRANES FOR REDOX FLOW BATTERIES

5.1 Abstract.

Sulfonated polybenzimidazole (s-PBI) gel membranes were prepared and shown to have a high stability in concentrated sulfuric acid and strongly oxidizing vanadium (V) solutions. These membranes were considered candidates for use in vanadium redox flow batteries, and compared to the commonly used "conventionally imbibed" *meta*-polybenzimidazole (m-PBI) membranes cast from N,N'-dimethylacetamide (DMAc) solutions. The s-PBI membranes exhibited high conductivities and low performance degradation during in-cell testing.

5.2 Introduction.

Increasing demands on the energy sector have created a new need for large-scale energy storage devices with additional implications in grid management and back-up power, coincidentally with the seamless integration of new renewable energy devices. Redox flow batteries have the potential to both efficiently store large amounts of energy as well as meet cost expectations.(1, 2) In a vanadium redox flow battery (VRB) a major portion of the cost is attributed to the vanadium electrolyte. This cost can be off-set with a cheaper cell stack design. Currently, in commercial VRBs, PFSA membranes are used in the stack component, which has limited the forward progress due to their low selectivity and high cost.(1-4) To reduce costs of VRBs and increase overall performance, there has been a surge in membrane development activities tailored to the specific needs of VRBs.

Phosphoric acid (PA) doped polybenzimidazole (PBI) membranes are most notably known for their performance in high temperature polymer electrolyte membranes (HT-PEMs). However, PBI membranes have been shown to be a favorable candidate for

multiple new devices, such as electrochemical hydrogen separation, SO_2 depolarized electrolyzers, and redox flow batteries. To date, research on PBI membranes for flow batteries has focused around *meta*-polybenzimidazole (m-PBI) and its derivatives, membranes prepared by solution casting in N,N'-dimethylacetamide (DMAc) to form a dense film and later imbibing the formed film in the desired electrolyte, coined the "conventional imbibing process."(5) Membranes prepared by this method typically have pore sizes that range from 0.5 nm to 2.0 nm,(6) which is much smaller than the pore sizes found in PFSA (e.g., Nafion) type membranes (2-4 nm).(7) This decrease in interstitial space allows for the dramatically decreased permeability of vanadium ions compared to PFSA membranes, but also accounts for its extremely low conductivities when imbibed in common VRB electrolyte solutions (<20 $mS \cdot cm^{-1}$).(6, 8-12) The focal point of these recent works is to enhance the proton conductivity while maintaining the inherently low permeability of m-PBI dense films. These techniques include: pre-swelling the PBI films in concentrated phosphoric acid before doping with sulfuric acid,(9) using the vapor induced phase inversion method(7) and non-solvent induced phase separation to create a spongy porous structure,(8) and the grafting of various substituents to the PBI polymer backbone.(12, 13) To the best of our knowledge, no research has been conducted on the use of PBI gel membranes, formed from the PPA Process,(14) as alternative membranes for redox flow batteries.

The conventional imbibing process of PBI membranes is a time consuming, environmentally unfriendly technique that adds cost to the membrane fabrication process. However, Xiao et al. developed the novel PPA process to prepare PBI gel membranes which consists of a direct casting of the polymerization solution(14) comprising the PBI

polymer in polyphosphoric acid (PPA). Subsequent exposure of the cast solution to atmospheric moisture or controlled humidity conditions at room temperature hydrolyzes the PPA solvent, a good solvent for PBI, to phosphoric acid (PA), which is a poor solvent for PBI. This process induces a solution to gel transition forming a PBI gel membrane inherently imbibed in phosphoric acid.(14) Although these membranes are "pre-imbibed" in phosphoric acid, it has been shown that these membranes are capable of undergoing acid exchange of the imbibed electrolyte. Garrick et al. exchanged the phosphoric acid in sulfonated *para*-polybenzimidazole (s-PBI) membranes with 50 wt% sulfuric acid solutions for testing in a SO_2 depolarized electrolyzer used to generate hydrogen. The membrane exhibited high stability in concentrated sulfuric acid, even at 120 °C. Furthermore, the membrane resistance in the SO_2 depolarized electrolyzer was found to be almost negligible in comparison to the anodic overpotential, and this is attributed to the high ionic conductivity of s-PBI.(15, 16) Due to the exceptional stability of the PBI derivative and it's high conductivity, we envisioned s-PBI polymer gel membranes to be a possible alternative membrane for vanadium redox flow batteries with increased rate capabilities.

5.3 Experimental.

5.3.1 Materials.

3,3',4,4'-Tetraaminobiphenyl (TAB, polymer grade, ~97.5%) was donated by BASF Fuel Cell, Inc. and used as received. Monosodium 2-sulfoterephthalate (>98.00% purity) was purchased from TCI and used as received. Polyphosphoric acid (115%) was supplied from FMC Corporation and used as received. α,α'-Dichloro-p-xylene (>98.0% purity) was purchased from TCI and used as received.

5.3.2 Polymer synthesis and membrane fabrication.

A typical polymerization consisted of 10.71 g tetraaminobiphenyl (TAB, 50 mmol), and 13.44 g monosodium 2-sulfoterephthalate (s-TPA, 50 mmol) added to 580 g polyphosphoric acid, mixed with an overhead stirrer and purged with dry nitrogen. The contents were heated in a high temperature silicone oil bath, and the temperature was controlled by a programmable temperature controller with ramp and soak features. In a typical polymerization, the final reaction temperature was approximately 195 °C and held for 12 hours. Once the reaction was completed, determined by visual inspection of viscosity, the polymer solution was cast onto clear glass plates using a doctor blade with a controlled gate thickness of 15 mils. The cast solution was hydrolyzed into membranes in a humidity chamber regulated to 55% R.H. at 25 °C.

5.3.3 Acid Exchange.

As cast membranes were placed in DI water baths, and the pH of the water was monitored using pH strips. Water baths were replaced every 8 hours until a pH of 7 recorded. At this point the membrane was either placed into a 2.6 M sulfuric acid bath for 24 hours to ensure equilibrium of acid doping, or the membrane was further modified by a crosslinking reaction.

5.3.4 Post-membrane Formation Crosslinking.

After PA removal from the PBI gel membranes they were allowed to soak in a bath of 0.0523 M solution of α,α'-dichloro-p-xylene in methanol. The bath was covered, heated to 30 °C, and agitated with a magnetic stir bar. Crosslinking reactions were typically allowed to proceed for 6 hours. The membrane was then washed with DI water and

methanol cyclically, at least three times. The membrane was then transferred to a 2.6 M sulfuric acid (SA) bath for 24 hours for acid doping.

5.3.5 Membrane composition.

The composition of sulfuric acid-doped PBI membranes was determined by measuring the relative amounts of polymer solids, water, and acid in the membranes. The sulfuric acid (SA) content of a membrane was determined by titrating a membrane sample with standardized sodium hydroxide solution (0.10 M) using a Metrohm 888 DMS Titrando autotitrator. Once titrated, the sample was thoroughly washed with DI water and dried at reduced pressures at 120 °C overnight. The dried sample was then weighed to determine the polymer solids content of the membrane.

Using **equations 1 and 2**, the polymer weight percentage and sulfuric acid weight percentage can be determined, respectively;

$$Polymer\ w/w\ \% = \frac{W_{dry}}{W_{sample}} \cdot 100 \qquad (1)$$

$$Acid\ w/w\ \% = \frac{M_{acid} \cdot V_{NaOH} \cdot c_{NaOH}}{2 \cdot W_{sample}} \qquad (2)$$

where W_{sample} is the weight of the sample before titration, W_{dry} is the weight of final dried sample after titration, M_{acid} is the molecular weight of sulfuric acid, and V_{NaOH} and c_{NaOH} are the volume and concentration of the sodium hydroxide solution required to neutralize the sulfuric acid to the first equivalence point. It is important to note that even though the second proton of sulfuric acid is much less acidic than the first, it is still a strong enough acid to cause both protons to be titrated simultaneously, $pK_{a1} = -3$ and $pK_{a2} = 2$.

The number of moles of sulfuric acid per mole of PBI repeat unit (or the SA doping levels, X) were calculated from the equation:

$$X = \frac{V_{NaOH} \cdot c_{NaOH}}{2 \cdot {W_{dry}}/{M_{polymer}}} \quad (3)$$

where V_{NaOH} and c_{NaOH} are the volume and concentration of the sodium hydroxide solution required to neutralize the sulfuric acid to the first equivalence point, W_{dry} is the final weight of the dried sample after titration, and $M_{polymer}$ is the molecular weight of the polymer repeat unit.

5.3.6 Conductivity.

The membranes were imbibed with sulfuric acid and V^{4+} ions by immersion in 2.6 M sulfuric acid and 1.5 M $VOSO_4$ +2.6 M sulfuric acid solution respectively. In-plane conductivity of the membrane was measured by a four-probe electrochemical impedance spectroscopy (EIS) method using a FuelCon (TrueData EIS PCM) electrochemical workstation over the frequency range from 1 Hz to 50 kHz. A membrane sample with a typical geometry of 1.0 cm × 4.0 cm was fixed into the measuring 4-electrode head of the measurement. The conductivity of the membrane was calculated using the following equation:

$$\sigma = \frac{d}{l \cdot w \cdot R_m} \quad (4)$$

Where d is the distance between the two inner probes, l is the thickness of the membrane, w is the width of the membrane, and R_m is the ohmic resistance determined by the model fitting. Conductivities were conducted at room temperature, to replicate normal operating conditions of vanadium redox flow batteries.

5.3.7 Vanadium Permeability.

The crossover of vanadium(IV) ($VOSO_4$) was measured utilizing a PermeGear "side-by-side" direct permeation cell. The cell has two chambers with a 45 mL volume separated by the membrane under test. The temperature of the chambers was regulated at 25 °C with a recirculating water bath. A typical test experiment contained 1.5 M $VOSO_4$ in 2.6 M sulfuric acid in the donor chamber and 1.5 M $MgSO_4$ in 2.6 M sulfuric acid in the receptor chamber. Vanadium(IV) has a strong absorption characteristic at 248 nm; utilizing this property, the concentration of the receptor chamber was measured with a Shimadzu UV-2450 UV/Vis spectrometer at various time intervals. The VO^{2+} permeability can be calculated using Fick's diffusion law, **equation 5**,

$$P_s t = ln\left[1 - 2\frac{c_r(t)}{c_r(0)}\right]\left[-\frac{Vd}{A}\right] \quad (5)$$

where: $c_r(t)$ is the receptor $VOSO_4$ concentration at time *t*, $c_r(0)$ is the donor initial $VOSO_4$ concentration, V is the donor and receptor solution volume, d is the membrane thickness, A is the active area of the membrane, and P_s is the salt permeability.(4)

5.3.8 Membrane Stability in Oxidative V(V) Solution.

Membranes were soaked in a solution of 1.5 M V^{5+} in 2.6 M sulfuric acid. The solution was periodically titrated using a Hiranuma Auto Titrator COM-1700 against a control solution that did not contain a polymer membrane to measure the concentration of V^{5+} and V^{4+} ions.

5.3.9 Flow Battery Testing.

Flow battery test cells with 23 cm^2 active areas and specialized interdigitated flow fields for liquid electrolyte solutions machined into carbon (Tokai G347B), designed and

assembled by United Technologies Research Center (UTRC), were utilized. Membranes were sandwiched between identical carbon paper electrodes provided by UTRC (undisclosed vendor) that were heat treated to 400 °C for 30 hours, and gasketed with polytetrafluoroethylene (PTFE). The flow battery cells were equipped with two reservoirs containing 100 mL of Riverside electrolyte; 1.60 M of vanadium species with a +3.55 average oxidation state and 3.8 M total sulfur content. Cells were charged via a two-step process, where [1] the positive and negative electrolytes were by prepared by charging the initial solution containing $VOSO_4$ (V^{4+}) in sulfuric acid forming V^{3+} and VO_2^+ (V^{5+}). The positive electrolyte solution was then replaced with the initial solution and [2] charging was repeated to generate V^{2+} and V^{5+}. Electrolytes were fed to the cell with KNF diaphragm liquid pumps at a constant 120 mL/min flow rate. Electrolyte solution temperature was not controlled and was approximately 20 °C. The electrolyte tanks were equipped with a nitrogen purge inlet and outlet. OCV was limited between 1.50 and 1.30 V during cycling. Cells were cycled between 0.7 and 1.65 V at various current densities and cells were cycled 25 times or until electrolyte utilization was below 35%.

5.4 Results and Discussion.

The rate capability of a flow battery is highly dependent on the conductivity of the membrane. m-PBI membranes prepared from the conventional imbibing process have relatively low conductivities, limiting stable operation at high current densities. Herein, we investigate the use of a highly proton conductive membrane, s-PBI, for their use in vanadium redox flow batteries, **Scheme 5.1**.

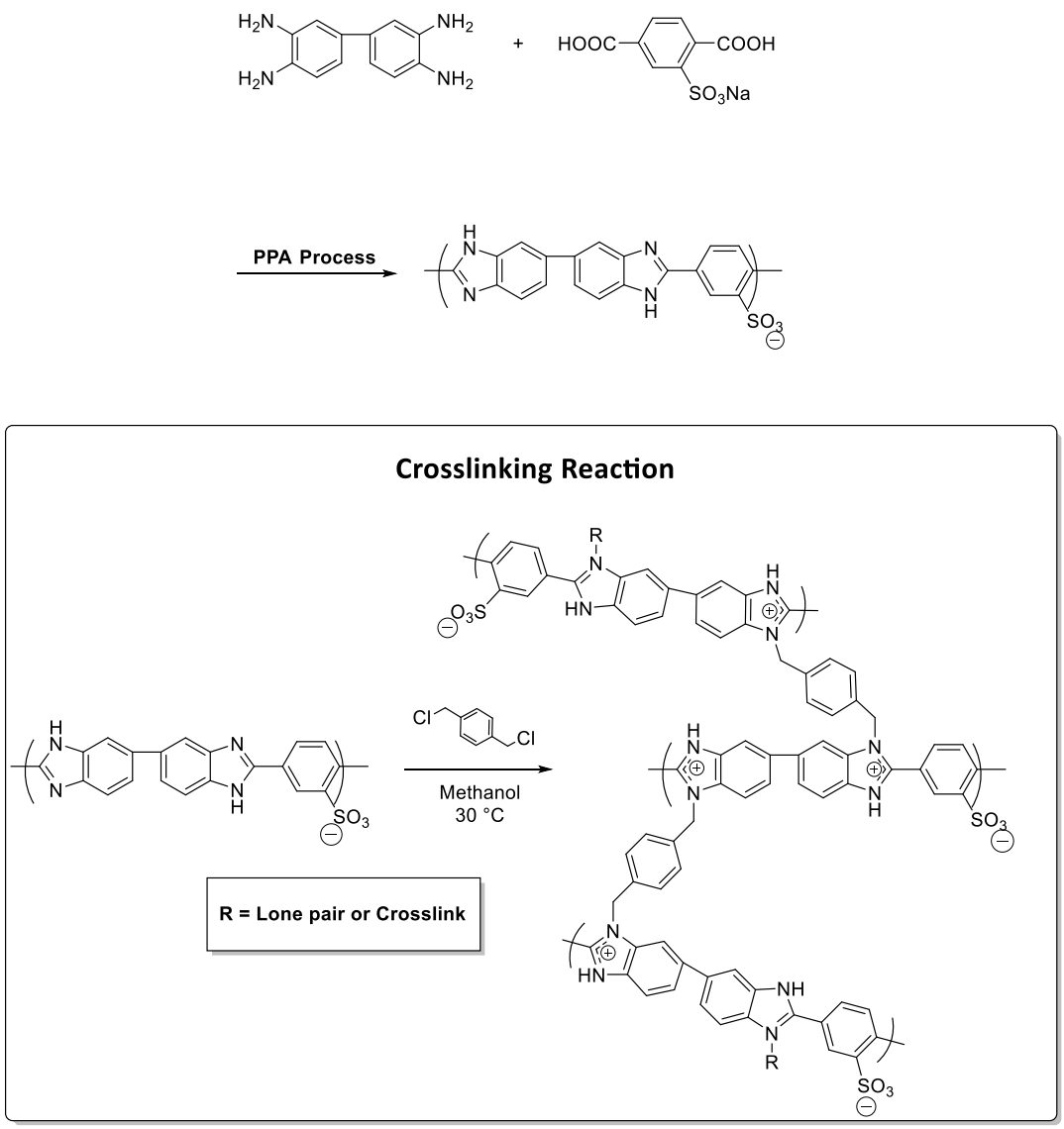

Scheme 5.1 Polymerization of s-PBI in PPA and membrane crosslinking modification reaction.

The *ex-situ* membrane properties for s-PBI gel membranes (both uncrosslinked and crosslinked) and m-PBI membranes formed from the conventional imbibing process are shown in **Table 5.1**. The room temperature conductivity of the membranes was evaluated in both 2.6 M sulfuric acid and a V(IV)/H^+ solution found in typical operating cell conditions. s-PBI gel membranes exhibit surprisingly high conductivities as

compared to the m-PBI membranes in both sulfuric acid and the acid electrolyte solution. The room temperature conductivities of the s-PBI and crosslinked s-PBI membranes were in the range of 537 – 593 $mS \cdot cm^{-1}$ compared to 13.1 $mS \cdot cm^{-1}$ for conventionally imbibed *m*-PBI in sulfuric acid and 240 – 242 $mS \cdot cm^{-1}$ compared to 12.2 $mS \cdot cm^{-1}$ in the vanadium acid electrolyte, respectively.

Table 5.1 Ex-situ properties of s-PBI gel membranes and conventionally imbibed m-PBI films.

Membrane	VO^{2+} Permeability ($cm^2 \cdot s^{-1}$)	Conductivity ($mS \cdot cm^{-1}$)[a]	Conductivity ($mS \cdot cm^{-1}$)[b]	% Polymer Solids	% Sulfuric Acid	% Water
s-PBI	5.74×10^{-7}	593	242	18.8	23.11	58.1
s-PBI-x	5.23×10^{-7}	537	240	30.6	35.6	33.8
m-PBI (conventionally imbibed)	2.53×10^{-11}	13.1	12.2	65.6	26.0	8.4

[a]Conductivity at r.t. after soaking in 2.6 M sulfuric acid
[b]Conductivity at r.t. after soaking in $V(IV)/H^+$ solution (1.5 M $VOSO_4$ + 2.6 M sulfuric acid) for 3 days

The slight difference in conductivity between the two s-PBI membranes is likely a result of cross-linking. s-PBI-x in **Table 5.1** is a s-PBI film that underwent a cross-linking modification post-hydrolysis of the membrane. The crosslinker forms bonds with the imidazole nitrogen and may slightly inhibit proton pathway through the hydrogen bond networks. When comparing imbibed solutions, the decrease in conductivity of the gel membranes in vanadium electrolyte solutions is thought to occur from two factors. The first is that vanadium ions may interact with the membrane by attractive forces with the negatively charged sulfonate group (pKa ~ -2), impeding the flow of protons. More so, the dramatic drop in conductivity in the PBI gel membranes is most likely attributed to the

intrinsic conductivity of the electrolyte solution containing vanadium ions.(17) Since the major contributor of proton conductivity is the mobility of ions, it is not surprising that an increase in vanadium concentration would diminish proton conductivity of the electrolyte solution solely with regards to an increase in viscosity of the electrolyte solution.(18) PBI gel membranes have a considerably open morphology that enhances proton conductivity by allowing not only proton transport via the Grotthuss mechanism but also mobility of the electrolyte in the membrane, thus proton transport through the membrane will also be affected by the increase in viscosity due to the incorporation of vanadium ions.

As a result, the electrolyte mobility in the PBI gel membrane is a plausible argument as to why vanadium permeability is significantly higher than its dense counterpart. This result is also not unexpected when considering the polymer solids of the membrane. From the data in **Table 5.1** it is evident s-PBI has a relatively small amount of polymer per the amount of electrolyte in the membrane compared to *m*-PBI membranes formed from the conventional imbibing process. Expecting PBI gel membranes to have high crossover of vanadium ions, we devised a mitigation route in which we could chemically crosslink the PBI chains together to fill interstitial space and limit chain mobility. Although the permeability of the s-PBI-x may still be too high for practical applications this slight modification does lower the permeability when compared to the non-crosslinked membrane and without having a dramatic effect on conductivity. Since this technique is impartial to the PBI derivative of choice, it could be used to hone the properties of PBI membranes as needed. At this time, we have not found a facile way to determine the cross-link density of the gel membrane, as typical gravimetric and rheological techniques carry large amounts of error with as-cast imbibed gel membranes.(19-21) However, to confirm

crosslinking occurred, a 50 mg sample of neutralized dried membrane was heated in 800 mL N,N'-dimethylacetamide at reflux for 48 hours. Under these conditions no membrane deterioration or solution color change was observed for the crosslinked sample, but dissolution was observed for the non-crosslinked polymer film.(22) Furthermore, the swell ratios of the crosslinked vs. non-crosslinked membranes affords noteworthy results. Utilizing a non-acid solvent (N,N'-dimethylacetamide), to ensure that unwanted solvent polymer interactions were suppressed, it was found that the non-crosslinked gel (3.94 wt% increase) absorbed approximately 0.75 wt% more solvent than the crosslinked membrane (3.25 wt% increase). Restriction of chain mobility by chemical crosslinks inhibits solvent swelling of the polymer gel, resulting in lower weight increase from solvent uptake.

Table 5.2 Oxidative stability of sulfonated PBI gel membranes in V^{5+} solutions.

Membrane	Date of Soak	Titration Date (2/16/2017)		Titration Date (6/30/2017)	
		V^{4+}	V^{5+}	V^{4+}	V^{5+}
V5+ Control	5/25/2016	Non-detectable	1.570	Non-detectable	1.583
s-PBI	5/25/2016	Non-detectable	1.551	Non-detectable	1.576

There are four common oxidation states for vanadium, all of which are present in VRB operation. Of these, VO_2^+ [V(V)] bears the highest oxidation state (+5). The facile reduction of this compound makes it a good oxidizing agent. During VRB operation, VO_2^+ is present in increasing concentrations as the battery is being charged. Due to its oxidative nature and the potential for prolonged interactions with the membrane separator, it is imperative to study the stability of the membrane under such conditions. The oxidative stability of the s-PBI base polymer was monitored by soaking a membrane in 2.6 M sulfuric

acid with approximately 1.5 M of V(V). Over the course of 1 year soaking in this solution various titration measurements were conducted to determine the concentration of V(V) remaining and the presence of V(IV) which would be produced consequently from membrane oxidation (vanadium reduction). **Table 5.2** shows that the concentration of V(V) is consistent with the control bath (no membrane) and the lack of V(IV) present suggests that s-PBI polymers are stable under these harsh conditions. This stability is not common for fully organic polymer membranes.(23)

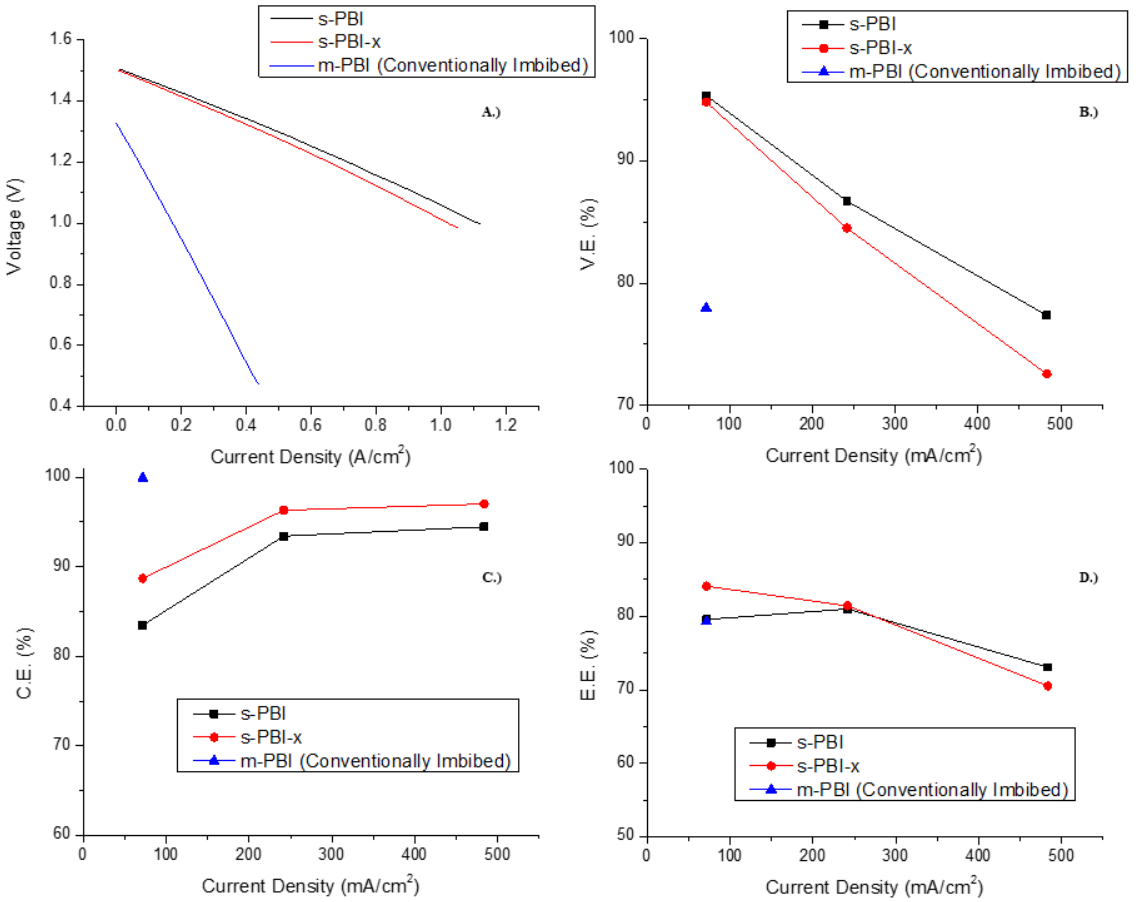

Figure 5.1 A.) Polarization curves with 80% state-of-charge electrolyte and cycling efficiencies [B.) voltage efficiencies, C.) coulombic efficiencies, and D.) energy efficiencies] of s-PBI, s-PBI-x, and m-PBI (conventionally imbibed) in a vanadium redox flow battery.

Membranes were tested in flow battery cells designed and assembled by United Technologies Research Center with specialized flow fields for liquid electrolytes. **Figure 5.1 A** shows polarization curves from 0 – 1.1 A/cm^2. The in-ability of conventionally imbibed m-PBI membranes to operate at current densities above 0.25 A/cm^2 is clearly apparent. This is attributed to the low ionic conductivity of the densely packed morphology. Both the s-PBI and its cross-linked form have relatively open structures and high ionic conductivity, which allows them to perform at higher currents densities. This is also seen with the relatively high voltage efficiencies, **Figure 5.1 B**, where the voltage ratio of discharge to charge at 483.3 mA/cm^2 is similar to that of conventionally imbibed m-PBI at 71.7 mA/cm^2. Since conventionally imbibed m-PBI performed poorly under these test conditions, cycling efficiencies could not be calculated beyond 200 mA/cm^2. Furthermore, there is only a slight difference in performance and voltage efficiency between the s-PBI and s-PBI-x. This can be explained by the slightly higher conductivity of s-PBI over s-PBI-x. However, the coulombic efficiency, a ratio of electrons discharged to charged, represents the downfall of such porous membranes as it is severely impacted by the crossover of reactive species. It is important to note that this contribution to inefficiency is dramatically reduced at high current densities where the increased reaction speed can outpace parasitic losses from crossover, **Figure 5.1 C**. The overall energy efficiency, a product of coulombic and voltage efficiencies, is a useful metric to determine the amount of energy lost during charge/discharge cycling. The results shown in **Figure 5.1 D** indicate a promising potential use of PBI gel membranes formed from the PPA process. Even at low current densities, where the coulombic inefficiency is most pronounced, both s-PBI and s-PBI-x have similar and even better energy efficiency compared to conventionally imbibed m-PBI because the

high voltage efficiency makes up for those losses. At high current densities the unmodified s-PBI membrane displays a slightly higher energy efficiency than the crosslinked s-PBI. Nonetheless, the high crossover imposes additional costs when considering the need to rebalance the reactive species and crosslinking proves to be a viable approach for reducing this need.

5.5 Conclusion.

s-PBI gel membranes were synthesized via the PPA process to afford membranes stable in sulfuric acid and oxidative V(V) solutions. The membranes exhibited high conductivities and good cell performance especially at high current densities. These membranes, however, have inherently high vanadium ion crossover due to the open morphology and low polymer solids content. Vanadium crossover was shown to be inhibited via chemical crosslinks, although still high compared to dense membranes. However, this crosslinking method is transferrable to many PBI chemistries and can be used to further decrease crossover in PBI gel membranes without significant losses in proton conductivity.

5.6 Acknowledgements.

The information, data, or work presented herein was funded in part by the Advanced Research Projects Agency – Energy (ARPA-E), U.S. Department of Energy, under Award Number DE-AR-0001478.

5.7 References.

1. M. L. Perry and A. Z. Weber, *Journal of The Electrochemical Society*, **163**, A5064 (2016).
2. C. Zhang, L. Zhang, Y. Ding, S. Peng, X. Guo, Y. Zhao, G. He and G. Yu, *Energy Storage Materials*, **15**, 324 (2018).
3. A. Parasuraman, T. M. Lim, C. Menictas and M. Skyllas-Kazacos, *Electrochimica Acta*, **101**, 27 (2013).
4. W. Xie, R. M. Darling and M. L. Perry, *Journal of The Electrochemical Society*, **163**, A5084 (2016).
5. K. A. Perry, K. L. More, E. Andrew Payzant, R. A. Meisner, B. G. Sumpter and B. C. Benicewicz, *Journal of Polymer Science Part B: Polymer Physics*, **52**, 26 (2014).
6. X. L. Zhou, T. S. Zhao, L. An, L. Wei and C. Zhang, *Electrochimica Acta*, **153**, 492 (2015).
7. Z. Yuan, Y. Duan, H. Zhang, X. Li, H. Zhang and I. Vankelecom, *Energy & Environmental Science*, **9**, 441 (2016).
8. T. Luo, O. David, Y. Gendel and M. Wessling, *Journal of Power Sources*, **312**, 45 (2016).
9. S. Peng, X. Yan, D. Zhang, X. Wu, Y. Luo and G. He, *RSC Advances*, **6**, 23479 (2016).
10. S. Peng, X. Yan, X. Wu, D. Zhang, Y. Luo, L. Su and G. He, *RSC Advances*, **7**, 1852 (2017).
11. C. Noh, M. Jung, D. Henkensmeier, S. W. Nam and Y. Kwon, *ACS Applied Materials & Interfaces*, **9**, 36799 (2017).
12. J.-K. Jang, T.-H. Kim, S. J. Yoon, J. Y. Lee, J.-C. Lee and Y. T. Hong, *Journal of Materials Chemistry A*, **4**, 14342 (2016).
13. Z. Chang, D. Henkensmeier and R. Chen, *ChemSusChem*, **10**, 3193 (2017).
14. L. Xiao, H. Zhang, E. Scanlon, L. S. Ramanthan, E. W. Choe, D. Rogers, T. Apple and B. C. Benicewicz, *Chem. Mater.*, **17**, 5328 (2005).
15. T. R. Garrick, C. H. Wilkins, A. T. Pingitore, J. Mehlhoff, A. Gulledge, B. C. Benicewicz and J. W. Weidner, *Journal of The Electrochemical Society*, **164**, F1591 (2017).
16. T. R. Garrick, A. Gulledge, J. A. Staser, B. Benicewicz and J. W. Weidner, *ECS Transactions*, **66**, 31 (2015).
17. M. Skyllas-Kazacos, L. Cao, M. Kazacos, N. Kausar and A. Mousa, *ChemSusChem*, **9**, 1521 (2016).
18. K.-Y. Chan and C. Y. V. Li, *Electrochemically Enabled Sustainability: Devices, Materials and Mechanisms for Energy Conversion*, p. 420, CRC Press (2014).
19. I. B. Valtcheva, P. Marchetti and A. G. Livingston, *Journal of Membrane Science*, **493**, 568 (2015).
20. Q. Li, J. O. Jensen, R. F. Savinell and N. J. Bjerrum, *Progress in Polymer Science*, **34**, 449 (2009).
21. M. Razali, C. Didaskalou, J. F. Kim, M. Babaei, E. Drioli, Y. M. Lee and G. Szekely, *ACS Applied Materials & Interfaces*, **9**, 11279 (2017).
22. J. Yang, H. Jiang, L. Gao, J. Wang, Y. Xu and R. He, *International Journal of Hydrogen Energy*, **43**, 3299 (2018).

23. T. Sukkar and M. Skyllas-Kazacos, *Journal of Applied Electrochemistry*, **34**, 137 (2004).

CHAPTER 6

SUMMARY AND OUTLOOK

6.1 Summary.

Polybenzimidazole (PBI) polymers, known for their thermal and chemical stabilities, demonstrate advantageous physical properties for use in high temperature and acidic environments such as those found in fuel cells, electrochemical hydrogen pumps, SO_2 depolarized electrolyzers, and flow batteries. Moreover, the synthetic flexibility of the PBI chemistry warrants polymer materials with tunable physical properties. With careful consideration, PBI polymers can be exploited for enhanced performance in different applications.

Chapter 2 of this dissertation discusses novel PBI copolymers comprised of *para* and *meta* PBI repeat units synthesized via the PPA Process and were evaluated for use in electrochemical devices. These PBI copolymers exhibited exceptional mechanical properties compared to PBI homopolymers previously reported, such as *p*-PBI. Recent work by Chen et. al. showed that polymer solids content in PBI gel membranes played a critical role in resistance to creep.(1) *p*-PBI homopolymers, due to their rigid linear nature, have decreased solubility compared to their *m*-PBI counterparts. This degree of rigidity is also partly responsible for the increased proton conductivity and electrochemical performance which is exploited in its commercial use in fuel cells. However, due to the creep deformation of these low solids membranes, long-term performance degradation is evident. A series of copolymers were constructed with varying *m/p* character. It was found that copolymers with a ratio of 7:1 *meta*:*para* the polymer greatly increased the polymer solubility leading to membranes with high solids content. These membranes performed exceptionally well in various electrochemical devices and long-term fuel cell performance was conducted demonstrating only a 0.69 $\mu V \cdot hr^{-1}$ degradation over two years. To the best

of our knowledge, this performance degradation and life-time surpasses all other PEMs reported in the literature.

The next part of this dissertation describes detailed studies of polymer membranes used in electrochemical hydrogen separation. To-date there has not been much work conducted studying the performance and efficiency of such devices, nor the purity that can be achieved from various gas streams. Novel membranes, such as the one found in chapter 1, and newly crosslinked membranes were compared to "off-the-shelf" *p*-PBI and studied under a variety of conditions including temperature, carbon monoxide content in feed stream, and differential pressures. *p*-PBI proved to have the best performance under standard operating conditions, as expected, due to its high conductivity. However, as the temperature was increased performance degradation was hastened. Operating at higher temperature allows for a higher carbon monoxide content in the feed stream because platinum catalyst poisoning is diminished. *p*-PBI was also not capable of operating under differential pressures for an extended period of time. The more mechanically robust *m/p*-PBI copolymer was capable of handling that mechanical load for well over 3,000 hours with minimal performance degradation. Further testing should be completed with crosslinked *p*-PBI, as the ex-situ data demonstrates similar mechanical stability to *m/p*-PBI and proton conductivities similar to *p*-PBI.

Sulfonated PBI membranes were then studied for use in an SO_2 depolarized electrolyzer for the generation of hydrogen from a thermal-chemical process. Membrane sulfonation was obtained by utilizing pre-sulfonated monomers that enhanced the stability of the sulfonate group in sulfuric acid. The sulfonate group also afforded membranes stable in concentrated sulfuric acid at elevated temperatures for long periods of time. This

membrane made it possible to operate the electrolyzer at temperatures greater than 100 °C generating sulfuric acid at concentrations above 8 M. Membranes further enhanced by crosslinking may provide a membrane more resilient to high acid concentrations and creep deformation that may lead to a poor interface between the membrane and electrode. Furthermore, the anodic overpotential was found to be the highest contributor to the overall voltage of the cell due to the reaction occurring on the anode suggesting a new catalyst should be investigated for increased performance.(2)

Similarly, sulfonated PBI was further tested as a membrane separator for redox flow batteries operating with a sulfuric acid electrolyte due to the increased chemical stability that was observed in SO_2 depolarizers. This membrane was also found to be oxidatively stable to V^{5+} which has not been reported for any other full organic polymer. This membrane allowed for flow battery operation at high current densities. Operating at high current densities decreases the number of cells needed in a stack and can greatly decrease the cost of a flow battery. However, s-PBI had increased vanadium crossover even when crosslinked. Additional techniques should be investigated to further reduce crossover without severely impacting proton conductivity. As these techniques are relatively new to PBI gel membranes more work is needed to determine industrial feasibility and reproducibility on a large scale.

6.2 Conclusion

PBI membranes formed from the PPA Process can have a wide range of properties. These works demonstrate tools that can be used to design and tune the chemistry and morphology of PBI membranes for use in electrochemical devices with different operating conditions and environments.

6.3 References.

1. X. M. Chen, G. Q. Qian, M. A. Molleo, B. C. Benicewicz and H. J. Ploehn, *Journal of Polymer Science Part B-Polymer Physics*, **53**, 1527 (2015).
2. T. R. Garrick, C. H. Wilkins, A. T. Pingitore, J. Mehlhoff, A. Gulledge, B. C. Benicewicz and J. W. Weidner, *Journal of The Electrochemical Society*, **164**, F1591 (2017).

APPENDIX A – PERMISSION TO REPRINT

SPRINGER NATURE LICENSE TERMS AND CONDITIONS

Sep 08, 2018

This Agreement between Andrew T Pingitore ("You") and Springer Nature ("Springer Nature") consists of your license details and the terms and conditions provided by Springer Nature and Copyright Clearance Center.

License Number	4397670578702
License date	Jul 28, 2018
Licensed Content Publisher	Springer Nature
Licensed Content Publication	Springer eBook
Licensed Content Title	Polybenzimidazole Fuel Cell Technology: Theory, Performance, and Applications
Licensed Content Author	Andrew T. Pingitore, Max Molleo, Thomas J. Schmidt et al
Licensed Content Date	Jan 1, 2018
Type of Use	Thesis/Dissertation
Requestor type	academic/university or research institute
Format	print and electronic
Portion	full article/chapter
Will you be translating?	no
Circulation/distribution	<501
Author of this Springer Nature content	yes
Title	Advanced Materials for Electrochemical Applications
Instructor name	Brian C. Benicewicz
Institution name	University of South Carolina
Expected presentation date	Nov 2018
Requestor Location	Andrew T Pingitore 541 Main St HRZ1 Room 210 COLUMBIA, SC 29201 United States Attn: Andrew T Pingitore
Billing Type	Invoice
Billing Address	Andrew T Pingitore 541 Main St HRZ1 Room 210 COLUMBIA, SC 29201 United States Attn: Andrew T Pingitore
Total	0.00 USD
Terms and Conditions	

Springer Nature Terms and Conditions for RightsLink Permissions